

**DEVELOPMENT AND ANALYSIS OF A COMPACT
DUAL-BAND COPLANAR ANTENNA**

A thesis submitted by

ROHITH K. RAJ

in partial fulfillment of the requirements for the degree of

DOCTOR OF PHILOSOPHY

Under the guidance of

Prof. P. MOHANAN

**DEPARTMENT OF ELECTRONICS
FACULTY OF TECHNOLOGY
COCHIN UNIVERSITY OF SCIENCE AND TECHNOLOGY
COCHIN-22, INDIA**

AUGUST 2007

CERTIFICATE

This is to certify that this thesis entitled “DEVELOPMENT AND ANALYSIS OF A COMPACT DUAL-BAND COPLANAR ANTENNA” is a bona fide record of the research work carried out by Mr. Rohith K. Raj under my supervision in the Department of Electronics, Cochin University of Science and Technology. The results embodied in this thesis or parts of it have not been presented for any other degree.

Cochin-22
August 2007




Dr. P. Mohanan
(Supervising Teacher)
Professor
Department of Electronics
Cochin University of Science and Technology
India

DECLARATION

I hereby declare that the work presented in this thesis entitled “DEVELOPMENT AND ANALYSIS OF A COMPACT DUAL-BAND COPLANAR ANTENNA” is a bona fide record of the research work done by me under the supervision of Dr. P. Mohanan, Professor, Department of Electronics, Cochin University of Science and Technology, India and that no part thereof has been presented for the award of any other degree.

Cochin-22
August 2007


ROHITH K. RAJ
Research Scholar
Department of Electronics
Cochin University of Science and Technology

ACKNOWLEDGEMENTS

It is with a deep sense of gratitude that I wish to place on record my indebtedness to my supervising guide Dr. Mohanan Pezholil, Professor, Department of Electronics, Cochin University of Science and Technology, whose valuable teaching, guidance and constant encouragement was indispensable for the progress and completion of this thesis. I remember the timely care he had given me throughout my research period. I really enjoyed the period of learning under him.

My sincere thanks Dr. K.G. Nair, Director, Centre for Science in Society, Cochin University of Science and Technology and former Head, Department of Electronics, Cochin University of Science and Technology for his constant encouragement, fruitful advice and suggestions for publishing this work in IEEE Transactions on Antennas & propagation.

In this context let me also thank Prof. K. Vasudevan, Head of the Department of Electronics for his whole hearted support, constant encouragement, and for extending the facilities of Department of Electronics for my research. I also wish to thank him for his valuable suggestion in my research.

I wish to express my sincere indebtedness to Dr. C. K. Anandan, Reader, Department of Electronics, Cochin University of Science and Technology for his timely care in my research, valuable suggestions and constant encouragement, which helped me very much to improve my research work.

Let me thank Prof. K. G. Balakrishnan, former Head, Department of Electronics, Prof. K. T Mathew and Prof. P.R.S Pillai, of Department of Electronics, for their whole hearted support, constant encouragement and valuable suggestions.

My sincere thanks to Dr. Tessamma Thomas, Mr. James Kurien, Mrs. M.H. Supriya, and all other faculty members of Department of Electronics for the help and cooperation extended to me.

In this context let me thank Prof. Ramesh Garg, IIT Kharagpur for spending his valuable time for discussing the FDTD analysis and other conceptual problems related to my thesis work, which helped me very much to improve my thesis.

I take this opportunity to express my sincere gratitude to Mrs. Sona O. Kundukulam, Scientist, LRDE, Defense Research and Development Organization for her constant encouragement and suggestions during my research period.

I thankfully bear in mind the sincere directions and enthusiastic words of Dr. Sebastian Mathew, K.E College, Mannanam about my laboratory during my graduation period very accidentally and fortunately.

Dr. P.A Praveen Kumar, Scientist, NPOL, DRDO lab Cochin, Dr. Joe Jacob, Department of Physics, Newman College, Thodupuzha, Dr. T. K. Mani, Model

Engineering College, Cochin and Mr. M. Deepu Kumar, Senior Engineer, Delphi, USA had helped me very much during my research period. I take this opportunity to express my sincere gratitude to them for their indispensable help.

Mr. Manoj Joseph had been with me throughout my research period. I take this opportunity to express my gratitude for his valuable suggestions and encouragement which were of immense value to me. I really enjoyed very much my period of association with him.

I take this opportunity to express my sincere thanks to Ms. Suma M.N and Mr. Deepu V for extending me an unparalleled way of support, constant encouragement, and fruitful discussions on my research topic.

My sincere thanks to Mr. K. Francis Jacob and Mrs. Shameena, for their whole hearted support, helps and above all the association with me.

I express my sincere thanks to Mr. M. Gopikrishna for his valuable suggestions and help while preparing this thesis.

I express my sincere thanks to Mr. Anupam R. Chandran and Mr. Shynu S.V, Post Doctoral fellow, Dublin institute of Technology, Mrs. Sreedevi K. Menon, Dr. Lethakumary B, M.G. University, Kottayam, Dr. Binu Paul and Dr. Mridula S, School of Engineering , CUSAT for their valuable help, fruitful discussions and constant encouragement.

My words are boundless to thank all my research colleagues in Centre for Research in Electromagnetics and Antennas, CUSAT centre for Ocean Electronics (CUCENTOL), Microwave Tomography and Material Research Laboratory (MTMR) and Audio and Image Research Lab (AIRL), Department of Electronics, Cochin University of Science and Technology.

In the course of my research work I received a Junior Research fellow ship from Cochin University of Science and Technology and a research project fellowship from University Grants Commission (UGC), Govt. of India. These financial supports are gratefully acknowledged.

My sincere thanks to all non teaching staff of Department of Electronics for their friendly behavior, encouragement and valuable helps.

My parents and my brother for their boundless love, care and their seamless effort, which gave me courage and stiffness to complete this work in this form.

ROHITHI K. RAJ

PREFACE

With the recent progress and rapid increase in mobile terminals, the design of antennas for small mobile terminals is acquiring great importance. In view of this situation, several design concepts are already been addressed by the scientists and engineers. Compactness, efficiency and radiation pattern are the major criteria for mobile terminal antennas. The challenging task of the microwave scientists and engineers is to device compact printed radiating systems having multi-band behavior, together with good efficiency. Printed antenna technology has received popularity among antenna scientists after the introduction of microstrip antenna in 1970s. The successors in this kind such as printed monopoles and Planar Inverted F Antenna (PIFA) are also equally important. Scientists and Engineers are trying to explore this technology as a viable cost effective solution for forthcoming microwave revolution. The transmission line perspectives of antennas are very interesting. Any electromagnetic system with a discontinuity will radiate. The size, shape and the orientation of the discontinuities controls the radiation characteristics of the system such as radiation pattern, gain, polarization etc. It can be either resonant or non resonant structure.

The coplanar waveguide is an attractive device in microwave integrated circuits due to its uniplanar nature, ease of fabrication and low production cost. Several attempts are already done to explore the radiating modes in coplanar waveguide transmission lines. Usually coplanar wave guides are excited by an SMA connector with its centre conductor connected to the exact middle of the centre strip and the outer ground conductor to the two ground strips. The mode excited on it is purely a bound mode. The E-field distribution in the two slots are out of phase and there for cancels at the far field. This thesis addresses an attempt to excite an in phase E-field distribution in the two slots of the coplanar waveguide by employing a feed asymmetry, in order to get radiation from the two large slot discontinuities of the coplanar waveguide. The omni directional distribution of the radiating energy can be achieved by widening the centre strip.

The first part of the thesis deals with the investigations on the resonance phenomena of conventional coplanar waveguides at higher frequency bands. Then an offset fed open circuited coplanar waveguide supporting resonance/radiation phenomena is analyzed. Finally, a novel compact coplanar antenna geometry with dual band characteristics, suitable for mobile terminal applications is designed and characterized using the inferences from the above study.

Chapter 1

Introduction...1

- 1.1 Introduction.....3
- 1.2 Over view of Antenna Research.....4
- 1.3 Small mobile terminal antenna performance and effect of ground plane.....6
- 1.4 State of the art technologies.....7
- 1.5 Microstrip Antennas.....9
- 1.6 Planar Inverted F Antennas.....11
- 1.7 Metamaterial Antennas.....12
- 1.8 Coplanar waveguide (CPW) and its application in antennas.....14
 - 1.8.1 Types of Coplanar Waveguide.....16
 - 1.8.2 Field distribution in CPW.....16
 - 1.8.3 Applications of CPW.....17
- 1.9 Motivation of present Research.....19
- 1.10 Thesis Organization.....24
- 1.11 References.....26

Chapter 2

Review of Literature.....31

- 2.1 Introduction.....33
- 2.2 Antennas for mobile applications.....33
- 2.3 Multi-band antenna design techniques.....39

2.4	Broad band antenna design techniques.....	45
2.5	Antenna Miniaturization Schemes.....	50
2.6	Coplanar Antennas.....	55
2.7	Resonance/Leakage Phenomena in Coplanar waveguides.....	57
2.8	FDTD for antenna analysis.....	59
2.9	References.....	63

Chapter 3

Methodology.....83

3.1	Fabrication method.....	85
3.2	Microwave substrates.....	86
3.3	Experimental characterization setup.....	87
3.3.1	HP 8510C Vector Network Analyzer.....	88
3.3.2	Anechoic Chamber.....	90
3.3.3	Turntable assembly for far field radiation pattern measurement.....	91
3.4	Measurement procedure.....	91
3.4.1	Return loss, Resonant frequency and Band width.....	92
3.4.2	Far field radiation pattern.....	93
3.4.3	Antenna gain.....	93
3.5	IE3D Electromagnetic simulator.....	94
3.6	HFSS: 3D Electromagnetic simulator.....	95
3.7	References.....	97

Chapter 4

Finite Difference Time Domain Method.....99

4.1	Introduction.....	101
-----	-------------------	------------

4.2	Three dimensional FDTD method.....	103
4.2.1	Finite Difference Equations.....	104
4.2.2	Stability criteria.....	106
4.2.3	Numerical dispersion.....	106
4.3	Absorbing Boundary conditions.....	107
4.3.1	Mur's first order ABC.....	109
4.3.2	Perfectly Matched Layer (PML).....	110
4.4	PML for Finite Difference Time Domain technique.....	111
4.5	Lubbers feed model for fast FDTD convergence.....	123
4.5.1	Resistive source model.....	124
4.5.2	Staircase transition for microstrip line feed.....	126
4.6	Excitation functions.....	127
4.6.1	Gaussian pulse.....	128
4.6.2	Sine function.....	128
4.7	General Flow chart of FDTD algorithm.....	129
4.8	Return loss calculation.....	130
4.9	References.....	131

Chapter 5

Investigations on Coplanar Waveguides (CPW)..133

5.1	Introduction.....	135
5.2	Resonance and radiation from finite ground open circuit CPW.....	136
5.2.1	Return loss characteristics.....	137
5.2.2	Far field radiation.....	138
5.2.3	3D radiation pattern.....	139
5.2.4	Gain and Efficiency.....	140
5.2.5	Conclusions.....	141
5.3	Resonance and radiation from offset fed open circuit CPW.....	142

5.3.1	FDTD analysis of offset fed open circuit CPW.....	143
5.3.1.1	Description of the problem and excitation schemes.....	143
5.3.1.2	FDTD flow chart.....	146
5.3.1.3	Input Gaussian pulse.....	148
5.3.1.4	PMI coefficients.....	149
5.3.1.5	Computed time domain characteristics at feed point.....	152
5.3.1.6	Return loss characteristics and input impedance.....	154
5.3.1.7	Computed fringing electric field values at the gaps.....	156
5.3.1.8	Conclusion.....	162
5.4	Parametric analysis.....	163
5.4.1	Effect of CPW length on resonance and radiation efficiency.....	163
5.4.2	Effect ground strip width resonance and radiation efficiency.....	164
5.4.3	Effect of centre strip width on resonance and radiation efficiency.....	165
5.4.4	Effect of substrate ϵ_r & thickness on resonance.....	166
5.5	Far field radiation and polarization.....	168
5.6	Current distribution.....	170
5.7	Radiation pattern and gain.....	172
5.8	Equivalent circuit representation and radiation mechanism.....	173
5.9	Conclusions.	178

Chapter 6

Development and analysis of a Compact

Microstrip-fed Dual-band Coplanar Antenna.....181

6.1	Introduction.....	183
6.2	Offset fed coplanar geometry with wide centre strip width.....	184
6.3	Dual-band coplanar antenna configuration.....	194
6.3.1	Microstrip line feed.....	195
6.3.2	Ground plane and its importance in the present design.....	196
6.3.3	Conducting pins or vias.....	199
6.3.4	Antenna configuration.....	200
6.4	FDTD analysis of coplanar antenna.....	202

6.4.1	Description of the problem.....	202
6.4.2	FDTD flow chart.....	204
6.4.3	Input Gaussian pulse.....	206
6.4.4	Computed time domain characteristics at feed point.....	207
6.4.5	Return loss characteristics.....	208
6.4.6	Computed electric field values at the top layer, middle layer and bottom layer of the substrate in the two bands.....	210
6.4.7	Conclusions.....	224
6.5	Parametric analysis.....	225
6.5.1	Effect of length 'l' on resonant frequencies and bandwidth.....	226
6.5.2	Effect of centre strip width 'w' on resonant frequencies and band width.....	228
6.5.3	Effect of lateral strip width 'c' on resonant frequencies and band width.....	230
6.5.4	Effect of gap 'g' on resonant frequencies and band width.....	232
6.5.5	Effect of conducting pin dimension on resonant frequencies.....	232
6.5.6	Effect of ground plane length 'L' on the two resonant frequencies and band width.....	234
6.5.7	Effect of ground plane width 'W' on the two resonant frequencies and band width.....	236
6.5.8	Effect of dielectric constant ϵ_r on resonant frequencies.....	238
6.6	Far field radiation and polarization.....	240
6.7	Principal plane radiation patterns.....	241
6.8	Gain and radiation efficiency in the two bands.....	245
6.9	Design procedure.....	246
6.10	Comparison with Rectangular microstrip antenna.....	251
6.11	Conclusions.....	253

Chapter 7

Conclusion.....255

7.1	Thesis highlights.....	257
7.2	Inferences from investigations on Coplanar waveguides.....	258
7.3	Inferences from investigations on 'Coplanar Antenna'.....	261
7.4	Demerits of present design.....	262
7.5	Suggestions for future works.....	263

Appendix A
**Compact planar Multi-band Antenna for GPS, DCS,
2.4/5.8 GHz WLAN applications.....265**

- A.1 Introduction.....267
- A.2 Antenna Design.....267
- A.3 Results and discussions.....269
- A.4 References.....273

Appendix B
**Compact Amplifier Integrated Microstrip
Antenna.....275**

- B.1 Introduction.....277
- B.2 Active Antenna Design.....278
- B.3 Results and discussions.....280
- B.4 References.....282

List of publications of the author.....283

Resume of the author.....287

Index.....291

Introduction

This chapter starts with a brief overview of the progress in antenna research. Microstrip antennas, Planar inverted F antennas (PIFA), metamaterial antennas are described to portrait the recent progress in antennas from half wavelength and quarter wave resonant antenna systems to sub-wavelength ultra miniaturized antennas. The chapter also presents the coplanar waveguide and its potential applications in microwave circuits and antennas. Finally the motivation behind the development of ‘coplanar antenna’ and the thesis organization are described.

1.1 Introduction

The foundations for wireless communication research and industry were established in 1864, when James Clerk Maxwell predicted that the electric and magnetic fields will allow energy to be transported through materials and space at a finite velocity [1]. Heinrich Rudolf Hertz demonstrated Maxwell's theory of electromagnetic radiation in 1888 by his classical spark transmitter. Hertz's apparatus demonstrated the first transmission of regulated radio waves, the 'new form of energy' [2].

The great Indian scientist Jagadish Chandra Bose made a revolutionary attempt to demonstrate radio communication. In 1895, Bose gave his first public demonstration of electromagnetic waves. The wavelengths he used ranged from 2.5 cm to 5 mm. He was playing at 60 GHz over one hundred years ago!. Bose's investigations included measurement of refractive index of a variety of substances. He also made dielectric lenses, oscillators, receivers, and his own polarization device.

Guglielmo Marconi, dubbed the father of the wireless communications, took the discoveries of Maxwell and Hertz. It was in 1897 that Marconi demonstrated the practical applications of wireless communication, when he established continuous radio communication between the shore and ships traveling in the English Channel [3]. By mid December in 1901, Marconi took a much greater step by performing the first transcontinental wireless communication, between England and Canada. This achievement triggered the scientists and engineers all over the world towards wireless communication.

1.2 Over view of Antenna Research

Prior to World War II, most antenna elements were of wire types such as long wires, dipoles, helices, rhombuses etc., and were used either as single elements or as arrays. In the year 1926 Yagi-Uda antenna was introduced [4], which received wide popularity due to the simple array structure and excellent radiation performance. It is still being used as home TV antenna.

World War II was the most flourishing period in antenna research. During and after World War II, many other radiators were introduced. Many of these were aperture type such as open ended waveguides, slots, horns, reflectors and lenses. They were employed for radar, remote sensing and deep space applications [5]. In 1950s a breakthrough in antenna evolution was created by V.H Ramsey [6] which extended the maximum bandwidth as great as 40:1 or more. The structure is specified entirely by angles, instead of linear dimensions, they offered an infinite bandwidth and popularly referred to as frequency independent antennas.

It was not until almost 20 years later that a fundamental new radiating element, which has received a lot of attention and many applications since its inception, was introduced. Microstrip antennas received considerable attention starting in the 1970s, although the idea of a microstrip antenna can be traced to 1953 [7]. Microstrip antenna is simple, lightweight, inexpensive, low profile and conformal to Aircraft, Missile etc. Major advances in millimeter wave antennas have been made in recent years,

including integrated antennas where active and passive circuits are combined with the radiating elements into one compact unit to form monolithic circuits [8].

The inherent narrow bandwidth properties of microstrip antennas has limited its usage from many applications. Recently, printed monopole elements have received wide acceptance due to its omni directional radiation characteristics and compact nature. Very recently ultra wideband communication has received wide popularity. It can provide high speed data transfer rate for short range applications. The wide band behavior of ultra short pulse used for this communication requires ultra wide band antennas to accommodate the large frequency spectrum. This is one of the developing areas in antenna design [9]. The time domain characterization of the antenna and formulation of transfer function for such antennas are active research topic in these days.

There has been much interest in electrically small antennas. Antennas that are electrically small, efficient, and have significant bandwidth would fill many needs if antenna engineers could reconcile these usually contradictory requirements. This is especially true recently with increased uses of wireless technologies for communications and sensor networks. It is well known that small electric dipole antenna is an inefficient radiator, i.e., because it has a very small radiation resistance with very large capacitive reactance. Consequently, to obtain a high overall efficiency, considerable effort must be expended on a matching network that produces an impedance that is conjugately matched to the dipole's impedance; i.e., it forces the total reactance to zero by introducing a very large inductive reactance which cancels the very large capacitive reactance of a small electric dipole, and that then matches this resonant system to a feed

network. Recently, this problem has been overcome by introducing metamaterial concept in antennas. A metamaterial medium is introduced in antennas to obtain electrically small antenna element with good efficiency [10].

Antenna research is now progressing rapidly. Active integrated antenna technology allows the integration of active devices with antenna elements, and the radiator is assigned with some other functions in addition to its role as a radiator in communication systems.

1.3 Small mobile terminal antenna performance and effect of ground plane

In designing antennas for small mobile terminals, the prime considerations have been taken into account are

1. small size
2. light weight
3. compact structure
4. low profile
5. robustness
6. flexibility
7. low cost
8. ease of mass fabrication

In addition to these, durability against the users rough handling, environmental conditions, such as temperature variations should be taken into account. From the 1980s to the present the downsizing of mobile terminals made remarkable progress and, accordingly, the size of the antennas are becoming smaller. The miniaturization of mobile handset is beneficial for users. It is a serious challenge for

antenna engineers. The miniaturization should not sacrifice the antenna performance [11].

Almost all of the equipment cases in these days are made of plastics, not of metals. Some 'conducting materials' existing in the equipment will also act as a radiator. The typical conducting material in the equipment is a rectangular shielding plate or box, where RF and other circuits are included. Usually a built-in antenna element is placed on this plate or box, and it acts as a ground plane.

As a ground plane performs as a part of a radiator, when a small antenna element is placed on it and induces currents on it, the antenna's size is effectively enlarged and, hence, the antenna's performance is enhanced. The gain and bandwidth may be increased, although this depends on the size of the ground plane and the type of the antenna. An important conclusion obtained from the research is that the role of ground planes in mobile communication equipments is very important. The ground plane contributes very much to the total radiation.

1.4 State of the Art technologies

Mobile communications, wireless interconnects, wireless local area networks (WLANs), and cellular phone technologies are the most viable cost effective communication systems enabling user mobility. Naturally, these applications require efficient antennas. The portable antenna technology has grown along with mobile and cellular technologies. It is important to have the proper antenna for a device. The proper antenna will improve transmission and reception, reduce power consumption and finally results a cute compact device with market demands.

Antennas used for early portable wireless handheld devices were the so-called 'whip' antennas. The quarter-wavelength whip antenna was very popular, mostly because of its simple structure and omnidirectional radiation pattern [12]. New antenna designs have appeared on radios with lower profile than the whip antenna and without significantly affecting the performance. The commonly used monopole antennas possess a number of drawbacks. Monopole antennas are relatively large in size and protrude from the handset case in an awkward way.

In the past few years, designs based on the Planar Inverted-F Antenna (PIFA) and Microstrip Antennas (MSA) have been popular for handheld wireless devices due to low profile geometry. Conventional PIFAs and MSAs are compact, with dimensions approximately a quarter to a half of the wavelength. These antennas can be further optimized by adding new parameters in the design, such as strategically shaping the conductive plate, or judiciously locating loads or slots etc.

The major limitation of many low-profile antennas is narrow bandwidth. Typical conventional PIFA's have 5% bandwidth, but advanced designs offer wider bandwidth. A variety of techniques for broadening bandwidth have been reported, including the addition of a parasitic structure whose resonant frequency is near that of the driving antenna structure. One example described in the literature is a stacked microstrip patch antenna [12].

In addition to broadband operation, one has to consider the development of multiband antennas. Dual-band and tri-band wireless phones have become popular recently because they permit people to use the same phone in two or three networks that have different frequencies.

The following sections describe the details of different antenna technologies widely used in advanced wireless communication systems.

1.5 Microstrip Antenna

A class of antennas that has gained considerable popularity in recent years is the *microstrip antenna*. A typical microstrip element is illustrated in Fig. 1.1

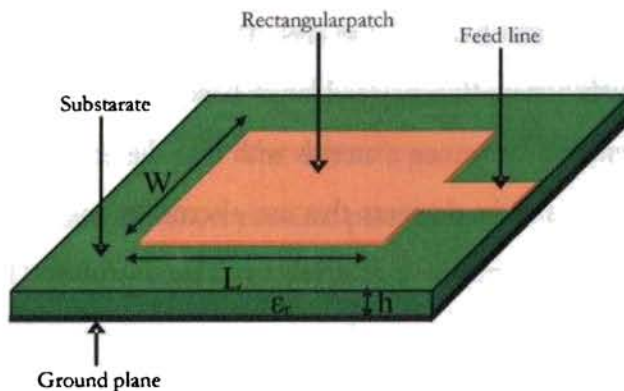


Fig. 1.1 Geometry of a conventional microstrip antenna excited using a microstrip line

There are different types of microstrip antennas, but their common features are:

1. A very thin flat metallic region often called radiating patch
2. Low loss isotropic and homogenous dielectric substrate of relative dielectric constant ϵ_r and thickness 'h'
3. Ground plane, which is usually much larger than the patch
4. Feed, which supplies the RF power to the radiating patch

Microstrip elements are often constructed by etching the radiating patch (and sometimes the feeding circuit) from a single double sided substrate. The length of the patch is typically about a half of the wavelength. A commonly used dielectric for such antennas is Poly Tetra Fluro Ethylene (PTFE), which has a relative dielectric constant of about 2.2. Sometimes a low-density “honeycomb” material is used to support the patch. This material has a relative dielectric constant near unity and usually results in an element with better efficiency and larger bandwidth [13] but at the expense of an increase in element size. Substrate materials with high dielectric constants can also be used. Such substrates result in elements that are electrically small in terms of free-space wavelengths and consequently have relatively small bandwidth and low efficiency.

The microstrip antennas are popular due to the following:

1. Low-profile structure
2. Easy and inexpensive to manufacture in large quantities using modern printed-circuit techniques.
3. When mounted to a rigid surface they are mechanically robust
4. It can be designed to produce variety of patterns and polarizations, depending on the mode excited and shape of the patch.

Active elements can be easily added by a via between the patch and the ground plane. Using such loaded elements, the antenna characteristics can be controlled. These advantages must be weighed against the disadvantages which can be most

succinctly stated in terms of antenna quality factor, Q . Microstrip antennas are high- Q devices. High- Q elements have small bandwidths. Increasing the thickness of the dielectric substrate will reduce the Q and increase its bandwidth. But thick substrate will excite unwanted surface waves and reduce the efficiency [13].

1.6 The Planar Inverted-F Antenna

The planar inverted F antenna (PIFA) is commonly employed in mobile hand sets [14]. The small size and low profile nature of the PIFA made it an excellent choice on portable equipment. The PIFA typically consists of a rectangular planar element, ground plane, and short circuited plate as shown in Fig. 1.2.

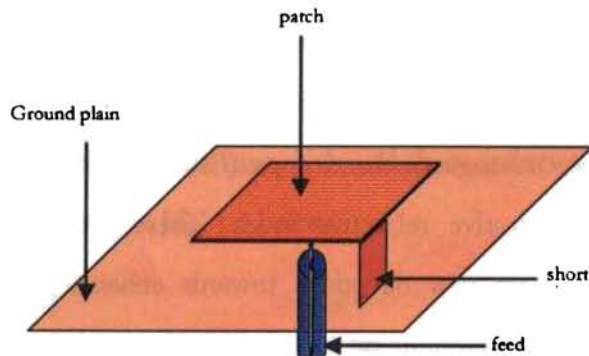


Fig. 1.2. Planar Inverted F antenna (PIFA) excited using a coaxial transmission line

The PIFA can be thought of as a combination of the inverted-F (IFA) antenna and the short circuited rectangular microstrip antennas (SCMSA), as shown in Fig. 1.2. Both the IFA and SCMSA have smaller bandwidths, but PIFA has sufficient bandwidth to cover popular communication bands (about 8%). The PIFA is an IFA in which the wire radiator element is replaced by a strip to increase the bandwidth.

The PIFA also can be viewed as a short-circuit microstrip antenna resonating at the dominant TM_{100} mode. The length of the rectangular element is halved by placing a short-circuit plate between the radiator element and ground plane. When the width of the short-circuit plate is narrower than that of the planar element, the effective inductance of the antenna element increases, and the resonant frequency becomes lower than that of a conventional short-circuit MSA having the same size. As a result, the size of the short-circuit MSA can be further reduced.

1.7 Metamaterial antennas

Over the last few years, there has been considerable research effort on the analysis and design of metamaterial structures for the microwave and millimeter wave frequency regimes [15, 16, 17]. Metamaterials have been developed and shown to exhibit properties such as electromagnetic band gaps (EBG), artificial magnetic conductor (AMC) behavior and negative refractive index. These properties of metamaterial structures have opened up new directions towards enhancing the performance of microwave components and overcoming current limitations.

Portable devices have become one of the necessary appliances for our daily lives. To conveniently carry these portable devices such as cell phones, media players and laptops, they are designed to be compact and lightweight, without sacrificing performance or functionality. The challenge to implement such small devices is to mount all the necessary circuits onto a small highly integrated transceiver unit. Among all

the components, the antenna is one of the most challenging device to be scaled down in size because the size of the conventional antennas depends on the operation frequency of the required applications, which is usually in the MHz or low GHz range.

The traditional half-wavelength antenna cannot be incorporated in the space limited RF front-end modules. Therefore, many researchers are investigating different methods to realize small antennas such as using high dielectric constant substrate, shorting pin and folded monopole etc. Recently, metamaterial based transmission lines have been developed and have been shown to exhibit unique features of anti-parallel phase and group velocities and zero propagation constant at a certain frequency at the fundamental operating mode. These metamaterials have been used to realize novel sub wavelength antennas. An interesting design consisting of a dipole with left-handed loading is explained [18]. The antenna is composed of a ladder network of periodic structure of unit cells having series capacitors and shunt inductors. The geometry of the proposed antenna is shown in Fig. 1.3 below.

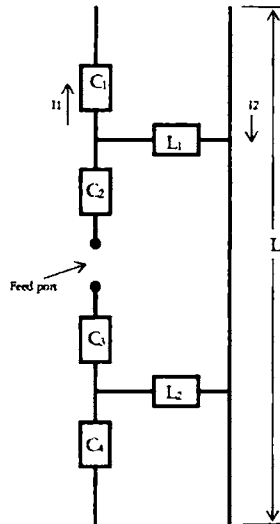


Fig. 1.3. Metamaterial based dipole antenna designed for sub wavelength resonance

Placing capacitors into one side of the network leads to out of phase currents with different amplitudes that allow strong radiation. The numerical analysis show that the antenna has a length of 0.15 wavelengths in free space, input impedance close to 50Ω and well behaved radiation patterns. The input impedance is close to 50Ω is achieved in a series resonance at 451 MHz. Note that the size of the device is less than 0.25λ , which is usually needed in any resonant antenna systems. Metamaterial antenna is becoming a promising area of research.

1.8 Coplanar Wave Guides and its applications

The coplanar waveguide (CPW) was proposed by Wen [19] in 1969. A conventional CPW on a dielectric substrate consists of a center strip conductor with semi-infinite ground planes on either side as shown in Fig. 1.4.

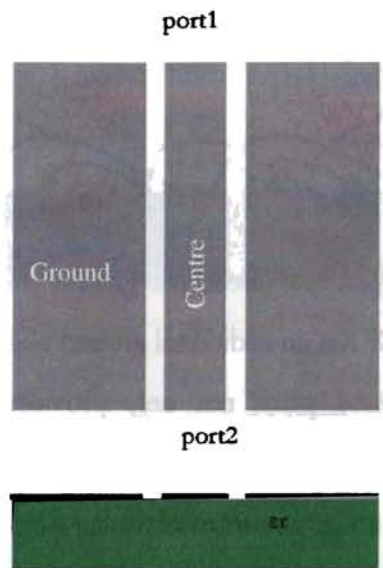


Fig. 1.4. Top view and side view of conventional Coplanar Wave Guide (CPW)

This structure supports a quasi-TEM mode of propagation. The CPW offers several advantages over conventional microstrip line. First, it simplifies fabrication, second it facilitates easy shunt as well as series surface mounting of active and passive devices [20] to [21]; third, it eliminates the need for wraparound and via holes [22] and [23], and fourth, it reduces radiation loss [24]. In addition a ground plane exists between any two adjacent lines, hence cross talk effects between adjacent lines are very weak [25]. As a result, CPW circuits can be made denser than conventional microstrip circuits. These, as well as several other advantages, make CPW ideally suited for MIC as well as MMIC applications

1.8.1 Types of Coplanar Waveguides

Coplanar waveguides can be broadly classified as follows:

- Conventional CPW
- Conductor backed CPW
- Micromachined CPW

In a conventional CPW, the ground planes are of semi infinite extent on either side. However, in a practical circuit the ground planes are made of finite extent. The conductor-backed CPW has an additional ground plane at the bottom surface of the substrate. This lower ground plane not only provides mechanical support to the substrate but also acts as a heat sink for circuits with active devices. The micro machined CPWs are of two types, namely, the microshield line [26] and the CPW suspended by a silicon dioxide membrane above a micromachined groove [27].

1.8.2 Field distribution in CPW

The electric and magnetic field distribution in CPW is depicted in Fig. 1.5 below. Usually the CPW is excited by giving signal to the centre strip with respect to the ground strips. This produce a field distribution similar to the Odd mode distribution in coupled slot lines. That is the power is coupled by the out of phase electric field distribution in the two slots and magnetic field encircling each strips. This produce a magnetic wall at the plane passing though the centre of the signal strip as shown in Fig. 1.5.

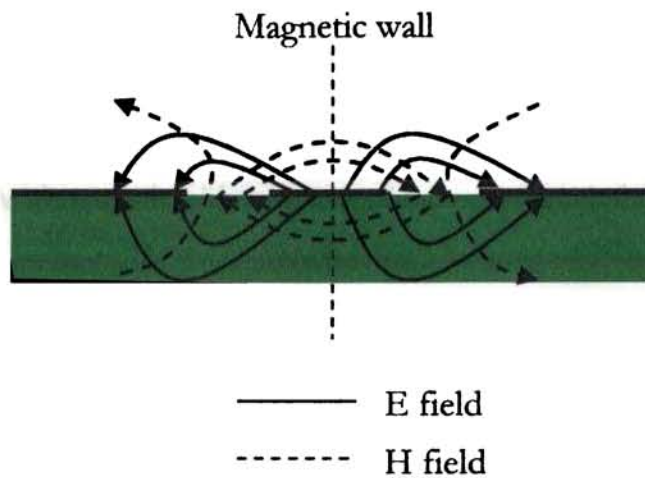


Fig. 1.5. Electric and Magnetic field distribution in CPW

The system is excited by connecting centre conductor of a coaxial connector to the signal strip and outer ground conductor to the two ground strips. This forcefully excites the odd mode field distribution in CPWs. In this case the field distributions in the slots are out of phase, and it cancels at the far field. This field distribution is maintained in this structure due to the feed symmetry.

1.8.3 Applications of CPW

The CPW finds application in almost all the fields of microwave engineering. The microwave circuits always prefer to use CPW based designs due to its uniplanar nature. The amplifiers, active combiners, frequency doublers, mixers, and switches has been realized using CPW. The CPW amplifier circuits include millimeter-wave amplifiers [28, 29 and 30] distributed amplifiers [31], cryogenically cooled amplifiers [32], cascade

amplifiers [33], transimpedance amplifiers [34], dual gate HEMT amplifiers [35], and low-noise amplifiers [36].

Another important area of its application is in Microelectromechanical Systems (MEMS) Switches. The rapid progress made in the area of semiconductor wafer processing has led to the successful development of MEMS based microwave circuits. In a CPW the conductors are located on the top surface of a substrate which makes it ideally suited for fabricating metal membrane, capacitive, shunt-type switches [37]. CPW MEMS shunt switches with low insertion loss, reasonable switching voltages, fast switching speed, and excellent linearity have recently been demonstrated. These switches offer the potential to build new generation of low-loss high-linearity microwave circuits for phased array antennas and communication systems.

The CPW is invariably using in antenna designs as the feed of the radiating element and as radiating system. Coplanar Waveguide Patch Antennas are available in literature [38]. The feed system in these antennas is directly coupled, electromagnetically coupled, or aperture coupled to the patch.

1.9 Motivation of the present research

‘Acceleration or deceleration of charges creates Electromagnetic radiation’ [39]. To create charge acceleration or deceleration there must be a bent, curve, discontinuity or termination. This is the fundamental idea behind any antenna system. Discontinuities in transmission lines excite spurious modes to satisfy the boundary conditions. In a normal closed transmission line, such as wave guide or coax, the spurious modes excited by discontinuities soon die out because they cannot propagate. The electric or magnetic fields in the region of the discontinuity appear as capacitive or inductive reactance to the transmission line.

If the transmission line is open or is opened by a discontinuity (a slot or hole), then the higher-order modes generated can radiate energy. The surface wave transmission lines will radiate at discontinuities. They include dielectric slabs, dielectric rods, and corrugated metal surfaces. At the point of excitation and at the point of termination, the higher-order modes generated will radiate.

It is worth noting that there are many antennas in use that can be viewed as a modification of transmission lines. For example consider a conventional half wave dipole antenna. It consists of two flared arms at the end of a balanced transmission line. The antenna becomes an efficient radiator when the two arms are flared apart. Here, the flaring makes a discontinuity, producing current distribution on the arms, and reinforced at far field to obtain omni directional radiation coverage. The transition of a twin wire balanced transmission line to a dipole is depicted in Fig. 1.8 (a) and (b).

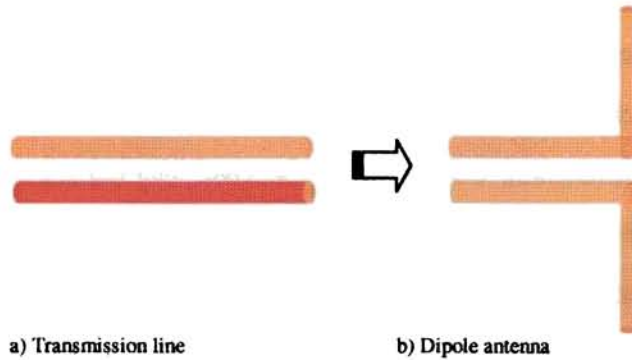


Fig. 1.8. Transformation of a twin wire transmission line to conventional half wave dipole antenna

In the case of a horn antenna, one end of the waveguide is transformed to a discontinuity. A field distribution is then formed at the aperture of the horn producing radiation intensity at far field. We can flare either E or H planes or both the planes. Fig. 1.9 shown below clearly shows the transformation of a rectangular waveguide to a pyramidal horn antenna.

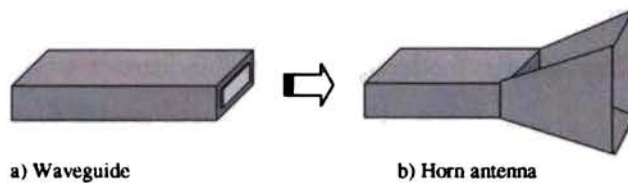


Fig. 1.9. Transformation of a rectangular waveguide to horn antenna

The printed antenna technology has gained the attention of mobile wireless system designers due to its attractive features like light weight, ease of fabrication and low cost of production. Microstrip antenna technology is the pioneer of this kind. The microstrip antennas are an extension of the microstrip transmission line. As long as the physical

dimension of the strip and the relative dielectric constant remains unchanged, virtually no radiation will occur. By shaping the microstrip line into a discontinuity, power will radiate off from the abrupt ends in the strip line. The transformation of a simple microstrip line to a microstrip antenna is depicted in Fig. 1.10 below.

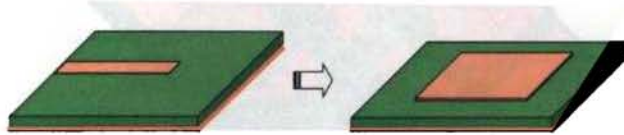


Fig. 1.10. Transition of microstrip line to a rectangular microstrip antenna

This is the fundamental principle behind radiation from a microstrip structure. The above discussion concludes as follows: *any transmission line can be configured as a radiating system by properly modifying its structural parameters, and or feed point.*

There are several papers in literatures regarding the leaky behavior of the CPW [40, 41 and 42]. They conclude that the structural parameters of the device strongly influences the leaky modes excited on the structure. But unfortunately the leaky modes are excited at higher microwave bands. This restricts the use of the leaky phenomenon for compact efficient radiator applications.

But according the transmission line perspective, the discussion above strongly says that the CPW can radiate electromagnetic energy if the feed point and structural parameters are properly optimized. This is the fundamental concept behind this thesis work. Consider the case of a conventional coplanar waveguide transmission line shown in Fig. 1.11

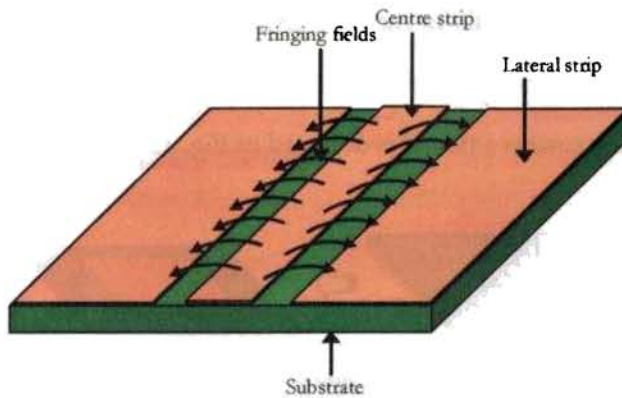


Fig. 1.11. Electric field distribution on Conventional coplanar wave guide when excited with a coaxial connector

The device carries the electromagnetic energy from one end to other by means of a slot mode. The fringing field distribution at the two slots are due to the air dielectric interface in the slots, as depicted in the above figure. The direction of the distribution is obviously out of phase and thus cancels at the far field. That is device behaves as a pure transmission line and thus the radiation from the structure is negligible. The only way to get radiation from the device is by means of transforming the slot modes in such a way that the fringing fields at the two slots are in phase, forming a reinforced radiation intensity at the far field. This is the key idea behind the present work.

By introducing an offset for the feed point location on the centre strip of a coplanar waveguide structure, a radiating mode is excited at lower microwave bands of

the EM spectrum. The E-field distribution at the slots of the device, for the new mode thus excited will look like as depicted in Fig. 1.12 below.

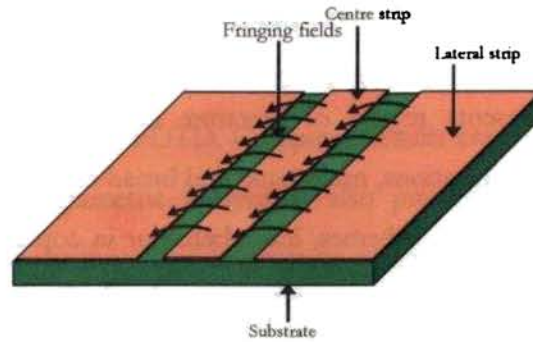


Fig. 1.12. Offset fed coplanar waveguide with in phase field distribution in the slots

The two slots are very close in terms of its operating wavelength and thus the radiation pattern of the device will not be suitable for mobile communication application. That is by properly optimizing the spatial distance between the slots and making the in-phase field distribution in the slots a new antenna element can be derived. The new antenna derived from the concept explained above is termed as 'coplanar antenna'. The conductor backed CPW (CBCPW) has not been selected purposefully for the study because the conductor backing will restrict the radiation pattern to a hemisphere.

1.10 Thesis Organization

Chapter 1 describes an overview of antenna research, state of the art technologies in antennas, coplanar waveguide, its applications and the motivation of present research.

Chapter 2 presents review of literature concerning the present work. Antennas for mobile communications, multi-band and broad-band techniques in printed antennas, antenna miniaturization schemes, leaky behavior in coplanar waveguides and different types of coplanar antennas are referred in detail. Finally, overview of the progress in FDTD analysis is referred.

In chapter 3, the antenna fabrication method and substrate materials used are described. The experimental facilities utilized are also described. The measurement methods employed for characterizing the antenna presented in the thesis is also described. Some part of the simulation is done using commercial packages like HFSS and HFSS. The basic characteristics about these packages are also explained in this chapter.

The principle behind the PML based FDTD computational method is described in Chapter 4. The theoretical investigations on offset fed coplanar waveguide resonance, radiation and the coplanar antenna are derived using PML based FDTD method.

Chapter 5 describes the theoretical investigations on the radiation and resonance phenomena in coplanar waveguide structures. Initially a conventional CPW is analyzed using FDTD. Then characteristics of the device are analyzed when the CPW structure is excited using offset feed. The computed field distributions and return loss characteristics are described. The Odd mode and Even mode like excitations schemes are separately studied using FDTD. Computed results are compared with the measured values. Finally the parametric analysis is also presented to confirm the resonance phenomenon on coplanar waveguide structure when an offset feed is employed.

The so called ‘coplanar antenna’ design is studied in Chapter 6. Experimental as well as theoretical observations are compared. Parametric analysis of the antenna and the empirical design equations are also presented.

Chapter 7 describes conclusions of this thesis. The scope for future works are also discussed.

Appendix I and II describes design of two other printed antennas. A compact planar multi-band antenna for GPS/PCS/WLAN applications is presented in Appendix I and a compact active microstrip antenna is presented in Appendix II.

1.11 References

1. K.Fujimoto and J.R.James, *Mobile Antenna Systems Handbook*, Artech House, 1994.
2. M.E Bialkowski, *Wireless: From Marconi – The Way Ahead*, IWTS 1997, Shah Alum, Malaysia 1997.
3. T.S. Rappaport, *Wireless Communications, Principles and Practice*, Prentice Hall, 1996.
4. S. Uda, *Wireless Beam of short electric waves*, J. IEE (Japan), pp. 273-282, March 1926 and pp. 1209-1219, Nov. 1927.
5. W.V. T. Rusch, *The current State of the Reflector Antenna Art-Entering the 1990's*, Proc. IEEE, vol. 80, No.1, pp. 113-126, Jan. 1992.
6. V. H. Rumsey, *Frequency Independent Antennas*, 1957 IRE National Convention Record, Part 1, pp. 114-118.
7. G.A. Deschamps, *Microstrip Microwave Antennas*, presented at the Third USAF symposium on Antennas, 1953
8. F.K. Schwering, *Millimeter wave antennas*, Proc. IEEE, vol. 80, No.1, pp. 92-102.
9. J.D. Kraus, Ronald J. Marhefka, *Antennas for all applications*, TATA McGraw-Hill Edition, 3rd Edition, pp. 785-788
10. Richard W. Ziolkowski and Aycan Erentok, *Metamaterial-Based Efficient Electrically Small Antennas*, IEEE Transactions on Antennas and Propagation, Vol. 54, NO. 7, July 2006, pp. 2113-2130

11. Hisashi Morishita, Yongho Kim, and Kyohei Fujimoto, Design Concept of Antennas for Small Mobile Terminals and the Future Perspective, *IEEE Antennas and Propagation Magazine*, Vol. 44, No. 5, pp. 30-43, Oct. 2002
12. L. Setian, *Practical Communication Antennas with Wireless Applications*, Prentice Hall PTR, New Jersey: 1998.
13. J.R. James et al., *Microstrip Antenna Theory and Design*, Peter Peregrinus, New-York: 1981.
14. Gabriel K. H. Lui and Ross D. Murch, Compact Dual-Frequency PIFA Designs Using LC Resonators, *IEEE Transactions on Antennas and Propagation*, VOL. 49, NO. 7, July 2001, pp. 10-16-1019
15. V. G. Veselago, *Soviet Physics. Usp.* 10, 509, 1968.
16. Nepa, G. Manara, A. A. Serra, and G. Nenna, *IEEE Antennas and Wireless Propagation Letters*, Vol. 4, 2005, pp. 349-350.
17. Special issue on Metamaterials, *IEEE Trans. Antennas Propagation*, 2003, Vol. 51
18. Iizuka H, Hall P. S, Borja A. L, Dipole Antenna with Left Handed Loading, *IEEE Antennas and Wireless Propagation Letters Issue 99*, 2006
19. C. P. Wen, Coplanar Waveguide: A Surface Strip Transmission Line Suitable for Nonreciprocal Gyromagnetic Device Applications, *IEEE Trans. Microwave Theory Tech.*, Vol. 17, No. 12, pp. 1087—1090, Dec. 1969.
20. J. Browne, Broadband Amps Sport Coplanar Waveguide, *Microwaves RF*, Vol. 26, No. 2, pp. 131—134, Feb. 1987.
21. Technology Close-Up, *Microwaves RF*, Vol. 27, No. 4, p. 79, April 1988.

22. J. Browne, Coplanar Waveguide Supports Integrated Multiplier Systems, *Microwaves RF*, Vol. 28, No. 3, pp.137—138, March 1989
23. J. Browne, Coplanar Circuits Arm Limiting Amp with 100-dB Gain, *Microwaves RF*, Vol. 29, No. 4, pp. 213—220, April 1990. .
24. J. Browne, Broadband Amp Drops through Noise Floor, *Microwaves RF*, Vol. 31, No. 2, pp. 141—144, Feb. 1992.
25. J. Browne, Coplanar MIC Amplifier Bridges 0.5 To 18.0 GHz, *Microwaves RF*, Vol. 26, No. 6, pp. 194—195, June 1987.
26. T. M. Weller, L. P. B. Katehi, and G. M. Rebeiz, High Performance Microshield Line Components, *IEEE Trans. Microwave Theory and Tech.*, Vol. 43, No. 3, pp. 534—543, March 1995.
27. V. Milanovic, M. Gaitan, E. D. Bowen, and M. E. Zaghoul, Micromachined Microwave Transmission Lines in CMOS Technology, *IEEE Trans. Microwave Theory Tech.*, Vol. 45, No. 5, pp. 630—635, May 1997.
28. G. S. Dow, T. N. Ton, and K. Nakano, Q-Band Coplanar Waveguide Amplifier, 1989 IEEE MTT-S Int. Microwave Symp. Dig. Vol. 2, pp. 809—812, Long Beach, California, June 13—15, 1989.
29. K. M. Strohm, J.-F. Luy, F. Schaffler, H. Jorke, H. Kibbel, C. Rheinfelder, R. Doerner, J. Gerdes, F. J. Schmuckle, and W. Heinrich, Coplanar Ka-Band SiGe-MMIC Amplifier, *Electron. Lett.*, Vol. 31, No. 16, pp. 1353—1354, Aug. 1995.
30. M. Riazat, S. Bandy, and G. Zdasiuk, Coplanar Waveguides for MMICs, *Microwave J.*, Vol. 30, No. 6, pp. 125—131, June 1987.

31. R. Majidi-Ahy, M. Riaziat, C. Nishimoto, M. Glenn, S. Silverman, S. Weng, Y. C. Pao, G. Zdasiuk, S. Bandy, and Z. Tan, 94 GHz InP MMIC Five-Section Distributed Amplifier, *Electron. Lett.*, Vol. 26, No. 2, pp. 91—92, Jan. 1990.
32. A. Cappello and J. Pierro, A 22-24-GHz Cryogenically Cooled GaAs FET Amplifier, *IEEE Trans. Microwave Theory Tech.*, Vol. 32, No. 3, pp. 226—230, March 1984.
33. R. Majidi-Ahy, C. Nishimoto, M. Riaziat, M. Glenn, S. Silverman, S.-L. Weng, Y.-C. Pao, G. Zdasiuk, S. Bandy, and Z. Tan, 100-GHz High-Gain InP MMIC Cascode Amplifier, *IEEE Journal of. Solid-State Circuits*, Vol. 26, No. 10, pp. 1370—1378, Oct. 1991.
34. K. W. Kobayashi, L. T. Tran, M. D. Lammert, A. K. Oki, and D. C. Streit, Transimpedance Bandwidth Performance of an HBT Loss-Compensated Coplanar Waveguide Distributed Amplifier, *Electron. Lett.*, Vol. 32, No. 24, pp. 2287—2288, Nov. 1996.
35. M. Schefer, H.-P. Meier, B.-U. Klepser, W. Patrick, and W. Bachtold, Integrated Coplanar MM-Wave Amplifier With Gain Control Using a Dual-Gate InP HEMT, *IEEE Trans. Microwave Theory Tech.*, Vol. 44, No. 12, pp. 2379—2383, Dec. 1996.
36. D. Leistner, Low Noise Amplifier at L- and Ku-Band for Space Applications in Coplanar Technology, 23rd European Microwave Conf. Proc., pp. 823—827, Madrid, Spain, Sept. 6—9, 1993.
37. M. Riaziat, E. Par, G. Zdasiuk, S. Bandy, and M. Glenn, Monolithic Millimeter Wave CPW Circuits, 1989 IEEE MTT-S Int. Microwave Symp. Dig., Vol. 2, pp. 525—528, Long Beach, CA, June 13—15, 1989.

38. J. W. Greiser, Coplanar Stripline Antenna, *Microwave J.*, Vol. 19, No. 10, pp. 47—49, October 1976.
39. Constantine A. Balanis, *Antenna Theory Analysis and Design*, 2nd edition, 1982, John Wiley and Sons Inc.
40. H. Shigesawa, M. Tsuiji, and A. A. Oliner, Power leakage from the dominant mode on coplanar waveguides with finite or infinite width, in 1990 URSI Radio Sci. Meeting Dig., Dallas, TX, May 1990, p. 340.
41. H. Shigesawa, M. Tsuiji, and A. A. Oliner, Dominant mode power leakage from printed-circuit wave guides, *Radio Sci.*, vol. 26, pp. 559- 564, Mar/Apr. 1991.
42. Mikio Tsuiji, Hiroshi Shigesawa and Arthur A. Oliner, New interesting leakage behaviour on coplanar waveguides of finite and infinite widths, *IEEE Trans. Microwave Theory and Techniques*, vol. 39, no. 12, Dec.1991.

Review of Literature

This chapter presents different technologies so far proposed by the research groups across the world for the development of antennas for mobile applications, multi band operation, broad band operation and for compact applications. The recent progress in the direction of coplanar antenna research is then presented. In the last section of this chapter relevant papers addressing leakage phenomena in coplanar waveguides and the progress in FDTD analysis are referred

2.1 Introduction

Progress in printed antenna technology is overwhelming. Modern wireless communication is using printed antenna technology, which is replacing almost all the wire antenna systems available so far. First generation mobile handsets used small monopole type antennas that protruded from the device cabinets. But today the industry prefers to use compact internal antennas for mobile communication applications.

The antennas for mobile communications require some inevitable characteristics. It should be compact, lightweight and capable of omni directional coverage. The rapid developments in mobile communications resulted in the introduction of different wireless communication standards. In order to integrate these communication standards into a single unit, compact wideband/multi band antennas are required.

The thesis highlights the development and analysis of a Compact Dual-band Coplanar antenna. The antenna has two wide resonant bands with 14% and 22% VSWR bandwidth in the lower and higher bands respectively. This chapter of the thesis describes the work done in this direction. Mobile handset antenna design techniques are first referred. Multi-band and broad banding techniques in antennas are then presented. Different antenna miniaturization schemes are also discussed. The leaky behavior in coplanar antennas and coplanar radiator designs are referred, because surface wave leaky modes in coplanar waveguides are the only reported leaky behavior in coplanar waveguides. In this thesis the experimental results are verified using Finite Difference Time Domain Method (FDTD) and most relevant contributions in this field are briefly described.

2.2 Antennas for mobile applications

The allocation of microwave spectrum for personal mobile communication has paved the way for the development of compact internal antennas. Due to the advantages like low attenuation and high coverage, lower microwave bands are used for mobile communications. Compactness of the antennas are the major challenge in this case because the mobile handset itself is very small compared to the wave length of operation. Following section describes different antennas proposed by the various microwave antenna groups working in this area.

K.L. Wong et al. [1] presented a Low-Profile Planar Monopole Antenna for Multiband Operation of Mobile Handsets. The proposed antenna has a planar rectangular radiating patch in which a folded slit is inserted at the patch's bottom edge. The folded slit separates the rectangular patch into two subpatches, one smaller inner subpatch encircled by the larger outer one. The proposed antenna is then operated with the inner subpatch resonating as a quarter-wavelength structure and the outer one resonating as both a quarter-wavelength and a half-wavelength structure.

Jeun-Wen Wu et al. [2] proposed a planar meander-line antenna consisting of three branched strips for very-low-profile GSM(global system for mobile communication)/DCS(digital communication system)/PCS(personal communication system)/WLAN (Wireless LAN) triple-band operation of mobile phones. The branch strips are designed to operate as quarter-wavelength structures at 900 and 1800 MHz, respectively, and covering GSM/DCS/PCS and WLAN bands.

Shun-Yun Lin, in [3] proposed a Multiband Folded Planar Monopole Antenna for Mobile Handset applications. It has a very low profile of about one twentieth of the wavelength of the lowest operating frequency. The effect is achieved by using a bended rectangular radiating patch and an inverted L-shape ground plane. The proposed antenna can be used in multiband operation, with omni directional radiation patterns for all operating bands.

A Miniature built-in multi-band Antennas for Mobile Handsets is described in [4] by Yong-Xin Guo, et al. Compared with the parasitic form with a shorted strip placed away from the main radiator, the size of the proposed antennas can be reduced by an order of 10-20%.

Yong-Sun Shin et al. [5] developed a broadband interior planar monopole type antenna for hand set applications. It is suitable to be built-in within the housing of a mobile phone. In order to achieve the broad bandwidth, the feed which is connected between the microstrip line and antenna is a trapezoidal shape with a tilted angle. By adjusting the width of the bottom and top side of a trapezoidal feed, the broad bandwidth can be achieved.

Fu-Ren Hsiao et al. [6] presented a novel broadband double-cavity planar antenna with a wide operating bandwidth (about 25% with respect to the center frequency of 900 MHz) for mobile-phone application as an internal antenna. The proposed planar antenna consists of a thin upper cavity and a relatively thick lower

cavity. In the lower cavity of the antenna, its partial volume is also be used to accommodate associated components of the mobile phone.

A Wide-Band Cylindrical Monopole Antenna for Mobile Phone applications [7] was introduced by K.L. Wong et al. The antenna is composed of an upper hollow conducting cylinder and a lower conducting cone and occupies a volume similar to that of the conventional helical monopole antenna.

K. L. Wong et al. [8] also proposed an internal shorted patch Antenna for UMTS Folder type mobile Phones. The patch antenna comprises of a simple rectangular patch that is fed through and short-circuited to a small ground plane which protrudes from the main or bottom ground of a folder-type mobile phone. With the presence of the small antenna ground, which can function as a shielding wall, the proposed antenna can be placed in close proximity to the RF shielding metal box in the mobile phone, with very small effects on the antenna performances.

An internal patch antenna for mobile device having electromagnetic compatibility (EMC) property with nearby conducting elements was presented [9] by Chih-Ming Su et al. Effects of the possible nearby conducting elements such as the RF/battery shielding metal case and the shielding metal cylinder for a charge-coupled device (CCD) of an embedded digital camera inside a mobile device on the performances are analyzed.

K.L. Wong et al. [10] developed a Thin Internal GSM/DCS Patch Antenna for portable mobile terminal applications. By incorporating a small portion of the top patch beyond the top edge of the system ground plane of the mobile terminal, enhanced bandwidths of the two resonant modes for covering the GSM and DCS bands.

Kin Lu Wong et al. [11] also introduced a shorted internal patch antenna suitable for application in sliding mobile phone. The shorted patch antenna is mounted at the bottom end of the lower ground plane of the mobile phone, and can generate a wide operating band for UMTS (1920-2170 MHz) operation.

Zhengwei Du et al. [12] designed a novel Compact Wide-Band Planar Antenna for Mobile Handsets. It can cover major wireless communication and navigation systems like GSM, GPS, DCS, PCS, UMTS, and WLAN. The radiating patch is jointly designed with the shape of the ground plane to optimize its performance.

P. Ciáis et al. [13] presented a penta-band planar inverted-F antenna (PIFA) suitable for handheld terminals. This antenna is made of capacitively loaded shorted patches, a slot, and an efficient antenna-chassis combination to achieve multiband and wideband performances to operate in the 850 MHz, 900 MHz, 1800 MHz, 1900 MHz, and UMTS bands

Saou-Wen Su et al. [14] proposed a wideband monopole antenna integrated within the front-end module package. The antenna was integrated within the front-end module package for WLAN and/or WiMAX operation in the 5 GHz band.

A Coupling Element Based Mobile Terminal Antenna Structure is reported in [15] by Juha Villanen et al. The work concentrates on the possibilities to reduce the

volume of mobile terminal antenna by efficiently utilizing the radiation of the currents on the mobile terminal chassis. Essentially non resonant coupling elements are used to optimally couple to the dominating characteristic wave modes of the chassis. The antenna structures are tuned to resonance with matching circuits.

Tieming Xiang et al. [16] proposed the design of a miniature mobile handset antenna using Genetic Algorithm and MoM. It can provide wide bandwidth to cover the operating bands for modern mobile communications, including GSM, DCS, PCS, and UMTS bands.

Kati Sulonen et al. discussed the effects of antenna radiation pattern on the performance of the mobile handset in [17]. In this work the effects of the different antenna radiation pattern characteristics on the performance of the antenna in different environments at 2 GHz are investigated.

Fa-Shian Chang et al. [18] presented a Folded Meandered-patch Monopole Antenna for Triple-Band Operation. The proposed antenna is suitable for applications in mobile phones for GSM, DCS and PCS triple-band operations.

An Internal GSM/DCS Antenna Backed by a Step-Shaped Ground Plane for a PDA Phone was proposed by K.L. Wong et al. [19]. The antenna has two radiating strips designed to operate at about 900 and 1800 MHz for GSM/DCS operation, and is backed by a short circuit to a step-shaped ground plane. With the use of the step-shaped ground plane, which is to be placed at the top edge of the system ground plane of a

PDA phone, the antenna can be employed in very close proximity to the possible RF shielding metal cases for battery and associated RF module/circuitry, with almost no degradation in the antenna performances.

An Internal Shorted Patch Antenna for UMTS Mobile Phone was proposed by Saou-wen Su et al. [20]. This internal mobile phone antenna design eliminate the required isolation distance between the antenna and the RF shielding metal box, thus providing a promising alternative for integrating various elements inside a mobile phone.

Shao-Lun Chien [21] proposed a Planar Inverted-F Antenna with a Hollow Shorting Cylinder for Internal Mobile Phone Antenna applications. The proposed PIFA and the embedded digital camera together occupy a minimum space, and very small or negligible coupling effects of the embedded camera with the PIFA was reported.

Saou-Wen Su [22] introduced a novel design of the internal patch antenna and integrated it with the shielding metal case for mobile phone application. The antenna mainly comprises of a simple rectangular patch as the antenna's top radiating patch and a shielding metal case form part of the antenna's ground plane.

2.3 Multi-band antenna design techniques

The advent of new, multi-standard mobile devices is an important challenge for antenna designers, as they have to implement integrated multi band antennas within a volume, which is rapidly shrinking. Following section describes different multi-band techniques so far developed by the antenna designers world across.

Puente C. et al. [23] introduced a new fractal antenna based on the Sierpinski gasket which presents a self-similar behavior at several bands. Such a behavior is based on the self-similarity properties of the antenna's fractal shape.

J. George et al. [24] presented a single-feed dual frequency compact microstrip antenna with a shorting pin. This new antenna configuration gives a large variation in frequency ratio of the two operating frequencies, without increasing the overall size of the antenna.

Sindou M et al. [25] presented the numerical and experimental results of a multiband fractal tree antenna generated by the elements of successive iteration levels.

Turski Z et al. [26] proposed a compact multi-band planar antenna for mobile wireless terminals. Multi-band operation is obtained by perturbing the shape of a conventional microstrip patch antenna in a prescribed manner.

Sona O. Kundukulam et al [27] presented a dual-frequency antenna achieved from a compact microstrip antenna by loading a pair of narrow slots close to its radiating edges. The two frequencies have parallel polarization planes and similar radiation characteristics.

Tang P et al. [28] examined the input characteristics of a hexagonal fractal based design and evaluated its suitability for multiband usage.

Steven R. Best [29] presented a multiband conical monopole antenna. The conical monopole exhibits broader impedance bandwidth and improved radiation pattern performance.

Junho Yeo et al. [30] presented some novel designs for conformal multiband antennas, based on fractal concepts, for application at three different frequencies.

Ali M. Hayes et al. [31] presented a novel triple-band antenna that consists of a driven meander-line element and two parasitic coupled elements. The geometrical configuration, size, and proximity of the driven and parasitic elements materialized the desired multiband operation.

Shun-Yun Lin [32] introduced a folded planar monopole antenna, which has a very low profile of about one twentieth of the wavelength of the lowest operating frequency. The proposed antenna can be used for multiband operation, with omnidirectional radiation patterns.

Duxian Liu et al. [33] proposed a multiband antenna for WLAN/cellular applications. This antenna has a smaller size, and can be built on a double-sided printed circuit board or stamped from thin metal sheets.

Sanz-Izquierdo B et al. [34] introduced a novel multiband PIFA. The antenna uses a novel technique to incorporate an extra band. The additional band is

incorporated by using a parasitic element in the plane of the ground that is excited by coupling from the surrounding finite-sized ground plane.

Liu W.-C [35] proposed a multiband monopole antenna. S-shaped meandered lines of different sizes, capable of generating a number of separate resonant modes are used for multiband operations. Raj et al. [36] proposed a compact single-feed multiband planar antenna configuration suitable for GPS, DCS, 2.4/5.8 GHz WLAN applications is presented. A reflector at the backside of the substrate was used to get the desired multiband operation.

Nepa P et al. [37] presented a Multiband PIFA for WLAN mobile terminals. The multiband behavior was obtained by combining a trapezoidal feed plate with two different resonance paths in the radiating structure.

Design synthesis of miniature multiband monopole antenna with application to ground-based and vehicular communication systems was presented by Werner P.L et al. [38]. The multiband response was achieved by placing a fixed number of thin stubs at strategic locations along the antenna. A robust genetic algorithm technique was introduced to determine the optimal lengths and locations of the stubs

Heejun Yoon et al. [39] presented the design of a multiband internal antenna for mobile handset applications. Two antenna elements are formed on top and bottom

of the common substrate and connected by metallic pin to obtain the multi band characteristics.

Liu W.-C et al [40] proposed a multiband CPW-fed notched planar monopole using a genetic algorithm in conjunction with the method of moments (MoM). By introducing a suitable notch to a rectangular CPW-fed patch, the desired multi-frequency resonant modes and broad impedance bandwidths can be obtained.

A Multiple Band-Notched Planar Monopole Antenna for Multiband Wireless Systems was proposed by Wang-Sang Lee et al. [41]. The proposed antenna consists of a wideband planar monopole antenna and the multiple U-shape slots, producing band-notched characteristics.

Amir Hossein Yamini et al. [42] presented a bow-tie printed antenna and simulation results based on dipole antenna concepts and compared it with simulation using FDTD.

Yu-Seng Liu et al. [43] presented two different geometries of antennas to satisfy the applications for WLAN/HIPERLAN/ISM triple band. The meander-line antenna with one or two inverted planar L-shaped antennas are used to excite three distinct resonant modes.

Jingjing Huang et al. [44] proposed a novel multiband fractal patch antenna. The self-similarity properties of the fractal shape are translated into its multiband

behavior. The characteristics of the novel fractal patch antenna is described by means of experimental and computational results.

Martinez-Vazquez M et al. [45] proposed an integrated planar multiband antennas for personal communication handsets. Triple band operation was achieved by combining spur-line techniques with parasitic patches, while the use of an additional slot introduces a fourth resonance with acceptable performance without increasing antenna volume so that a quad-band antenna is obtained.

Sanz-Izquierdo B et al. [46] proposed a Single and double layer planar multiband PIFA for WLAN applications. The antenna size was reduced by removing metallization in areas of low current density. The construction is simple with the metal etched from a thin mylar sheet folded around a honeycomb former.

Jean-Marie et al. [47] presented a multiband printed dipole antennas using parasitic elements for multiple wireless services. First, an elementary dipole antenna was studied and characterized at the operating frequency of 2.9 GHz. Next, two compact dual-band planar-antenna configurations were presented.

Suma M.N et al. [48] proposed a compact dual band planar antenna for a digital communication system (DCS)/2.4-GHz WLAN application. The two resonant modes of the proposed antenna are associated with various lengths of the monopoles, in

which a longer arm contributes for the lower resonant frequency and a shorter arm for higher resonant frequency.

Sheng-Bing Chen et al. [49] reported a novel modified T-shaped planar monopole antenna, with two asymmetric horizontal strips as additional resonators to produce the lower and upper resonant modes. As a result, a dual-band antenna for covering 2.4- and 5-GHz wireless local area network (WLAN) bands is implemented.

Wen-Jiao Liao et al. [50] proposed a novel microstrip antenna applicable for multiband. The design was evolved from a conventional parallel stripline dipole with modifications in the dipole geometry and feeding structure.

2.4 Broad band antenna design techniques

The demand for broadband wireless communication is rapidly increasing due to the need to support more users and to provide more information with higher data rates. Broad band antennas are essential front-end element for broadband wireless communications. This section describes different broad band antenna designs available in the open literature.

C. K. Aanandan et al. [51] presented a broad band gap coupled microstrip antenna for broad band operation using parasitic elements. The antenna is compact and produces less distortion in the radiation pattern. The closed form expression for calculating the impedance bandwidth of a wide band printed dipole is proposed by S. Dey et al. [52]

Li M.-Y et al. [53] presented a novel broadband coplanar waveguide-coplanar strip-fed spiral antenna. The antenna has good radiation patterns and a return loss better than 10dB over a wide bandwidth. M. Deepukumar et al. [54] proposed a new dual port microstrip antenna geometry for dual frequency operation. The structure consists of the intersection of two circles of the same radius with their centers displaced by a small fraction of the wavelength. This antenna provides wide impedance bandwidth and excellent isolation between its ports.

Barker S.J [55] proposed the use of silica aerogels in broadband planar antennas. The first application is the use of an aerogel as a thick, low-permittivity substrate in a broadband millimetre-wave antenna. A broadband, robust, low-profile monopole incorporating top loading, dielectric loading, and a distributed capacitive feed mechanism have been reported by McLean J et al. [56]. Broadband printed antennas for point-to-point and point-to-multipoint wireless millimeter-wave applications has been proposed by Waterhouse R.B et al. [57].

Zhi Ning Chen et al. [58] proposed a broadband monopole antenna. A parasitic planar thin conductive element is placed in parallel with the monopole, and electromagnetically coupled to the monopole. K. P. Ray et al. [59] presented a paper describing a broadband planar rectangular monopole antenna. Both theoretical and experimental investigations have been carried out to draw an analogy between this monopole antenna and a rectangular microstrip antenna.

S. Mridula et al. [60] reported a broadband rectangular microstrip antenna utilizing an electromagnetically coupled L-strip feed is presented. Experimental study shows a 2:1 VSWR bandwidth of 10% and excellent cross-polarization performance with a radiation coverage almost as same as that of the rectangular microstrip antenna fed by conventional methods.

Designs of broad-band dual-polarized patch antennas fed by promising feeding structures of a capacitively coupled feed, slot-coupled feed, two capacitively coupled feeds of 180° phase shift with a slot feed, and two capacitively coupled feeds of a 180° phase shift with a slot feed, and two slot-coupled feeds were proposed and experimentally studied by Kin-Lu Wong et al. [61].

An electromagnetically coupled T-shaped microstrip feed to enhance the impedance bandwidth of a rectangular microstrip antenna has been proposed by Lethakumary. B et al. [62]. Manju Paulson et al. [63] described an arrow-shaped microstrip antenna with a pair of narrow slots embedded near the non-radiating edges to provide wide impedance bandwidth.

By embedding properly arranged L-shaped slots in a circular patch, a novel broadband dual-frequency design was proposed by Jui-Han Lu [64]. Impedance bandwidth of about 7.0% to 12.5% for the lower band and 18.9% to 21.5% for the higher band is achieved.

A planar monopole broadband antenna with a parasitic radiator has been presented Xing Jiang et al. [65]. Measurements show that the bandwidth of the monopole antenna has been considerably improved with a parasitic element earthed with a matching inductor.

A broadband coplanar waveguide fed inductive slot antenna has been proposed by Xian-Chang Lin et al. [66]. It consists of a conventional CPW inductive slot and a CPW inductively coupled slot antenna as the feeding network. Wen-Shan Chen et al. [67] explained that by introducing a small rectangular slot protruded from the triangular slot, a new resonant mode in the vicinity of the fundamental resonant mode of the triangular slot can be excited.

M. Joseph et al. [68] proposed a novel compact wideband antenna for wireless local area network (WLAN) applications in the 2.4 GHz band. The proposed low profile antenna offers 18.6% bandwidth and an average gain of 5 dBi. The antenna is excited directly using a 50 ohm coaxial probe. B. Lethakumary et al. [69] introduced a hook shaped feeding technique for bandwidth enhancement of a rectangular microstrip antenna. This antenna offers an impedance bandwidth of 22% without degrading the efficiency.

Guiping Zheng et al. [70] proposed a broadband printed bow-tie antenna with a simplified balanced feeding network and modified tapering is presented. Microstrip and parallel-strip transmission lines printed on the substrate with high

dielectric permittivity realize the proposed feeding network. The ground-plane transition between the microstrip line and the parallel-strip line is exponentially tapered so as to reduce the reflection losses and produce a balanced feed for the antenna.

Filipovic D.S [71] proposed a low profile 4-arm slot spiral for broadband commercial applications. The antenna is designed for circularly polarized dual-mode, normal mode and split-beam mode. Phase progressions at arm ports are realized through the odd and even coplanar waveguide excitations.

Chao-An Shen et al. [72] designed a broadband interior-type planar monopole with an omni directional radiation pattern over a wide operation band using a slanted feeding shape.

Suma M. N et al. [73] proposed a planar monopole antenna suitable for broadband wireless communication. With the use of a truncated ground plane, the proposed printed monopole antenna offers nearly 60% 2:1 VSWR bandwidth and good radiation characteristics for the frequencies across the operating band. The antenna can be easily integrated into wireless circuitry and is convenient for application in laptop computers.

Seong-Youp Suh et al. [74] summarized broadband antennas and proposes an evolution process from the monopole disc antennas to broadband dual-polarized antennas. The design of a short-circuited triangular patch antenna with broadband operation has been proposed by Row J.S et al. [75]. By placing two shorting walls at the

opposite edges of a tip-truncated triangular patch antenna with a V-shaped slot, two resonant modes can be excited simultaneously and they can be coupled together to achieve the broadband operation.

Pan B et al. [76] has been developed a low-profile broadband and dual-frequency monopole antennas. The broadband monopole consists of an S-strip and a folded T-strip which are separately printed on the two sides of a thin planar substrate.

K. Francis Jacob et al. [77] proposed the development of a compact microstrip-fed, branched monopole antenna for ultra wide band (UWB) applications. By suitably embedding branches on the top edge of the strip monopole, UWB response can be easily achieved by merging different resonances.

2.5 Antenna Miniaturization Schemes

The topic of small antennas has been a subject of interest for more than half a century, but in recent years, it has gained significant attention because of an exorbitant demand for mobile wireless communication systems. The need for antenna miniaturization stem from the fact that most mobile platforms have a limited space for antennas. Compact antennas are needed so that more antennas can be closely packed together without the risk of mutual and parasitic coupling between them. The following section describes different antenna miniaturization techniques reported in the open literature.

Miniaturization on planar printed-circuit antennas by loading the substrate of very high permittivity materials has been experimentally demonstrated by Hwang Y [78]. The results show that the size reduction is achieved with the gain comparable with that of the same type of antenna with low dielectric constant.

A printed antenna occupying the same physical volume as a rectangular patch was designed by Herscovici N et al. [79] to resonate at a frequency that is 37% lower than the resonance frequency of the patch. A Genetic algorithm optimization procedure was used in the design.

Skrivervik A.K et al. [80] presented some basic rules about electrically small antennas, and gave clues and guidelines about efficient antenna miniaturization. The Fractal based antenna miniaturization technique has been discussed by Gianvittorio J.P et al. [81]. Sharma S.K et al. [82] presented the simulation results of a low-profile wide band microstrip slot antenna, which shows the polarization diversity in radiation characteristics.

Elkamchouchi H.M et al. [83] presented a miniaturization model of a square loop antenna using a non-return to zero pulse as a generator instead of the square pulse in Minkowski fractal model that allows an increase in the total electric length without occupying more space. This led to an easily matched compact loop antenna, but with a small sacrifice in the gain.

Azadegan R et al. [84] concluded that with the virtual enforcement of the required boundary condition (BC) at the end of a slot antenna, the area occupied by the resonant antenna can be reduced. To achieve the required virtual BC, the two short circuits at the end of the resonant slot are replaced by some reactive BC, including inductive or capacitive loadings. The application of these loads is shown to reduce the size of the resonant slot antenna for a given resonant frequency.

Behdad N et al. [85] investigated the effect of inserting an array of series inductors to a resonant slot antenna on size, bandwidth and gain of the antenna. The results show that the antenna size can be reduced efficiently without adverse effect on the impedance matching and gain. However, as it is expected the antenna bandwidth is reduced as a result of this miniaturization process.

A topology for designing an electrically small resonant slot antenna has been demonstrated by Sarabandi K et al. [86]. A major size reduction was achieved by constructing a resonant slot rather than the traditional antenna. This was accomplished by generating a virtual open circuit at one end of the slot. Further miniaturization was achieved by bending the slot into three pieces in order to use the area of the board more efficiently.

The dependence of the resonant frequency and input impedance of printed Hilbert antenna on the various parameters were studied by Xuan Chen et al. [87], at UHF band. Hala Elsadek et al. [88] has miniaturized a multi-band planar inverted-F

antenna (PIFA) by adding lumped load and employing fractal concept. The results show that a 68%-82% size reduction can be achieved.

Schulteis S et al. [89] concluded that the size of a PIFA for integration in mobile devices can be reduced by inductive or capacitive loading. In addition by using a symmetrical feed, it is possible to enlarge the input impedance and to connect the antenna easily to a state of the art front end.

A triangular-ring slot antenna fed by coplanar waveguide feed line with protruded tuning stub and a back-patch at the bottom of the substrate for miniaturization has been demonstrated by Jin-Sen Chen et al. [90]. The resonant frequency can be significantly reduced as compared with CPW fed conventional ring-slot antennas. Mosallaei H et al. [91] introduced a novel reactive impedance substrate for antenna miniaturization with enhanced bandwidth performance.

Volakis J.L et al. [92] demonstrated methods for miniaturizing spirals and other antennas using dielectric loading, artificial lumped loads, textured dielectrics and other approaches. The aim of the study was to achieve miniaturization without compromising gain and bandwidth.

Kawano Y et al. [93] investigated the downsizing technique of antennas for handset by utilizing a magnetic material at 900MHz and 2GHz band. A Planar Inverted-F Antenna (PIFA), which is the popular built-in antenna for handset was used for the investigation.

The effect of slot loading on microstrip patch antennas was investigated by Hung Tien et al. [94]. Initially, Koch island fractal and H-shape slots are introduced to microstrip patch antennas and their effect on reduction of the resonant frequency is determined. Additional slots of more complex geometry are implemented on the H-shaped patch to further bring down its resonance frequency.

A miniaturized printed monopole antenna suitable for cellular handset terminals was designed by Robert Borowiec et al. [95]. A substantial reduction in antenna size was achieved due to the use of the inverted-F antenna concept combined with a capacitive feeding system. The antenna operates in three frequency bands, that is, GSM 1800, PCS 1900, and UMTS, with VSWR ≤ 2.5 .

Chi-Hun Lee et al. [96] proposed a compact printed hook-shaped monopole antenna for 2.4/5-GHz WLAN applications. The designed antenna is compact and the radiation patterns are nearly omni-directional.

A novel compact antenna operating at GSM, DCS, PCS and IMT2000 bands has been presented by Peng Sun et al. [97]. With a loosely coupled ground branch, the antenna covers all 2G and 3G wireless communication bands. Wen-Chung Liu et al. [98] presented a coplanar waveguide (CPW)-fed monopole antenna with dual folded strips for the radio frequency identification (RFID) application. The proposed antenna has a very compact size including ground plane.

A novel approach for the realization of compact antennas has been described by Cheng-Jung Lee Leong et al. [99]. The proposed antenna designs are based on the unique fundamental left-handed mode propagation properties of the composite right/left-handed transmission line (CRLH-TL). At frequencies near cutoff the propagation constant approaches infinity, therefore using the CRLH-TL in this region an electrically large, small sized antenna can be realized depending on the unit cell optimization and miniaturization.

A new variation of the conventional open-sleeve dipole antenna called an end-loaded planar open-sleeve dipole has been introduced by Spence T. G et al. [100]. This configuration provides miniaturization while retaining a comparable bandwidth in terms of the VSWR response to that of conventional open-sleeve dipoles. Psychoudakis D et al. [101] presented a miniaturization scheme for a square circularly polarized, cavity-backed antenna using textured dielectric loading and a folded metallic strip feed.

2.6 Coplanar Antennas

A Coplanar patch antenna consists of a patch surrounded by closely spaced ground conductor on a dielectric substrate. The CPW fed coplanar antenna is useful to directly connect to an active device such as a photo detector in a radio-over-fiber system. The antenna was considered as a loop slot antenna up to recent years, since it looks very similar to the loop slot antenna which usually has no back ground conductor. But very recently it has been found that the antenna behaves more like a microstrip patch antenna

rather than a loop slot antenna. Relevant papers in this area are summarized in the following section.

A novel coplanar waveguide fed coplanar strip dipole antenna has been presented by Tilley K. et al. [102]. The antenna was matched with the use of a novel, wideband balun. They also presented a paper [103] on coplanar waveguide (CPW) fed coplanar strip (CPS) dipole antenna which operates at dual frequencies. The transition from CPW to CPS is accomplished with the use of a wideband balun which exhibits less than 1 dB insertion loss up to 4.8 GHz.

K. F Tong et al. [104] presented simulation and experimental results of wideband coplanar waveguide fed coplanar patch antennas. The antennas were developed to widen the narrow bandwidth of the newly suggested coplanar patch antennas. This was achieved by introducing two identical parasitic patches next to the resonant edges of the main patch.

An aperture-coupled coplanar patch antennas (CPA) were investigated by Cheng et al. [105]. The result shows that the return loss and the radiation pattern of the CPA are similar to the microstrip patch antenna, and the front-to-back ratio and gain of the CPAs are better than that of microstrip antennas.

K. Li et al. [106] presented broadband stacked coplanar patch antennas. The antennas were designed based on the stacked patch technique developed for microstrip

patch antennas, in which the lower patch is a coplanar patch which is fed by a conductor-backed coplanar waveguide, and the upper patch is a microstrip patch. They also presented [107] the simulation and experiment of CPAs, and demonstrated that the CPA behaves, particularly the resonant property, more similar to the microstrip patch antenna rather than a loop slot antenna.

The feeding characteristics of coplanar patch antennas fed at the non radiating edge are discussed in [108] by Pandey S et al. Li K et al. [109] demonstrated the performance of the coplanar patch antenna. The simulation and experimental results on the field distributions in the CPAs were presented to reveal the physics in the CPA. The operating frequency of a coplanar patch antenna is tuned by Holland B et al. [110] using a varactor mounted at one of the radiating edges.

2.7 Resonance/Leakage Phenomena in Coplanar waveguides

At higher frequencies most of the transmission lines starts radiating. When the frequency of operation is increased more and more, the structural parameter values of the transmission line becomes comparable with the operating wavelength, and thus starts radiating. Coplanar waveguides are also found to be radiating when the frequency of operation is sufficiently high. The radiation is mainly in the form of surface waves. Following section describes the most relevant papers in this area to get an over view of the leakage phenomena in coplanar waveguides.

Mikio Tsuji et al. [111] showed that when the frequency of operation of a circuit that utilizes coplanar waveguide is increased sufficiently, leakage of power away from the waveguide occurs in the form of a surface wave. This power leakage can cause

unwanted cross talk between neighboring portions of the circuit and produce unexpected package effects. They also presented a paper on [112] the new type of pulse shape degradation when a narrow pulse is transmitted on conventional coplanar waveguide. This degradation is not caused by the well-known dispersion of the phase constant of the CPW dominant mode, but by the complicated dispersion behavior of its attenuation constant due to the leakage effect.

The resonant phenomena in conductor backed coplanar waveguides through-line circuits were investigated by Wen-Teng Lo et al. [113]. The patch antenna model and the multi-mode model were applied to help understanding the origin of resonances. They also presented another paper [114] on the resonant phenomena in conductor backed coplanar waveguides.

Dispersion and radiation properties of the conductor-backed CPW were studied by Wolfgang Heinrich et al. [115]. A frequency domain finite-difference method using the PML absorbing boundary condition was used in the study. The different types of higher-order modes are identified and design rules to avoid parasitic effects are given.

Although the leakage/resonance phenomena in coplanar waveguide circuits is a drawback as far as a microwave circuit is concerned, it can be successfully used to design millimeter wave antennas by employing the aforesaid surface wave modes. But it is not suitable for compact antenna applications, because the dimensions of the device

becomes large compared to the operating wavelengths. The investigations in this direction will not yield a new compact efficient radiator.

2.8 FDTD for antenna analysis

The Finite-Difference Time-Domain (FDTD) method is arguably the most popular numerical method for the solution of problems in electromagnetics. Although the FDTD method has existed for nearly 40 years, its popularity continues to grow as computing costs continue to decline. Furthermore, extensions and enhancements to the method are continually being published, which further broaden its appeal. Most relevant papers concerning the FDTD computation of printed antenna problems are referred in this section.

The Finite-Difference Time-Domain (FDTD) method, as first proposed by Yee in 1966 [116], is a simple and elegant way to discretize the differential form of Maxwell's equations. Yee used an electric-field grid, which was offset both spatially and temporally from a magnetic-field grid, to obtain update the present fields throughout the computational domain, in terms of the past fields.

The original Yee FDTD algorithm is second-order accurate in both space and time. Numerical-dispersion and grid-anisotropy errors can be kept small by having a sufficient number of grid spaces per wavelength. Taflove was among the first to rigorously analyze these errors [117]. Taflove was also the first to present the correct stability criteria for the original orthogonal-grid Yee algorithm [118].

D. M. Sheen et. al. [119] described application of 3D FDTD method for the analysis of microstrip antenna and other microstrip circuits. The most relevant advance in material-based ABCs was put forward by Berenger [120]. His ABC, termed the perfectly-matched-layer (PML) absorbing boundary condition, appears to yield a major improvement in the reduction of boundary reflections, compared to any ABC proposed previously.

Reineix and Jecko [121] used the FDTD method for the analysis of microstrip antennas. In 1992, Leveque et al. [122] modeled frequency-dispersive microstrip antennas, while Wu et al. [123] used the FDTD method to accurately measure the reflection coefficient of various microstrip-patch configurations.

Uehara and Kagoshima [124] presented an analysis of the mutual coupling between two microstrip antennas, while Oonishi et al. [125] and Kashiwa et al. [126] used one of the conformal FDTD approaches to analyze microstrip antennas on a curved surface.

In 1994, Qian et al. [127] used the FDTD method to design twin-slot antennas. Reineix and co-workers [128, 129, 130] have expanded their FDTD analysis to include the input impedance of micro strips with slots, to obtain the radar cross section of microstrip-patch antennas, and to model the radiation from microstrip patches with a ferrite substrate.

Luebbers et al. [131] and Chen et al. [132] analyzed hand-held on a monopole antenna on a conducting or dielectric box using FDTD. Toftgird et al. [133] calculated the effect the presence of a person on the radiation from such antennas. In 1994, Jensen and Rahmat-Samii [134] presented results for the input impedance and gain of monopole, PIFA, and loop antennas on hand-held transceivers.

The interaction of a hand held antenna and a human were also studied by Jensen and Rahmat-Samii [135]. Chen and Wang [136] calculated the currents induced in the human head with a dipole-antenna model from a cellular phone. Martens et al. [137] have used a dipole model and a full model for a hand-held antenna to compute the fields induced in the human head.

Analysis of CPW-fed folded-slot and multiple-slot antennas on thin substrates were carried out using FDTD method [138]. M. Kar and P.F Wahid [139] described the FDTD analysis of dual-feed microstrip patch antennas. S. Dey et al. [140] proposed conformal FDTD analysis technique for modeling cylindrical DRs. FDTD analysis of radiation pattern of antenna on truncated ground plane was investigated by Yamamoto et al. [141].

The 3-D FDTD design analysis of a 2.4-GHz polarization-diversity printed dipole antenna with integrated balun and polarization-switching circuit for WLAN and wireless communication applications was carried out by Huey-Ru Chuang et al. [142]. Pattern reconfigurable leaky-wave antenna analysis using FDTD method was introduced by Shaoqiu Xiao et al. [143].

Indeed, the FDTD algorithm, or one of its variant forms, has been successfully applied in a number of disciplines outside of “traditional” electromagnetics, including acoustics, optics, and biology.

2.9 References

1. A Low-Profile Planar Monopole Antenna for Multiband Operation of Mobile Handsets Kin-Lu Wong, Gwo-Yun Lee, and Tzung-Wern Chiou, *IEEE Transactions on Antennas and Propagation*, Vol. 51, No. 1, January 2003 pp. 121-125
2. A planar meander-line antenna for triple-band operation of mobile handsets Jeun-Wen Wu, Chun-Ren Lin , Jui-Han Lu, *Microwave and optical technology letters*, Vol. 41, Issue 5 , Apr 2004, pp. 380 – 386
3. Multiband Folded Planar Monopole Antenna for Mobile Handset, Shun-Yun Lin, *IEEE Transactions on Antennas and Propagation*, Vol. 52, No. 7, July 2004, pp. 1790-1794.
4. Miniature Built-In Multiband Antennas for Mobile Handsets, Yong-Xin Guo, Michael Yan Wah Chia, and Zhi Ning Chen, *IEEE Transactions on Antennas and Propagation*, Vol. 52, No. 8, August 2004, pp. 1936-1941.
5. A Broadband Interior Antenna of Planar Monopole Type in Handsets, Yong-Sun Shin, Seong-Ook Park, and Manjai Lee. *IEEE Antennas and Wireless Propagation Letters*, Vol. 4, 2005, pp. 9-12
6. Broadband double-cavity internal planar antenna for mobile phones, Fu-Ren Hsiao, Kin-Lu Wong , *Microwave and optical technology letters*, Vol. 46, Issue 2 , May 2005, pp. 125 – 128

7. Wide-Band Cylindrical Monopole Antenna for Mobile Phone, Kin-Lu Wong and Shao-Lun Chien, *IEEE Transactions on Antennas and Propagation*, Vol. 53, No. 8, August 2005, pp. 2756-2758.
8. Internal Shorted Patch Antenna for a UMTS Folder-Type Mobile Phone, Kin-Lu Wong, Saou-Wen Su, Chia-Lun Tang, and Shih-Huang Yeh, *IEEE Transactions on Antennas and Propagation*, Vol. 53, No. 10, October 2005, pp. 3391-3394.
9. EMC Internal Patch Antenna for UMTS Operation in a Mobile Device, Chih-Ming Su, Kin-Lu Wong, Chia-Lun Tang, and Shih-Huang Yeh, *IEEE Transactions on Antennas and Propagation*, Vol. 53, No. 11, November 2005, pp. 3836-3839
10. Thin Internal GSM/DCS Patch Antenna for a Portable Mobile Terminal, Kin-Lu Wong, Yuan- Chih Lin, and Ting-Chih Tseng, *IEEE Transactions on Antennas and Propagation*, Vol. 54, No. 1, January 2006, pp. 238-241.
11. Internal UMTS patch antenna for a sliding mobile phone, Kin-Lu Wong, Chun-Yi Lin, Fa-Shian Chang, *Microwave and optical technology letters*, Vol. 48, Issue 4 , Feb 2006, pp. 726 – 729
12. A Novel Compact Wide-Band Planar Antenna for Mobile Handsets, Zhengwei Du, Ke Gong and Jeffrey Shiang Fu, *IEEE Transactions on Antennas and Propagation*, Vol. 54, No. 2, Feb. 2006, pp. 613-619.
13. Pentaband internal antenna for handset communication devices, P. Ciais, C. Luxey, A. Diallo, R. Staraj, G. Kossiavas, *Microwave and optical technology letters*, Vol. 48, Issue 8 , 30 May 2006, pp. 1509 - 1512

14. Wideband Monopole Antenna Integrated Within the Front-End Module Package, Saou-Wen Su, Kin-Lu Wong, Chia-Lun Tang, and Shih-Huang Yeh, *IEEE Transactions on Antennas and Propagation*, Vol. 54, No. 6, June 2006, pp. 1888-1891
15. Coupling Element Based Mobile Terminal Antenna Structures, Juha Villanen, Jani Ollikainen, Outi Kivekäs, and Pertti Vainikainen, *IEEE Transactions on Antennas and Propagation*, Vol. 54, No. 7, July 2006, pp. 2142-2153
16. Design of Multiband Miniature Handset Antenna by MoM and HGA, Tieming Xiang, K. F. Man, K. M. Luk, and C. H. Chan, *IEEE Antennas and Wireless Propagation Letters*, Vol. 5, 2006, pp. 179-182
17. Effects of Antenna Radiation Pattern on the Performance of the Mobile Handset, Kati Sulonen, Pertti Vainikainen, *IEEE Antennas and Propagation International symposium* pp. 354-357,
18. Folded Meandered-Patch Monopole Antenna for Triple-Band Operation Fa-Shian Chang, Wen-Kuan Su and Kin-Lu Wong, *IEEE Antennas and Propagation International symposium* pp. 278-281.
19. Internal GSM/DCS Antenna Backed by a Step-Shaped Ground Plane for a PDA Phone Kin-Lu Wong and Chun Lin, *IEEE Transactions on Antennas and Propagation*, Vol. 54, No. 8, August 2006 pp. 2408-2410.
20. Internal Shorted Patch Antenna for UMTS Mobile Phone, Saou-Wen Su, Kin-Lu Wong, Chia-Lun Tang, and Shih-Huang Yeh, *IEEE Antennas and Propagation International symposium*, pp. 343-346.

21. Planar Inverted-F Antenna with a Hollow Shorting Cylinder for Internal Mobile Phone Antenna, IEEE Antennas and propagation International symposium, pp. 1947-1950.
22. Integrated internal patch antenna for UMTS mobile phone application, Saou-Wen Su, Austin Chen, Kin-Lu Wong, Yuan-Chih Lin, Microwave and optical technology letters, Vol. 49, Issue 2 , Dec 2006, pp. 349 - 351
23. Fractal multiband antenna based on the Sierpinski gasket, Puente C, Romeu, J, Pous, R, Garcia, X., Benitez F, Electronics Letters, Vol. 32, Issue 1, 4 Jan. 1996 pp. 1 - 2
24. Dual frequency miniature microstrip antenna, J. George, K. Vasudevan, P. Mohanan and K.G. Nair, Electronics Letters, 11th June 1998 Vol. 34 No. 12, pp. 1168-1170
25. Multiband and wideband properties of printed fractal branched antennas, Sindou M., Ablart G, Sourdois C, Electronics Letters, Vol. 35, Issue 3, 4 Feb. 1999 pp. 181 – 182
26. Compact multi-band planar antenna for mobile wireless terminals Turski Z, Fathy A.E, McGee D, Ayers G, Kanamalum S, Antennas and Propagation Society International Symposium, 2001. IEEE, Vol. 4, 8-13 July 2001 pp. 454 - 457 vol.4
27. Slot-loaded compact microstrip antenna for dual-frequency operation, Sona O. Kundukulam, Manju Paulson, C. K. Aanandan, P. Mohanan, Microwave and optical technology letters, Vol. 31, Issue 5 , Oct 2001, pp. 379 – 381

28. Hexagonal fractal multiband antenna, Tang P, Wahid P, IEEE Antennas and Propagation Society International Symposium, 2002., Volume 4, 16-21 June 2002 pp. 554 - 557.
29. A multi-band conical monopole antenna derived from a modified Sierpinski gasket, Best S.R, Antennas and Wireless Propagation Letters, Vol. 2, Issue 1, 2003 pp. 205 – 207
30. Design of conformal multiband antennas based on fractal concepts, Junho Yeo, Raj Mittra, Microwave and optical technology letters, Vol. 36, Issue 5 , Feb 2003, pp. 333 – 338
31. Design of a multiband internal antenna for third generation mobile phone handsets, Ali M, Hayes, G.J, Huan-Sheng Hwang, Sadler, R.A., IEEE Transactions on Antennas and Propagation Vol. 51, Issue 7, July 2003 pp. 1452 – 1461
32. Multiband folded planar monopole antenna for mobile handset, Shun-Yun Lin, IEEE Transactions on Antennas and Propagation, Vol. 52, Issue 7, July 2004 pp.1790 – 1794
33. A new multiband antenna for WLAN/cellular applications, Duxian Liu, Gaucher, B, IEEE Vehicular Technology Conference 2004. Vol. 1, 26-29 Sept. 2004 pp. 243 - 246
34. Multiband printed PIFA antenna with ground plane capacitive resonator, Sanz-Izquierdo B., Batchelor, J Langley R, IEE Electronics Letters, Vol. 40, Issue 22, 28 Oct. 2004 pp. 1391 – 1392
35. Printed double S-shaped monopole antenna for wideband and multiband operation of wireless communications, Liu W.-C, Chen, W.-R., Wu, C.-M., IEE

Proceedings -Microwaves, Antennas and Propagation, Vol. 151, Issue 6, 19 Dec. 2004 pp. 473 – 476

36. Compact planar multiband antenna for GPS, DCS, 2.4/5.8 GHz WLAN applications, Raj R.K., Joseph M., Paul B., Mohanan P, Electronics Letters, Vol. 41, Issue 6, 17 March 2005 pp. 290 – 291
37. Multiband PIFA for WLAN mobile terminals, Nepa P, Manara G, Serra A.A, Nenna G, Antennas and Wireless Propagation Letters, Vol. 4, 2005 pp. 349 – 350
38. Design synthesis of miniature multiband monopole antennas with application to ground-based and vehicular communication systems, Werner P.L, Werner,D.H, Antennas and Wireless Propagation Letters Vol. 4, 2005 pp. 104 – 106
39. Internal antenna for multiband mobile handset applications, Heejun Yoon, Harackiewicz F.J Rhyu, H Myun-Joo Park Byungje Lee, Antennas and Propagation Society International Symposium, 2005 Vol. 1B, 3-8 July 2005 pp. 463 - 466
40. Design of a CPW-fed notched planar monopole antenna for multiband operations using a genetic algorithm Liu W.-C, IEE proceedings -Microwaves, Antennas and Propagation , Vol. 152, Issue 4, 5 Aug. 2005 pp. 273 – 277
41. Multiple band-notched planar monopole antenna for multiband wireless systems, Wang-Sang Lee, Lim W.-G Jong-Won Yu, IEEE Microwave and Wireless Components Letters, , Vol. 15, Issue 9, Sept. 2005 pp. 576 – 578
42. Multiband behavior of wideband Sierpinski fractal bow-tie antenna, Yamini A.H, Soleimani M., The European Conference on Wireless Technology 2005 , 3-4 Oct. 2005 pp. 503 – 506

43. New multiband printed meander antenna for wireless applications, Yu-Seng Liu 1, Jwo-Shiun Sun, Rui-Han Lu, Yi-Jay Lee , Microwave and optical technology letters, Vol. 47, Issue 6 , Oct 2005, pp. 539 – 543
44. A novel multiband fractal patch antenna, Jingjing Huang, Ning Li, Jingzhao She, Zhenghe Feng, Asia-Pacific Microwave Conference Proceedings, APMC 2005. , Vol.4, 4-7 Dec. 2005
45. Integrated planar multiband antennas for personal communication handsets, Martinez-Vazquez M., Litschke O, Geissler M., Heberling D, Martinez-Gonzalez A.M, Sanchez-Hernandez, IEEE Transactions on Antennas and Propagation Vol. 54, Issue 2, Part 1, Feb. 2006 pp. 384 – 391
46. Single and double layer planar multiband PIFAs, Sanz-Izquierdo B, Batchelor J.C, Langley R.J, Sobhy M.I, IEEE Transactions on Antennas and Propagation, Vol.54, Issue 5, May 2006 pp. 1416 – 1422
47. Design of multiband printed dipole antennas using parasitic elements, Jean-Marie Floch, Hatem Rmili, Microwave and optical technology letters, Vol. 48, Issue 8 , May 2006, pp. 1639 – 1645
48. A Compact Dual Band Planar Branched Monopole Antenna for DCS/2.4-GHz WLAN Applications, M. N. Suma, Rohith K. Raj, Manoj Joseph, P. C. Bybi, and P. Mohanan, IEEE Microwave and Wireless Components Letters, Vol. 16, No. 5, May 2006, pp. 275-277
49. Modified T-shaped planar monopole antennas for multiband operation, Sheng-Bing Chen, Yong-Chang Jiao, Wei Wang, Fu-Shun Zhang, IEEE Transactions on Microwave Theory and Techniques, Vol.54, Issue 8, Aug. 2006 pp. 3267 – 3270

50. A novel multiband dipole antenna with a microstrip loop feed, Wen-Jiao Liao, Yu-Cheng Lu, Hsi-Tseng Chou, *Microwave and optical technology letters*, Vol. 49, Issue 1, Nov 2006, pp. 237 – 241
51. Broad band gap coupled microstrip antenna, C. K. Aanandan, P. Mohanan and K. G. Nair, *IEEE Transactions on Antennas and Propagation*, Vo. 38, No. 10, Oct. 1990, pp. 1581-1586.
52. Analysis of cavity backed printed dipoles, S. Dey, C.K. Aanandan, P. Mohanan and K.G. Nair, *Electronics Letters*, 3rd February 1994 Vol. 30 No. 3, pp. 173-174
53. Broadband coplanar waveguide-coplanar strip-fed spiral antenna, Li M.-Y, Tilley K, McCleary J, Chang K, *Electronics Letters* Vol. 31, Issue 1, 5 Jan. 1995 pp. 4 – 5.
54. Broadband dual frequency microstrip antenna, M. Deepukumar, J. George, C.K. Aanandan, P. Mohanan and K.G. Nair, *Electronics Letters*, 15th August 1996 Vol. 32 No. 17, pp. 1531-1532
55. A Study of the Application of Silica Aerogels in Broadband Millimetre-Wave Planar Antennas Barker S.J, Kot J.S, Nikolic N, *IEEE Antennas and Propagation Society International Symposium, 1998*, Vol. 2, 21-26 June 1998 pp. 1116 - 1119
56. Broadband, robust, low profile monopole incorporating top loading, dielectric loading, and a distributed capacitive feed mechanism, McLean J, Foltz H, Crook G, *IEEE Antennas and Propagation Society International Symposium 1999*. Vol. 3, 11-16 July 1999 pp. 1562 - 1565
57. Broadband printed antennas for point-to-point and point-to-multipoint wireless millimeter-wave applications, Waterhouse, R.B, Novak, D, Nirmalathas, A, Lim, C,

- Antennas and Propagation Society International Symposium, 2000. IEEE , Vol. 3, 16-21 July 2000 pp. 1406 - 1409
58. Broadband monopole antenna with parasitic planar element, Zhi Ning Chen, Y. W. M. Chia, *Microwave and optical technology letters*, Vol. 27, Issue 3 , Sep 2000, pp. 209 – 210
 59. Broadband planar rectangular monopole antennas, K. P. Ray, P. V. Anob, R. Kapur, Girish Kumar, *Microwave and optical technology letters*, Vol. 28, Issue 1, Nov 2000, pp. 55 – 59
 60. Planar L-strip fed broadband microstrip antenna, S. Mridula, Sreedevi K. Menon, B. Lethakumary, Binu Paul, C. K. Aanandan, P. Mohanan, *Microwave and optical technology letters*, Vol. 34, Issue 2 , Jun 2002, pp. 115 – 117
 61. Broadband dual-polarized patch antennas fed by capacitively coupled feed and slot-coupled feed, Kin-Lu Wong, Tzung-Wern Chiou, *IEEE Transactions on Antennas and Propagation*, Vol. 50, Issue 3, March 2002 pp. 346 - 351
 62. A wideband rectangular microstrip antenna using an asymmetric T-shaped feed, B. Lethakumary, Sreedevi K. Menon, C. K. Aanandan, P. Mohanan, *Microwave and optical technology letters*, Vol. 37, Issue 1 , Feb 2003, pp. 31 – 32
 63. Compact microstrip slot antenna for broadband operation, Manju Paulson, Sona O. Kundukulam, C. K. Aanandan, P. Mohanan, K. Vasudevan, *Microwave and optical technology letters*, Vol. 37, Issue 4 , Mar 2003, pp. 248 – 250
 64. Broadband dual-frequency operation of circular patch antennas and arrays with a pair of L-shaped slots, Jui-Han Lu, *IEEE Transactions on Antennas and Propagation*, Vol. 51, Issue 5, May 2003 pp. 1018 – 1023

65. Broadband planar antenna with parasitic radiator, Xing Jiang, Li S, Guangjie Su, *Electronics Letters* Vol. 39, Issue 23, 13 Nov. 2003 pp. 1626-1627
66. A broadband CPW-fed inductive slot antenna, Xian-Chang Lin, Ling-Teng Wang, Cheng-Liang Lai, Yu-Seng Liu, *Microwave and optical technology letters*, Vol. 41, Issue 1, Feb 2004, pp. 12 – 14
67. Broadband design of the printed triangular slot antenna, Wen-Shan Chen, Fu-Mao Hsieh, *IEEE Antennas and Propagation Society International Symposium 2004*. Vol. 4, 20-25 June 2004 pp. 3733 – 3736
68. Compact wideband antenna for 2.4 GHz WLAN applications, Joseph M., Paul B, Raj, R.K, Mohanan P, *Electronics Letters*, Volume 40, Issue 23, 11 Nov. 2004, pp. 1460 - 1461
69. Wideband microstrip antenna using hook-shaped feed, B. Lethakumary, Sreedevi K. Menon, Priya Francis, C. K. Aanandan, K. Vasudevan, P. Mohanan, *Microwave and optical technology letters*, Vol. 44, Issue 2, Dec 2004, pp. 169 - 171
70. A broadband printed bow-tie antenna with a simplified balanced feed, Guiping Zheng, Ahmed A. Kishk, Allen W. Glisson, Alexander B. Yakovlev, *Microwave and optical technology letters*, Vol. 47, Issue 6, Oct 2005, pp. 534 - 536
71. Low-profile broadband dual-mode four-arm slot spiral antenna with dual Dyson balun feed, Filipovic D.S, Bhohe A.U, Cencich T.P, *IEE Proceedings of Microwaves, Antennas and Propagation*, 9 Dec. 2005 pp. 527 – 533
72. A broadband internal planar monopole antenna for mobile phone, Chao-An Shen, Ken-Huang Lin, *Microwave and optical technology letters*, Vol. 48, Issue 4, Feb 2006, pp. 768 – 769

73. A wideband printed monopole antenna for 2.4-GHz WLAN applications, M. N. Suma, P. C. Bybi, P. Mohanan, *Microwave and optical technology letters*, Vol. 48, Issue 5, Mar 2006, pp. 871 – 873
74. Evolution of broadband antennas from monopole disc to dual-polarized antenna, Seong-Youp Suh, Waltho A.E, Nair V.K, Stutzman W.L, Davis W.A, *IEEE Antennas and Propagation Society International Symposium 2006*, 9-14 July 2006 p. 1631 - 1634
75. Broadband short-circuited triangular patch antenna, Row J.-S, Yen-Yu Liou, *IEEE Transactions on Antennas and Propagation* Vol. 54, Issue 7, July 2006 pp. 2137 – 2141
76. Low-Profile Broadband and Dual-Frequency Two-Strip Planar Monopole Antennas, Pan B, Li R.L, Papapolymerou J, Laskar J, Tentzeris M.M, *IEEE Antennas and Propagation Society International Symposium 2006*, 9-14 July 2006 pp. 2665 – 2668
77. Planar branched monopole antenna for UWB applications, K. Francis Jacob, M. N. Suma, Rohith K. Raj, Manoj Joseph, P. Mohanan, *Microwave and optical technology letters*, Nov 2006, Vol. 49, Issue 1, pp. 45 - 47
78. Miniaturization on planar antennas with very high permittivity materials, Hwang Y, Zhang Y.P, Lo T.K.C, Luk K.M, Yung E.K.N, *APMC '97, 1997 Asia-Pacific* Vol. 1, 2-5 Dec. 1997 pp.217 - 220
79. Minimization of a rectangular patch using genetic algorithms, Herscovici N, Osorio M, Peixeiro, *IEEE Antennas and Propagation Society International Symposium 2001*, Vol. 4, 8-13 July 2001 pp.34 - 37

80. PCS antenna design: the challenge of miniaturization, Skrivervik A.K, Zurcher J.-F, Staub O, Mosig J.R, IEEE Antennas and Propagation Magazine, Vol. 43, Issue 4, Aug. 2001 pp.12 – 27
81. Fractal antennas: a novel antenna miniaturization technique, and applications, Gianvittorio J.P, Rahmat-Samii Y, IEEE Antennas and Propagation Magazine, Vol. 44, Issue 1, Feb. 2002 pp.20 – 36
82. Low profile wide band slot antenna for wireless communications, Sharma S.K, Jacob N, Shafa, IEEE Antennas and Propagation Society International Symposium, 2002. Vol. 1, 16-21 June 2002 pp.390 – 393
83. Square loop antenna miniaturization using fractal geometry, Elkamchouchi H.M, Abd El-Salam M.N, Radio Science Conference, 2003 18-20 March 2003 pp.B4 - 1-8
84. A novel approach for miniaturization of slot antennas, Azadegan R, Sarabandi K, IEEE Transactions on Antennas and Propagation, , Vol. 51, Issue 3, March 2003 pp.421 – 429.
85. Slot antenna miniaturization using distributed inductive loading, Behdad N, Sarabandi K, IEEE Antennas and Propagation Society International Symposium 2003, Vol. 1, 22-27 pp.308 - 311
86. Design of an efficient miniaturized UHF planar antenna, Sarabandi K, Azadegan R, IEEE Transactions on Antennas and Propagation, Vol. 51, Issue 6, June 2003 pp.1270 - 1276

87. A down-sized printed Hilbert antenna for UHF band, Xuan Chen, Safieddin Safavi Naeini, Yaxin Liu, IEEE Antennas and Propagation Society International Symposium, 2003, Vol. 2, 22-27 June 2003 pp.581 - 584
88. Multiband miniaturized PIFA for compact wireless-communication applications, Hala Elsadek, Dalia Nashaat, Hani Ghali, Microwave and optical technology letters, Vol. 42, Issue 3 , Jun 2004, pp. 230 – 234
89. A small planar inverted F antenna with capacitive and inductive loading, Schulteis S, Waldschmidt C, Sorgel W, Wiesbeck W, IEEE Antennas and Propagation Society International Symposium, 2004. Vol. 4, 20-25 June 2004 pp.4148 - 4151
90. CPW-fed compact equilateral triangular-ring slot antenna, Jin-Sen Chen, IEEE Antennas and Propagation Society International Symposium, 2004, Vol. 3, 20-25 June 2004 pp.2416 - 2419
91. Antenna miniaturization and bandwidth enhancement using a reactive impedance substrate Mosallaei H, Sarabandi K, IEEE Transactions on Antennas and Propagation, Vol. 52, Issue 9, Sept. 2004 pp.2403 – 2414
92. Miniaturization methods for narrowband and ultrawideband antennas Volakis J.L, Chi-Chih-Chen Ming Lee, Kramer B, Psychoudakis D, IEEE International Workshop on Antenna Technology: Small Antennas and Novel Metamaterials, 2005. IWAT 2005. 7-9 March 2005 pp.119 – 121
93. A study on miniaturization of 900 MHz and 2 GHz band antennas utilizing magnetic material, Kawano Y, Hayashida S, Bae S, Koyanag Y, Morishita H, IEEE Antennas and Propagation Society International Symposium, 2005 Vol. 3B, 3-8 July 2005 pp.347 – 350

94. Microstrip patch miniaturization by slots loading, Hung Tien Nguyen, Noghianian S, Shafai L, IEEE Antennas and Propagation Society International Symposium, 2005, Vol. 1B, 3-8 July 2005 pp.215 – 218
95. A miniaturized antenna for 2G/3G frequency-band applications, Robert Borowiec, Piotr M. Słobodzian, Microwave and optical technology letters, Vol. 48, Issue 2 , Dec 2005, pp. 399 - 402
96. A compact printed hook-shaped monopole antenna for 2.4/5-GHz wlan applications, Chi-Hun Lee, Seong-Ook Park, Microwave and optical technology letters, Vol. 48, Issue 2 , Dec 2005, pp. 327 - 329
97. Compact planar monopole antenna with ground branch for GSM/DCS/PCS/IMT2000 operation, Peng Sun, Zhenghe Feng, Microwave and optical technology letters, Vol. 48, Issue 4 , Feb 2006, pp. 719 – 721
98. Compact CPW-fed dual folded-strip monopole antenna for 5.8-GHz RFID application, Wen-Chung Liu 1, Ping-Chi Kao 2, Microwave and optical technology letters, Vol. 48, Issue 8 , May 2006, pp. 1614 – 1615
99. Composite right/left-handed transmission line based compact resonant antennas for RF module integration Cheng-Jung Lee Leong, K.M.K.H, Itoh T, IEEE Transactions on Antennas and Propagation Vol. 54, Issue 8, Aug. 2006 pp.2283 – 2291
100. A Novel Miniature Broadband/Multiband Antenna Based on an End-Loaded Planar Open- Sleeve Dipole, Spence T. G, Werner D. H, IEEE Transactions on Antennas and Propagation, Vol. 54, Issue 12, Dec. 2006 pp.3614 – 3620

101. Cavity-Backed Miniature Wideband UHF Circular Polarized Antenna With Textured Dielectrics Psychoudakis D, Volakis J. L, Wing Z, Halloran J. H, IEEE Transactions on Antennas and Propagation , vol. 54, Issue 12, Dec. 2006 pp.3586 – 3592
102. Coplanar waveguide fed coplanar strip dipole antenna, Tilley K, Wu, X.-D, Chang K, Electronics Letters, Vol. 30, Issue 3, 3 Feb. 1994 pp.176 - 177
103. Dual frequency coplanar strip dipole antenna, Tilley K, Xiao-Dong Wu, Kai Chang, Antennas and Propagation Society International Symposium 1994, Vol. 2, 20-24 June 1994 pp.928 - 931
104. Wideband coplanar waveguide fed coplanar patch antenna, Tong K.F, Li K, Matsui T, Izutsu M, IEEE Antennas and Propagation Society International Symposium, 2001 Vol. 3, 8-13 July 2001 pp.406 - 409
105. Aperture-coupled coplanar patch antennas, Cheng C.H, Li K Tong, K.F Matsui, T, IEEE Antennas and Propagation Society International Symposium 2001, Vol. 3, 8-13 July 2001 pp.506 - 509
106. Broadband Stacked Coplanar Patch Antennas, K. Li, C. H. Cheng, K. F. Tong, T. Matsui, European Microwave Conference 2001, pp.1 – 4
107. Coplanar patch antennas: principle, simulation and experiment, Li. K, Cheng, C.H, Matsui, T, Izutsu, M, IEEE Antennas and Propagation Society International Symposium, 2001 Vol. 3, 8-13 July 2001 pp.402 - 405
108. Coplanar patch antenna fed at the non-radiating edge, Pandey S, RamadossR, Antennas and Propagation Society International Symposium, 2004, Vol. 3, 20-25 June 2004 pp.3397 - 3400

109. Electric field in coplanar patch antenna (CPA) - simulation and measurement, Li K, Chun-Ping Chen, Anada, T Matsui, Asia-Pacific Conference Proceedings , Vol. 1, 4-7 Dec. 2005
110. Tunable coplanar patch antenna using varactor, Holland B, Ramadoss, R Pandey, S Agrawal P, Electronics Letters, Vol. 42, Issue 6, 16 March 2006 pp.319 – 32
111. New Interesting Leakage Behavior on Coplanar Waveguides of Finite and Infinite Widths, Mikio Tsuji, Hiroshi Shigesawa, and Arthur A. Oliner, IEEE Transactions on Microwave Theory and Techniques, Vol. 39, NO. 12, Dec. 1991, pp. 2130-2137.
112. The Feature of the Narrow-Pulse Transmission on Conventional Coplanar Waveguides when Power Leakage is Present, IEEE Transactions on Microwave Theory and Techniques, Vol. 41, No. 617, Jan. 1993, pp. 1017-1023
113. Resonant Phenomena in Conductor-Backed Coplanar Waveguides, Wen-Teng Lo, Ching-Kuang C. Tzuang, Song-Tsuen Peng, Chung-Chi Chang, Jenq-Wen Huang, and Ching-Cheng Tien, IEEE MTT Digest 1993, pp. 1199-1202
114. Resonant Phenomena in Conductor-Backed Coplanar Waveguides (CBCPW ' s), IEEE Transactions on Microwave Theory and Techniques, Vol. 41, No.12, Dec. 1993 pp. 2099-2108
115. Dispersion and Radiation Characteristics of Conductor- Backed CPW With finite Ground width, Wolfgang Heinrich, Frank Schnieder, and Thorsten Tischler, IEEE MTT Digest 2000, pp. 1663-1666

116. Numerical solution of initial boundary value problems involving Maxwell's equations in isotropic media, K. S. Yee, IEEE Transactions on Antennas and Propagation, 1966, AP-14, pp. 302-307
117. Review of the formulation and applications of the finite-difference time-domain method for numerical modeling of electromagnetic wave interactions with arbitrary structures, Taflove, Wave Motion, 1988, pp. 547-582
118. Numerical solution of steady state electromagnetic scattering problems using the time-dependent Maxwell's equations, A. Taflove and M. E. Brodwin, IEEE Transactions on Microwave Theory Techniques, 1975, MTT-23, 8, pp. 623-630
119. Application of the 3D FDTD method to the analysis of planar microstrip circuits, D.M. Sheen, Sami. M. Ali, Mohamed D. Abouzahra and Jin Au Kong, IEEE Transactions on Microwave Theory and Techniques, Vol. 38, No. 7, pp. 849-857, July 1990.
120. A perfectly matched layer for the absorption of electromagnetic waves, J. P. Berenger, Journal of Computational Physics, 1994, pp. 185-200
121. Analysis of microstrip patch antennas using finite difference time domain method, Reineix and B. Jecko, IEEE Transactions on Antennas and Propagation, , 1989.AP-37, 1 1 , pp. 1361-1369
122. Modelling dielectric losses in microstrip patch antennas: Application of FDTD method, P. Leveque, A. Reineix, and B. Jecko, Electronics Letters, 1992, 28, 6, pp. 539-540
123. Accurate characterization of planar printed antennas using finite-difference time domain method, C. Wu, K.-L. Wu, Z.-Q. Bi, and J. Litva, IEEE Transactions on Antennas and Propagation, 1992, AP-40, 5, pp. 526-533

124. FDTD method analysis of mutual coupling between microstrip antennas, K. Uehara and K. Kagoshima, *IEICE Transactions on Communication*, 1993, E76-B, 7, pp. 762-764
125. Analysis of microstrip antennas on a curved surface using the conformal grids FDTD method, T. Oonishi, T. Kashiwa, and I. Fukai, *Electronics and Communications in Japan, Part 1*, 1993, pp. 73-81
126. Analysis of microstrip antennas on a curved surface using the conformal grids FDTD method, T. Kashiwa, T. Onishi, and I. Fukai, *IEEE Transactions on Antennas and Propagation*, AP-42, 3, 1994, pp. 423-427
127. Optimal design of an offset-fed, twin-slot antenna element for millimeter-wave imaging arrays, Y. Qian, S. Iwata, and E. Yamashita, *IEEE Microwave and Guided Wave Letters*, 4, 7, pp. 232-234, 1994.
128. A time domain theoretical method for the analysis of microstrip antennas composed by slots, A. Reineix and B. Jecko, *Annales des Telecommunications*, 48, 112, pp. 29-34, 1993.
129. FDTD method applied to the study of radar cross section of microstrip patch antennas, A. Reineix, J. Paillol, and B. Jecko, *Annales des Telecommunications*, 48, 11/12, pp. 589-593, 1993.
130. The FDTD method applied to the study of microstrip patch antennas with a biased ferrite substrate, A. Reineix, C. Melon, T. Monediere, and F. Jecko, *Annales des Telecommunications*, 49, 314, pp. 137-142, 1994.
131. FDTD calculation of radiation patterns, impedance, and gain for a monopole antenna on a conducting box, R. Luebbers, L. Chen, T. Uno, and S. Adachi,

- IEEE Transactions on Antennas and propagation, AP-40, 12, pp, 1577-1583, 1992.
132. FDTD analysis of a monopole antenna mounted on a conducting box covered with a layer of dielectric, L. Chen, T. Uno, S. Adachi, and R. J. Luebbers, IEICE Transactions on Communications, E76-B, 12, pp. 1583-1586, 1993.
 133. Effects on portable antennas of the presence of a person, Toftgird, S. N. Hornsleth, and J. B. Andersen, IEEE Transactions on Antennas and Propagation, vol. 41, No.6, pp, 739-746, 1993.
 134. Performance analysis of antennas for hand-held transceivers using FDTD, M. A. Jensen and Y. Rahmat-Samii, IEEE Transactions on Antennas and Propagation, vol. 42, No.8 , pp. 1106-1 113, 1994.
 135. EM interaction of handset antennas and a human in personal communications, M. A. Jensen and Y. Rahmat-Samii, Proceedings of the IEEE, 83, 1, pp, 7-17, 1995.
 136. Current and S A R induced in a human head model by electromagnetic fields irradiated from a cellular phone, H. Y . Chen and H. H. Wang, IEEE Transactions on Microwave Theory Techniques, MTT-42, 12, pp. 2249-2254, 1994.
 137. Calculation of the electromagnetic fields induced in the head of an operator of a cordless telephone, L. Martens, J. De Moerloose, D. De Zutter, J. De Poorter, and C. De Wagter, Radio Science, 30, 1, pp. 283-290, 1995.
 138. FDTD analysis of CPW-fed folded-slot and multiple-slot antennas on thin substrates Huan-Shang Tsai, York R.A., IEEE Transactions on Antennas and Propagation, Vol. 44, Issue 2, Feb. 1996, pp. 217 – 226

139. The FDTD analysis of a microstrip patch antenna with dual feed lines, M. Kar and P.F Wahid, Proc. IEEE southeast conference, April 24-26, 1988.
140. A conformal Finite Difference Time Domain technique for modeling cylindrical dielectric resonators, Supriyo Dey and Raj Mittra, IEEE Trans. Microwave Theory and Tech., Vol. 47, no. 9, pp. 1737-1739, September 1999.
141. FDTD analysis of radiation pattern of antenna on truncated ground plane, Yamamoto D, Arai H, Microwave Conference, 2000 Asia-Pacific, 3-6 Dec. 2000 pp. 378 – 381
142. 3-D FDTD design analysis of a 2.4-GHz polarization-diversity printed dipole antenna with integrated balun and polarization-switching circuit for WLAN and wireless communication applications, Huey-Ru Chuang, Liang-Chen Kuo, IEEE Transactions on Microwave Theory and Techniques, , Vol. 51, Issue 2, Part 1, Feb. 2003 pp. 374 – 381
143. Pattern reconfigurable leaky-wave antenna design by FDTD method and Floquet's Theorem, Shaoqiu Xiao, Zhenhai Shao,, Fujise M, Bing-Zhong Wang, IEEE Transactions on Antennas and Propagation, Vol. 53, Issue 5, May 2005 pp. 1845 – 1848

Methodology

This chapter describes the experimental and simulation facilities utilized to characterize the behavior of the coplanar waveguide and final antenna configuration. The coplanar waveguide and proposed antenna are fabricated using the in-house photolithography facility. The antenna characteristics such as return loss, radiation pattern and gain are measured using vector network analyzer and associated instrumentation. Theoretical analysis of the offset fed coplanar waveguide and antenna are done using in-house developed MATLAB based FDTD codes. The Method of Moment based 3D EM solver and FEM based HFSS are also employed for simulation.

3.1 Fabrication method

The offset fed coplanar waveguide and the printed coplanar antenna are fabricated on different substrate materials using standard photolithography facility available in the laboratory. Photolithography method gives good accuracy for the etched patterns. This is very critical when the frequency of operation of the device is in higher microwave bands. The step by step process for the fabrication is very simple and illustrated in Fig. 3.1 below.

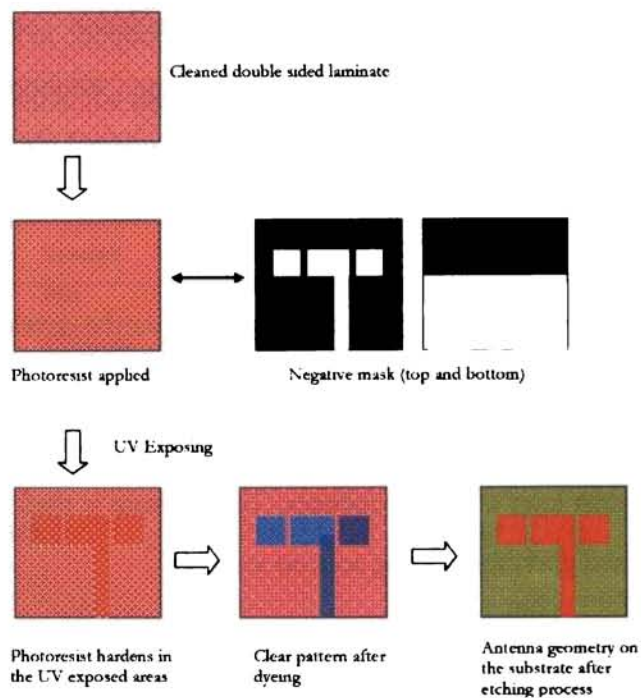


Fig. 3.1 Step by step process involved in Photo lithographic process

The computer aided design of the geometry is initially made and a negative mask of the geometry to be generated is printed on a butter paper. A double sided copper clad lamination of suitable dimension required for the antenna is cleaned very well and dried. Any dust or impurities on it will produce small discontinuity on the copper traces etched on the substrate. This will shift the resonant frequency from the predicted values, especially when the operating frequency is very high. Now, the negative photo resist material is applied on copper surfaces. It is then exposed to ultra violet radiation through the mask. The layer of photo-resist material in the exposed portions hardens. Now the board is immersed in developer solution for few minutes. The hardened portions will not be washed out by the developer solution. The board is then dipped in the dye solution in order to clearly view the hardened photoresist portions on the copper coating.

The unwanted copper traces now exposes after the developing phase is to be etched off to get the required antenna geometry on the substrate. Ferric Chloride (FeCl_3) solution is used for this purpose. FeCl_3 dissolves the copper parts except underneath the hardened photo resist layer after few minutes. The laminate is then cleaned carefully to remove the hardened photoresist using acetone solution.

3.2 Microwave substrates

Selection of substrates in microwave circuits is very important. Low loss substrates are very important at microwave bands. As frequency of operation increases, the loss tangent of the material used for substrates slightly increases, which in turn

adversely affect the efficiency of the antenna. The power handling capability of the antenna depends on the substrate materials also. At high power certain substrate materials cannot withstand. A variety of substrate materials are available in the market. Flexible substrate materials are also available, so that the antenna can be mounted on curved surfaces. The selection of dielectric constant of the substrate depends on the application of the antenna and the radiation characteristics specifications. It is worth noting that surface waves will be excited in high dielectric constant substrates. This will generate spurious radiations in unwanted directions from the antenna. In this thesis importance is given to compactness of the antenna structure. Table 3.1 shows the details of the substrates used in the thesis.

TABLE 3.1
DETAILS OF THE MICROWAVE SUBSTRATES USED IN THE THESIS

Sl. No.	Substrate	Relative dielectric constant, loss tangent and dielectric thickness
1	FR4	$\epsilon_r=4.4$, $\tan \delta=.02$, $h=1.6$ mm
2	RT duroid	$\epsilon_r=2.2$, $\tan \delta=.002$, $h=1.5$ mm

Prototype of offset fed coplanar waveguide and antennas were fabricated on FR4 and RT duroid substrates.

3.3 Experimental characterization setup

Antenna characteristics such as return loss, radiation pattern and gain are measured using the HP8510C and associated setup. The indigenously developed CREMA SOFT is used for the automatic measurement of the radiation properties using HP 8510C Network analyzer. The important systems used for the antenna

characterization are Vector network Analyzer, Anechoic Chamber, Automated turn table etc.

3.3.1 HP 8510C Vector Network Analyzer

This is a sophisticated Vector Network Analyzer (VNA) from Hewlett Packard with time domain and frequency domain operation capability [1]. The microprocessor based system can measure two port network parameters such as s_{11} , s_{12} , s_{21} and s_{22} very accurately. The in built signal processing algorithms of the network analyzer process the transmit and receive data and finally displays the measured values in many plot formats. The schematic of the VNA is shown in Fig. 3.2.

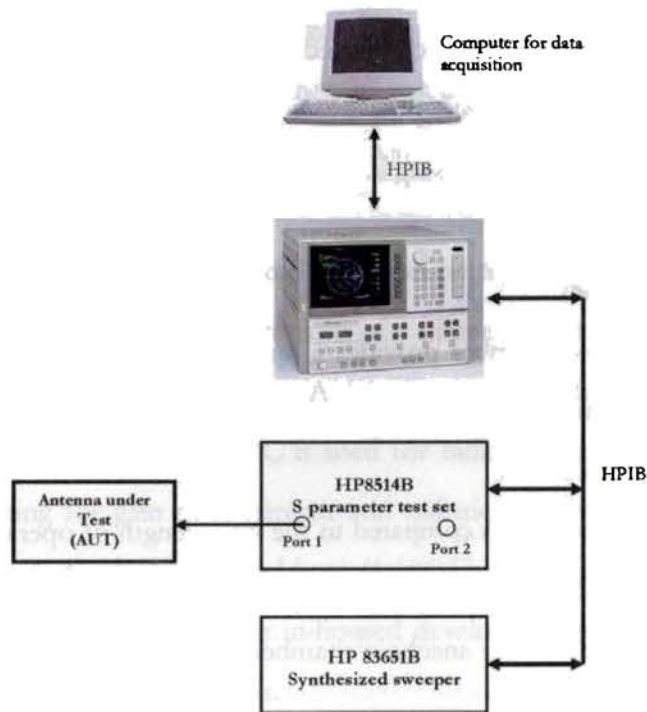


Fig. 3.2 Schematic diagram of the HP8510C vector network analyzer setup used for the characterization of the antennas

The network analyzer consists of a microwave generator, S parameter test set, signal processor and the display unit as illustrated in Fig. 3.2. The synthesized sweep generator HP 83651B uses an open loop YIG tuned element to generate the RF stimulus. It can synthesize frequencies from 10 MHz to 50 GHz. The frequencies can be set in step mode or ramp mode depending on the required measurement accuracy.

The antenna under test (AUT) is connected to the port of the S-parameter test set HP8514B and the forward and reflected power at the measurement point is separated and down converted to 20MHz using frequency down converter. It is again

down converted to lower frequency and processed in the IIP8510C processing unit. All the systems discussed above are interconnected using GPIB bus. A computer interfaced to the system is used for coordinating the whole operation remotely. Measurement data can be saved on a storage medium using it.

3.3.2 Anechoic Chamber

The anechoic chamber provides a 'quiet zone', free from all types of EM distortions. All the antenna characterizations are done in an Anechoic chamber to avoid reflections from nearby objects.

It is a very big room compared to the wave length of operation, consists of microwave absorbers [2] fixed on the walls, roof and the floor to avoid the EM reflections. A photograph of the anechoic chamber used for the study is shown in Fig. 3.3 below.



Fig. 3.3 Photograph of the anechoic chamber used for the antenna measurements

The absorbers fixed on the walls are highly lossy at microwave frequencies. They have tapered shapes to achieve good impedance matching for the microwave power impinges upon it. The chamber is made free from the surrounding EM interferences by covering all the walls and the roof with aluminium sheet.

3.3.3 Turn table assembly for far field radiation pattern measurement

The turn table assembly consists of a stepper motor driven rotating platform for mounting the Antenna Under Test (AUT). The in-house developed microcontroller based antenna positioner STIC 310C is used for radiation pattern measurement. The main lobe tracking for gain measurement and radiation pattern measurement is done using this setup. A standard wideband horn (1-18GHz) is used as receiving antenna for radiation pattern measurements. The in-housed developed automation software '*Crema Soft*' coordinates all the measurements.

3.4 Measurement procedure

The experimental procedures followed to determine the antenna characteristics are discussed below. The network analyzer in real practice is connected to large cables and connectors. The connectors and cables will have its losses associated at higher microwave bands. Thus the instrument should be calibrated with known standards of open, short and matched loads to get accurate scattering parameters. There are many calibration procedures available in the network analyzer. Single port, full two port and TRL calibration methods are usually used. The two port passive or active device scattering parameters can be accurately measured using TRL calibration method.

Return loss, VSWR and input impedance can be characterized using single port calibration method.

3.4.1 Return loss, Resonant frequency and Bandwidth

The return loss characteristic of the antenna is obtained by connecting the antenna to any one of the network analyzer port and operating the VNA in s_{11}/s_{22} mode. The calibration of the port is done for the frequency range of interest using the standard open, short and matched load. The calibrated instrument including the port cable is now connected to the device under test. The frequency vs reflection parameter (s_{11}/s_{22}) values is then stored on a computer using the 'Crema Soft' automation software.

The frequency for which the return loss value is minimum is taken as resonant frequency of the antenna. The range of frequencies for which the return loss value is within the -10dB points is usually treated as the bandwidth of the antenna. The antenna bandwidth is usually expressed as percentage of bandwidth, which is defined as

$$\%Bandwidth = \frac{bandwidth}{centrefrequency} * 100$$

At -10dB points the VSWR is ~ 2 . The above bandwidth is sometimes referred to as 2:1 VSWR bandwidth.

3.4.2 Far field radiation pattern

The measurement of far field radiation pattern is conducted in an anechoic chamber. The AUT is placed in the quiet zone of the chamber on a turn table and connected to one port of the network analyzer. A wideband horn is used as a transmitter and connected to the other port of the network analyzer. The turn table is controlled by a STIC positioner controller. The automated radiation pattern measurement process is coordinated by the '*Crema Soft*' software in the remote computer.

In order to measure the radiation pattern, the network analyzer is kept in S_{21}/S_{12} mode with the frequency range within the -10dB return loss bandwidth. The number of frequency points are set according to the convenience. The start angle, stop angle and step angle of the motor is also configured in the '*Crema Soft*'. The antenna positioner is boresighted manually. Now the THRU calibration is performed for the frequency band specified and saved in the CAL set. Suitable gate parameters are provided in the time domain to avoid spurious radiations if any. The *Crema Soft* will automatically perform the radiation pattern measurement and store it as a text file

3.4.3 Antenna Gain

The gain of the antenna under test is measured in the broadside direction. The gain transfer method using a standard gain antenna is employed to determine the absolute gain of the AUT [3-4]. The experimental setup is similar to the radiation pattern measurement setup. An antenna with known gain is first placed in the antenna positioner and the THRU calibration is done for the frequency range of interest. Standard antenna is then replaced by the AUT and the change in S_{21} is noted. Note that the AUT should be aligned so that the gain in the main beam direction is measured. This is the relative

gain of the antenna with respect to the reference antenna. The absolute gain of the antenna is obtained by adding this relative gain to the original gain of the standard antenna.

3.5 IE3D Electromagnetic Simulator

The IE3D Electromagnetic simulator works based on Method of Moment [5]. This full wave simulator is capable of simulating microwave circuits such as microstrip circuits, printed antennas and some types of wire antennas. There is no limitation on the size and shape of the antennas to be simulated. The CURVIEW post-processor of IE3D provides colorful 3D and 2D display of current distribution and radiation patterns. CURVIEW also provides complete information on the directivity, return loss, efficiency, axial ratio, 3 dB beam width, and RCS. Most field solvers assume infinite ground planes in solving circuit and antenna problems. In many microwave applications one may not be able to find a big ground plane. Therefore, infinite ground plane assumption is not applicable. IE3D is able to model structures with finite ground plane.

The different port types available in IE3D are very useful for microwave circuit simulators to excite the devices according to the convenience of the designer. Coplanar waveguide ports, probe feed are widely used in IE3D. In this thesis the study of the radiation pattern, gain and efficiency of the coplanar waveguide with corner feed is done using IE3D. The edge port schemes suitable for coplanar wave guide applications are used in the study. The first step in IE3D simulation is to define the

material parameter such as substrate thickness, dielectric constant, and metallic properties in MGRID window. Then draw the required circuit geometry in MGRID. The simulation setup in the window is then used to specify the frequency range of simulation, number of frequency points etc. The simulation results are available in MODUA window available with IE3D.

3.6 HFSS: 3D Electromagnetic simulator

HFSS utilizes a 3D full-wave Finite Element Method (FEM) to compute the electrical behavior of high-frequency and high-speed components [6]. With HFSS one can extract the parameters such as S, Y, and Z, visualize 3D electromagnetic fields (near- and far-field), and optimize design performance. An important and useful feature of this simulation engine is the availability of different kinds of port schemes. It provides lumped port, wave port, incident wave scheme etc. The accurate simulation of coplanar waveguides and microstrip lines can be done using wave port.

In this thesis some parts of the investigations are done using HFSS. The optimization algorithm available with HFSS is very useful for antenna engineers to optimize the dimensions very accurately. There are many kinds of boundary schemes available in HFSS. Radiation boundary and PML boundary are the important are widely used in this work. The vector as well as scalar representation of E, H, J values of the device under simulation gives a good insight in to the problem under simulation.

The first step in simulating a system in HFSS is to define the geometry of the system by giving the material properties and boundaries for 3D or 2D elements

available in HFSS window. The suitable port excitation scheme is then given. A radiation boundary filled with air is then defined surrounding the structure to be simulated. Now, the simulation engine can be invoked by giving the proper frequency of operations and the number of frequency points. Finally the simulation results such as scattering parameters, current distributions and far field radiation pattern can be displayed.

References

1. HP8510C Network Analyzer operating and programming manual, Hewlett Packard, 1988.
2. Design, Development and Performance Evaluation of an Anechoic Chamber for Microwave Antennas Studies, E. J. Zachariah, K. Vasudevan, P. A. Praveen Kumar, P. Mohanan and K. G. Nair, Indian Journal of Radio and Space Physics, Vo. 13, February 1984, pp. 29-31.
3. C. A. Balanis, Antenna Theory: Analysis and Design, Second Edition, John Wiley & Sons Inc. 1982
4. John D. Kraus, Antennas Mc. Graw Hill International, second edition, 1988
5. IE3D User's manual, Release 7, Zeland Software Inc. December 1997
6. HFSS User's manual, version 10, Ansoft Corporation, July 2005

Finite Difference Time Domain Method

A brief introduction to the fundamentals of PML based FDTD computation technique is presented in this chapter. The PML based FDTD was found to be the best suited method to describe the radiation and resonance in coplanar waveguides and 'coplanar antenna'. The MATLAB based FDTD codes developed for this specific research topic is based on the PML based FDTD concept explained in this chapter.

4.1 Introduction

The finite difference time domain (FDTD) method proposed by Yee [1] in 1966 for Maxwell's equations has become the state of the art for solving Maxwell's equations in complex geometries. It is a fully vectorial method that naturally gives both time domain, and frequency domain information to the user, offering unique insight into all types of problems and applications in electromagnetics. The technique is discrete in both space and time. The electromagnetic fields and structural materials of interest are described on a discrete mesh made up of so-called Yee cells. Maxwell's equations are solved discretely in time, where the time step used is related to the mesh size through the speed of the propagating wave.

Multiple sources may be added to the simulation and subsequent iteration results in the electromagnetic field propagation in time. Typically, the simulation is continued until there are essentially no electromagnetic fields left in the simulation region. Time domain information can be recorded at any spatial point (or group of points). This data can be recorded for the duration of the simulation, or it can be recorded as a series of "snapshots" at times specified by the user.

Frequency domain information at any spatial point may be obtained through the Fourier transform of the time domain information at that point. Thus the frequency dependence of power flow may be obtained over a wide range of frequencies from a single simulation.

The FDTD has been used by many investigators, because it has the following advantages over other techniques:

1. From the mathematical point of view, it is a direct implementation of Maxwell's curl equations. Therefore, analytical processing of Maxwell's equations is almost negligible.
2. It is capable of predicting broadband frequency response because the analysis is carried out in the time domain
3. It is capable of analyzing complex systems, including wave interaction with human body, non linear devices, complex bodies and so on.
4. It is capable of analyzing structures having different types of materials

Analysis of any problem using FDTD starts with dividing the structure into various regions based on the material properties. The unbounded region, if any, is then bounded by terminating it with absorbing medium or a termination free from reflections. Next, the problem's physical space is discretized in the form of a number of cubes. The time domain is also discretized. The structure is then excited by an electromagnetic pulse. The wave thus launched by the pulse in the structure is then studied for its propagation behavior. The stabilized time-domain waveform is numerically processed to determine the time-domain and frequency domain characteristics of the structures.

4.2 Three dimensional FDTD method

The FDTD method is implemented by discretizing Maxwell's curl equations over a finite volume and approximating the derivatives with center difference approximations. Conducting surfaces are treated by vanishing tangential electric field components. The walls of the outer boundary however require special treatment to prevent reflections from mesh termination.

Formulation of the FDTD method begins by considering the differential form of Maxwell's two curl equations which govern the propagation of fields in the structures. For simplicity, the media is assumed to be uniform, isotropic, and homogeneous and lossless.

With these assumption, Maxwell's equations can be written as

$$\mu \frac{\partial H}{\partial t} = -\nabla \times E \quad (1)$$

$$\epsilon \frac{\partial E}{\partial t} = \nabla \times H \quad (2)$$

In order to find an approximate solution to these set of equations, the problem is discretized over a finite three dimensional computational domain with appropriate boundary conditions enforced on the source, conductors, and mesh walls. The divergence equations are automatically satisfied by the FDTD method.

4.2.1 Finite Difference Equations

To obtain discrete approximations to these continuous partial differential equations the centered difference approximation is used on both the time and space. Fig. 4.1 shows the Yee cell used in FDTD computation. The entire computational domain is obtained by stacking these rectangular cubes into a larger rectangular volume. The x , y and z dimensions of the unit cell are Δx , Δy and Δz , respectively. The advantages of this field arrangement are that centered differences are realized in the calculation of each field component and that continuity of tangential field components is automatically satisfied. There are only six unique field components within the unit cell. Each unit cell is described by the subscript indices i , j , and k corresponding to the node numbers in the x , y and z directions.

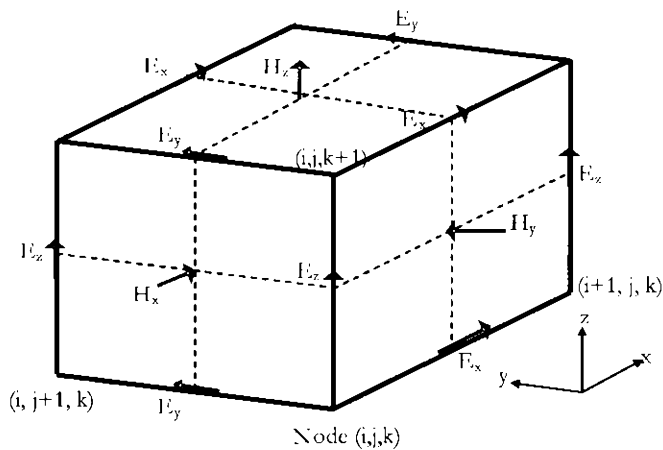


Fig. 4.1 Yee Cell using in FDTD with Electric and Magnetic field components

The notation implicitly assumes the $\pm 1/2$ space indices and thus simplifies the notation, rendering the formulas directly implementable on the computer.

The time steps are indicated with the superscript 'n'. Using this field component arrangement, the above notation, and the centered difference approximation, the explicit finite difference approximations to (1) and (2) are

$$H_{x,j,k}^{n+1/2} = H_{x,j,k}^{n-1/2} + \frac{\Delta t}{\mu\Delta z} (E_{y,j,k}^n - E_{y,j,k-1}^n) - \frac{\Delta t}{\mu\Delta y} (E_{z,j,k}^n - E_{z,j-1,k}^n) \quad (3)$$

$$H_{y,j,k}^{n+1/2} = H_{y,j,k}^{n-1/2} + \frac{\Delta t}{\mu\Delta x} (E_{z,j,k}^n - E_{z,j-1,k}^n) - \frac{\Delta t}{\mu\Delta z} (E_{x,j,k}^n - E_{x,j,k-1}^n) \quad (4)$$

$$H_{z,j,k}^{n+1/2} = H_{z,j,k}^{n-1/2} + \frac{\Delta t}{\mu\Delta y} (E_{x,j,k}^n - E_{x,j-1,k}^n) - \frac{\Delta t}{\mu\Delta x} (E_{y,j,k}^n - E_{y,j-1,k}^n) \quad (5)$$

$$E_{x,i,j,k}^{n+1} = E_{x,i,j,k}^n + \frac{\Delta t}{\epsilon\Delta y} (H_{z,i,j,k+1}^{n+1/2} - H_{z,i,j,k}^{n+1/2}) - \frac{\Delta t}{\epsilon\Delta z} (H_{y,i,j,k+1}^{n+1/2} - H_{y,i,j,k}^{n+1/2}) \quad (6)$$

$$E_{y,i,j,k}^{n+1} = E_{y,i,j,k}^n + \frac{\Delta t}{\epsilon\Delta z} (H_{x,i,j,k+1}^{n+1/2} - H_{x,i,j,k}^{n+1/2}) - \frac{\Delta t}{\epsilon\Delta x} (H_{z,i+1,j,k}^{n+1/2} - H_{z,i,j,k}^{n+1/2}) \quad (7)$$

$$E_{z,i,j,k}^{n+1} = E_{z,i,j,k}^n + \frac{\Delta t}{\epsilon\Delta x} (H_{y,i,j,k+1}^{n+1/2} - H_{y,i,j,k}^{n+1/2}) - \frac{\Delta t}{\epsilon\Delta y} (H_{x,i,j+1,k}^{n+1/2} - H_{x,i,j,k}^{n+1/2}) \quad (8)$$

The half time steps indicate that E and H are alternately calculated in order to achieve centered differences for the time derivatives. In these equations, the permittivity and the permeability are set to the appropriate values, depending on the location of each field component. For the dielectric-air interface the average of the two permittivities $(\epsilon_{r+1})/2$ is used [2]

4.2.2 Stability criteria

The numerical algorithm for Maxwell's curl equations derived requires the time increment Δt to have a specific upper bound relative to the space increments Δx , Δy and Δz . This bound is necessary to avoid numerical instability that can cause the computed results to increase spuriously without limit as time marching continues. The cause for numerical instability is the finite difference implementation of the derivate. The final expression for the upper bound on Δt can be written as,

$$\Delta t \leq \frac{1}{V_{\max}} \frac{1}{\sqrt{1/\Delta x^2 + 1/\Delta y^2 + 1/\Delta z^2}} \quad (9)$$

Where V_{\max} is the maximum phase velocity of the signal in the problem being considered. Typically V_{\max} will be the velocity of light in free space unless the entire volume is filled with dielectric. These equations will allow the approximate solution of E and H in the volume of the computational domain or mesh. In practice, the maximum value of Δt used is about 90% of the value given by above equation.

4.2.3 Numerical Dispersion

Dispersion is defined as the variation of the phase constant of the propagating wave with frequency. The discretization of Maxwell's equations in space and time causes dispersion of the simulated wave in an otherwise dispersion-free structure. That is the phase velocity of the wave in an FDTD grid can differ from the analytical value. This dispersion is called numerical dispersion. The amount of dispersion depends on the wavelength, the direction of propagation in the grid, and the discretization size.

Numerical dispersion can be reduced to any degree that is desired if one uses a fine enough FDTD mesh.

4.3 Absorbing Boundary Conditions

A large number of electromagnetic problems have associated open space regions, where the spatial domain is unbounded in one or more directions. The solution of such a problem in this form will require an unlimited amount of computer resources. Therefore, the domain must be truncated such that the error involved is minimal. For this, the domain can be divided into two regions: the interior region and the exterior region as shown in Fig. 4.2.

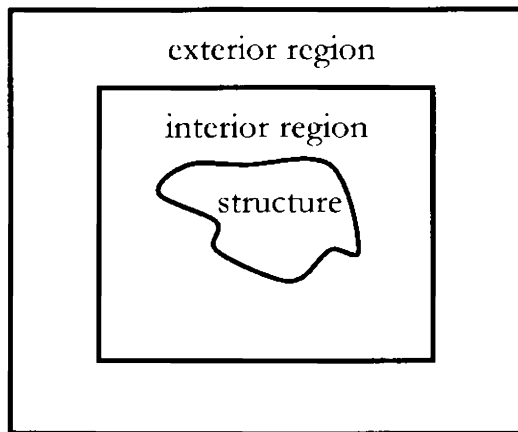


Fig. 4.2 Truncation of the domain by the exterior region in FDTD algorithm

The interior region must be large enough to enclose the structure of interest. The exterior region simulates the infinite space. The FDTD algorithm is applied in the interior region. It simulates wave propagation in the forward and backward directions. However, only the outward propagation in the exterior region is desired so that infinite free-space conditions are simulated. These reflections must be suppressed to an acceptable level so that the FDTD solution is valid for all time steps.

Two options are available to simulate the open region surrounding the problem physical space.

1. Terminate the interior region with equivalent currents on the surface of the interior region and use the Green's function to simulate the fields in the exterior region
2. To simulate the exterior region with absorbing boundary conditions to minimize reflections from the truncation of the mesh.

Simulation of the open region with the help of equivalent currents yields a solution whereby the radiation condition is satisfied exactly. But the values of fields on the surface enclosing the interior region are needed, for which CPU time and storage requirement increases rapidly with the surface size. On the other hand, the absorbing boundary concept truncates the computation domain and reduces the computational time and storage space. The absorbing boundary condition (ABC) can be simulated in a number of ways. These are classified as analytical (or differential) ABC and material ABC. The material ABC is realized from the physical absorption of the incident signal by means of a lossy medium [3], whereas analytical ABC is simulated by approximating the

wave equation on the boundary [4]. The material ABC holds great promise of truncating the computation domain. It can reach an ideal limit extending the FDTD numerical modeling capabilities to a -80 to -120 dB reflection coefficient at the boundaries.

4.3.1 Mur's first order ABC

The simple and optimal analytical ABC, named Mur's first-order absorbing boundary condition, is described below. Analysis of Mur's first-order ABC is based on the work of Enquist and Majda [4] and the optimal implementation given by Mur [5]. An arbitrary wave can be expanded in terms of a spectrum of plane waves. If a plane wave is incident normally on a planar surface, and if the surface is perfectly absorbing, there will be no reflected wave. A numerical wave traveling along the negative x direction has a solution given by,

$$\left(\frac{\partial}{\partial x} - \frac{1}{c} \frac{\partial}{\partial t} \right) \phi(x, t) = 0 \quad (10)$$

If we impose the above condition on a wave normally incident on the planar surface, the wave should not be reflected. Consequently, an absorbing condition for a normally incident wave is

$$\frac{\partial \phi(x, t)}{\partial x} = \frac{1}{c} \frac{\partial \phi(x, t)}{\partial t} \quad \text{Where } x = \Delta x / 2, t = (n + 1/2) \Delta t \quad (11)$$

For updating of the electric field at a $x = \Delta x / 2, t = (n + 1) \Delta t$.

In finite-difference form it can be written as follows:

$$\frac{\phi_1^{n+1/2} - \phi_0^{n+1/2}}{\Delta x} = \frac{1}{c} \frac{\phi_{1/2}^{n+1} - \phi_{1/2}^n}{\Delta t} \quad (12)$$

In this form, the finite-difference approximation is accurate to the second order in Δx and Δt . But the values at the half grid points and half time steps are not available, and can be averaged as

$$\phi_m^{n+1/2} = \frac{\phi_m^{n+1} + \phi_m^n}{2} \text{ and } \phi_{m+1/2}^n = \frac{\phi_{m+1}^n + \phi_m^n}{2} \quad (13) \ \& \ (14)$$

The approximation of above equation is also accurate to a second order if $\Phi(x,t)$ is a smooth function. Use of (12), (13) and (14) yields

$$\phi_0^{n+1} = \phi_1^n + \left(\frac{c\Delta t - \Delta x}{c\Delta t + \Delta x} \right) (\phi_1^{n+1} - \phi_0^n) \quad (15)$$

This equation can be used for updating the fields lying on the outer boundary of the interior region. Above equation can be shown to be unconditionally stable [5]. The boundary condition for (10) is exact only for a plane wave at normal incidence. Hence, the wave will still be reflected for an oblique incidence. To take care of this eventuality, one needs to use higher order absorbing boundary conditions.

4.3.2 Perfect Matched Layer (PML)

The implementation of FDTD using Yee algorithm is the usual straight forward way to simulate the EM problems. The field equations (1) to (8) together with proper boundary conditions can simulate the EM problems with good accuracy. As discussed

above, the Mur's first order absorbing boundary condition has some disadvantages. This ABC is not useful to absorb oblique incident power. One of the most flexible and most efficient ABC is the perfectly matched layer (PML) developed by Berenger [6]. PML provides the perfect absorption of all the incident power at the boundary of the problem space. The absorption is independent of the incident angle.

It should be noted that the thesis investigates the radiation and resonance phenomena of a coplanar waveguide in order to obtain a novel radiating structure with coplanar configuration. Thus the field values at the two slots of the waveguide is very important in order to explain the phenomena. Thus PML is selected for the present analysis.

4.4 PML for Finite Difference Time Domain technique

The Yee algorithm described in the previous sections compute the propagation of EM signal by calculating E with initial excitation signal with proper boundary conditions. Then H field values are updated using the calculated E field values. In this thesis the FDTD method with PML concept is implemented by introducing Electric Flux Density (D) in discretized Maxwell's equations [7].

Initially the implementation of PML concept in FDTD is described and then discretized Maxwell's equations are derived. An interesting thing is that the iterative FDTD algorithm does not use separate computer codes for PML section, but the generalized equation can be used for both normal media and PML by suitably enabling or disabling some medium dependent parameters in the equations.

Consider the following Maxwell's equations,

$$\frac{\partial D}{\partial t} = \frac{1}{\sqrt{\epsilon_0 \mu_0}} \nabla_x H \quad (16.a)$$

$$D(\omega) = \epsilon^*_r(\omega) E(\omega) \quad (16.b)$$

$$\text{Where } \epsilon^*_r(\omega) = \epsilon_r + \frac{\sigma}{j\omega\epsilon_0}$$

$$\frac{\partial H}{\partial t} = -\frac{1}{\sqrt{\epsilon_0 \mu_0}} \nabla_x E \quad (16.c)$$

Consider a transverse magnetic wave (TM) propagating in a medium. The E and H field components are Ez, Hx and Hy. Now the above equations are reduced to

$$\frac{\partial D_z}{\partial t} = \frac{1}{\sqrt{\epsilon_0 \mu_0}} \left(\frac{\partial H_y}{\partial x} - \frac{\partial H_x}{\partial y} \right) \quad (17.a)$$

$$D(\omega) = \epsilon^*_r(\omega) E(\omega) \quad (17.b)$$

$$\frac{\partial H_x}{\partial t} = -\frac{1}{\sqrt{\epsilon_0 \mu_0}} \frac{\partial E_z}{\partial y} \quad (17.c)$$

$$\frac{\partial H_y}{\partial t} = \frac{1}{\sqrt{\epsilon_0 \mu_0}} \frac{\partial E_z}{\partial x} \quad (17.d)$$

If a wave is propagating in medium A and it impinges upon medium B, the amount of reflection is dictated by the intrinsic impedances of the two media

$$\Gamma = \frac{\eta_A - \eta_B}{\eta_A + \eta_B} \quad (18)$$

Which are determined by the dielectric constant and permeability of the respective media

$$\eta = \sqrt{\frac{\mu}{\epsilon}} \quad (19)$$

Up to now, it is assumed that μ is a constant, so when a propagating pulse travels from ϵ_1 to ϵ_2 , it sees a change in impedance and reflects a portion of the pulse. However, if μ changed with ϵ so that η remains a constant, Γ would be zero and no reflection will occur. This still doesn't solve the problem, because the pulse will continue propagating in the new medium. What we really want is a medium that is also lossy so that the pulse will die out before it hits the boundary. This is accomplished by making both ϵ and μ of Eq. (19) complex because the imaginary part represents attenuation or loss.

Consider Eq. (17) and move everything to the Fourier domain.

$$j\omega D_z = c_0 \left(\frac{\partial H_y}{\partial x} - \frac{\partial H_x}{\partial y} \right) \quad (20.a)$$

$$D_z(\omega) = \epsilon_r^*(\omega) E_z(\omega) \quad (20.b)$$

$$j\omega H_x = -c_0 \frac{\partial E_z}{\partial y} \quad (20.c)$$

$$j\omega H_y = c_0 \frac{\partial E_z}{\partial x} \quad (20.d)$$

It should be noted that ϵ and μ are eliminated from the spatial derivatives in the above equations for the normalized units. Instead of putting them back to implement the PML, we will add fictitious permittivities and permeabilities.

$$j\omega D_z \varepsilon_{Fz}^*(x) \varepsilon_{Fz}^*(y) = c_0 \left(\frac{\partial H_y}{\partial x} - \frac{\partial H_x}{\partial y} \right) \quad (21.a)$$

$$D_z(\omega) = \varepsilon_{Fz}^*(\omega) E_z(\omega) \quad (21.b)$$

$$j\omega H_x \mu_{Fx}^*(x) \mu_{Fx}^*(y) = -c_0 \frac{\partial E_z}{\partial y} \quad (21.c)$$

$$j\omega H_y \mu_{Fy}^*(x) \mu_{Fy}^*(y) = c_0 \frac{\partial E_z}{\partial x} \quad (21.d)$$

It is worth noting that the fictitious values added in the equations have nothing to do with the real values of $\varepsilon_{Fz}^*(\omega)$ which specify the medium

Sacks et al. [8] showed that there are two conditions to form a PML:

1. The impedance going from the background medium to the PML must be constant

$$\eta_0 = \eta_m = \sqrt{\frac{\mu_{Fx}^*}{\varepsilon_{Fz}^*}} = 1 \quad (22)$$

2. In the direction perpendicular to the boundary the relative dielectric constant and relative permeability must be the inverse of those in the other directions

That is,

$$\varepsilon_{Fx}^* = \frac{1}{\varepsilon_{Fy}^*} \quad (23.a)$$

$$\mu_{Fx}^* = \frac{1}{\mu_{Fy}^*} \quad (23.b)$$

Each of these is a complex quantity of the form

$$\epsilon_{Fm}^* = \epsilon_{Fm} + \frac{\sigma D_m}{j\omega\epsilon_0} \quad \text{for } m=x \text{ or } y \quad (24.a)$$

$$\mu_{Fm}^* = \mu_{Fm} + \frac{\sigma H_m}{j\omega\mu_0} \quad \text{for } m=x \text{ or } y \quad (24.b)$$

The following selection of parameters satisfies Eq. (23.a) and (23.b)

$$\epsilon_{Fm} = \mu_{Fm} = 1 \quad (25.a)$$

$$\frac{\sigma D_m}{\epsilon_0} = \frac{\sigma H_m}{\mu_0} = \frac{\sigma D}{\epsilon_0} \quad (25.b)$$

Substituting (25) above values to (24), the values of (22) becomes

$$\eta_0 = \eta_m = \sqrt{\frac{\mu_{Fx}^*}{\epsilon_{Fx}^*}} = \sqrt{\frac{1 + \sigma(x)/j\omega\epsilon_0}{1 + \sigma(x)/j\omega\epsilon_0}} = 1$$

This fulfills the first requirement above. If σ increases gradually as it goes into the PML, the field components Dz, Hx and Hy experience attenuation.

The PML is first implemented in the X direction. Therefore, the x dependent values of ϵ_{Fm}^* and μ_{Fm}^* will be retained.

$$j\omega D_z \varepsilon^*_{Fz}(x) = c_0 \left(\frac{\partial H_y}{\partial x} - \frac{\partial H_x}{\partial y} \right)$$

$$j\omega H_x \mu^*_{Fx}(x) = -c_0 \frac{\partial E_z}{\partial y}$$

$$j\omega H_y \mu^*_{Fy}(x) = c_0 \frac{\partial E_z}{\partial x}$$

using the values of (25)

$$j\omega \left(1 + \frac{\sigma_D(x)}{j\omega\varepsilon_0} \right) D_z = c_0 \left(\frac{\partial H_y}{\partial x} - \frac{\partial H_x}{\partial y} \right) \quad (26.a)$$

$$j\omega \left(1 + \frac{\sigma_D(x)}{j\omega\varepsilon_0} \right)^{-1} H_x = -c_0 \frac{\partial E_z}{\partial y} \quad (26.b)$$

$$j\omega \left(1 + \frac{\sigma_D(x)}{j\omega\varepsilon_0} \right) H_y = c_0 \frac{\partial E_z}{\partial x} \quad (26.c)$$

In the above equations, the permeability of Hx is the inverse of that of Hy. Therefore the second requirement for the PML is fulfilled.

Now the above equations have to be put into the FDTD formulation. Consider the left side of (26.a)

$$j\omega \left(1 + \frac{\sigma_D(x)}{j\omega\varepsilon_0} \right) D_z = j\omega D_z + \frac{\sigma_D(x)}{\varepsilon_0} D_z$$

Moving to the time domain, and then taking the finite difference approximations,

$$\begin{aligned} \frac{\partial D_z}{dt} + \frac{\sigma_D(i)}{\epsilon_0} D_z &\cong \frac{D_z^{n+1/2}(i,j) - D_z^{n-1/2}(i,j)}{\Delta t} + \frac{\sigma_D(i)}{\epsilon_0} \frac{D_z^{n+1/2}(i,j) + D_z^{n-1/2}(i,j)}{2} \\ &= D_z^{n+1/2}(i,j) \frac{1}{\Delta t} \left[1 + \frac{\sigma_D(i)\Delta t}{2\epsilon_0} \right] - D_z^{n-1/2}(i,j) \frac{1}{\Delta t} \left[1 - \frac{\sigma_D(i)\Delta t}{2\epsilon_0} \right] \end{aligned}$$

If this is substituted into Eq. (26.a) along with the spatial derivatives,

$$\begin{aligned} D_z^{n+1/2}(i,j) &= gi3(i)D_z^{n-1/2}(i,j) + \\ gi2(i)0.5 &\left[H_y^n(i+1/2,j) - H_y^n(i-1/2,j) - H_x^n(i,j+1/2) - H_x^n(i,j-1/2) \right] \end{aligned} \quad (27)$$

The parameters $gi(2)$ and $gi(3)$ are given by

$$gi2(i) = \frac{1}{1 + \sigma_D(i)\Delta t / 2\epsilon_0} \quad (28.a)$$

$$gi3(i) = \frac{1 - \sigma_D(i)\Delta t / 2\epsilon_0}{1 + \sigma_D(i)\Delta t / 2\epsilon_0} \quad (28.b)$$

Similarly H_y can be formulated as,

$$H_y^{n+1}(i+1/2,j) = fi3(i+1/2)H_y^n(i+1/2,j) + fi2(i+1/2)0.5 \left[E_z^{n+1/2}(i+1,j) - E_z^{n+1/2}(i,j) \right] \quad (29)$$

where

$$fi2(i+1/2) = \frac{1}{1 + \sigma_D(i+1/2)\Delta t / (2\epsilon_0)} \quad (30.a)$$

and

$$fi3(i+1/2) = \frac{1 - \sigma_D(i+1/2)\Delta t / (2\epsilon_0)}{1 + \sigma_D(i+1/2)\Delta t / (2\epsilon_0)} \quad (30.b)$$

These parameters are calculated at $i+1/2$ positions due to the $1/2$ cell position of the H component.

(26.b) can be written as,

$$j\omega H_x = -c_0 \left[\frac{\partial E_z}{\partial y} + \frac{\sigma_D(x)}{\epsilon_0} \frac{1}{j\omega} \frac{\partial E_z}{\partial y} \right]$$

The spatial derivative will be written as,

$$\frac{\partial E_z}{\partial y} \cong \frac{E_z^{n+1/2}(i, j+1) - E_z^{n+1/2}(i, j)}{\Delta x} = -\frac{curl_e}{\Delta x}$$

Implementing this into FDTD gives

$$\frac{H_x^{n+1}(i, j+1/2) - H_x^n(i, j+1/2)}{\Delta t} = -c_0 \left[\frac{-curl_e}{\Delta x} - \frac{\sigma_D(x)}{\epsilon_0} \Delta t \sum_{n=0}^T \frac{curl_e}{\Delta x} \right]$$

The extra Δt in front of the summation is the part of the approximation of the time domain integral.

$$\begin{aligned} H_x^{n+1}(i, j+1/2) &= H_x^n(i, j+1/2) + \frac{c_0 \Delta t}{\Delta x} curl_e + \frac{\Delta t c_0}{\Delta x} \frac{\sigma_D(x) \Delta t}{\epsilon_0} I_{Hx}^{n+1/2}(i, j+1/2) \\ &= H_x^n(i, j+1/2) + \frac{c_0 \Delta t}{\Delta x} curl_e + \frac{\sigma_D(x) \Delta t}{2\epsilon_0} I_{Hx}^{n+1/2}(i, j+1/2) \end{aligned}$$

(26.b) is implemented as the following series of equations:

$$curl_e = \left[E_z^{n+1/2}(i, j) - E_z^{n+1/2}(i, j+1) \right] \quad (31.a)$$

$$I_{Hx}^{n+1/2}(i, j+1/2) = I_{Hx}^{n-1/2}(i, j+1/2) + curl_e \quad (31.b)$$

$$H_x^{n+1}(i, j+1/2) = H_x^n(i, j+1/2) + 0.5 curl_e + fl(i) I_{Hx}^{n+1/2}(i, j+1/2) \quad (31.c)$$

With

$$fl(i) = \frac{\sigma(i) \Delta t}{2\epsilon_0} \quad (32)$$

In calculating the f and g parameters, it is not necessary to actually vary conductivities. Instead, we calculate an auxiliary parameter,

$$x_n = \frac{\sigma \Delta t}{2\epsilon_0}$$

that increases as it goes into the PML. The f and g parameters are then calculated:

$$x_n(i) = 0.333 \left(\frac{i}{\text{length_pml}} \right)^3 \quad i=1,2, \dots, \text{length_pml} \quad (33)$$

$$fi1(i) = x_n(i) \quad (34.a)$$

$$gi2(i) = \left(\frac{1}{1 + x_n(i)} \right) \quad (34.b)$$

$$gi3(i) = \left(\frac{1 - x_n(i)}{1 + x_n(i)} \right) \quad (34.c)$$

The factor 0.333 is found empirically to be the largest number that remained stable. The cubic factor is also found empirically to be the most effective variation

The parameters vary in the following manner:

$$fi1(i) \text{ from } 0 \text{ to } 0.333 \quad (35.a)$$

$$gi2(i) \text{ from } 1 \text{ to } 0.75 \quad (35.b)$$

$$gi3(i) \text{ from } 1 \text{ to } 0.5 \quad (35.c)$$

Throughout the main problem space, fi1 is zero, while gi2 and gi3 are 1. Therefore, there is a transition from the main part of the program to the PML. The above equations refer to the implementation of PML in x direction. Now the PML is to be implemented in y direction. Therefore instead of (26) one can write

$$j\omega \left(1 + \frac{\sigma_D(x)}{j\omega\epsilon_0} \right) \left(1 + \frac{\sigma_D(y)}{j\omega\epsilon_0} \right) D_z = c_0 \left(\frac{\partial H_y}{\partial x} - \frac{\partial H_x}{\partial y} \right) \quad (36.a)$$

$$j\omega \left(1 + \frac{\sigma_D(x)}{j\omega\epsilon_0}\right)^{-1} \left(1 + \frac{\sigma_D(y)}{j\omega\epsilon_0}\right) H_x = c_0 \left(-\frac{\partial E_z}{\partial y}\right) \quad (36.b)$$

$$j\omega \left(1 + \frac{\sigma_D(x)}{j\omega\epsilon_0}\right) \left(1 + \frac{\sigma_D(y)}{j\omega\epsilon_0}\right)^{-1} H_y = c_0 \frac{\partial E_z}{\partial x} \quad (36.c)$$

Employing the same procedure in the previous section D, and H values becomes

$$D_z^{n+1/2}(i, j) = gi3(i)gj3(j)D_z^{n-1/2}(i) + gi2(i)gj2(j)0.5 \begin{bmatrix} H_y^n(i+1/2, j) - H_y^n(i-1/2, j) \\ -H_x^n(i, j+1/2) + H_x^n(i, j-1/2) \end{bmatrix}$$

In Y direction, Hy will require an implementation similar to the one used for Hx in the x direction.

$$curl_e = [E_z^{n+1/2}(i+1, j) - E_z^{n+1/2}(i, j)] \quad (37.a)$$

$$I_{Hy}^{n+1/2}(i+1/2, j) = I_{Hy}^{n-1/2}(i+1/2, j) + curl_e \quad (37.b)$$

$$H_y^{n+1}(i+1/2, j) = fi3(i+1/2)H_y^n(i+1/2, j) - fi2(i+1/2)0.5curl_e + ff1(j)I_{Hy}^{n+1/2}(i+1/2, j) \quad (37.c)$$

Finally, Hx in the x direction becomes

$$curl_e = [E_z^{n+1/2}(i, j) - E_z^{n+1/2}(i, j+1)]$$

$$I_{Hx}^{n+1/2}(i, j+1/2) = I_{Hx}^{n-1/2}(i, j+1/2) + curl_e$$

$$H_x^{n+1}(i, j+1/2) = fj3(j+1/2)H_x^n(i, j+1/2) + fj2(j+1/2)0.5curl_e + fi1(i)I_{Hx}^{n+1/2}(i, j+1/2)$$

The full set of parameters associated with the PML are,

$$fi1(i) \& ff1(j) \quad \text{from 0 to 0.333} \quad (38.a)$$

$$fi2(i), gi2(i), fj2(j) \text{ and } gj2(j) \quad \text{from 1 to 0.75} \quad (38.b)$$

$$fi3(i), gi3(i), fj3(j) \text{ and } gj3(j) \quad \text{from 1 to 0.5} \quad (38.c)$$

The PML can be turn off in the main part of the problem space by setting f_{i1} and f_{j1} to 0, and other parameters to 1.

The free space equations for D and H in three dimensions are,

$$\frac{\partial D_x}{\partial t} = \frac{1}{\sqrt{\epsilon_0 \mu_0}} \left(\frac{\partial H_z}{\partial y} - \frac{\partial H_y}{\partial z} \right) \quad (39.a)$$

$$\frac{\partial D_y}{\partial t} = \frac{1}{\sqrt{\epsilon_0 \mu_0}} \left(\frac{\partial H_x}{\partial z} - \frac{\partial H_z}{\partial x} \right) \quad (39.b)$$

$$\frac{\partial D_z}{\partial t} = \frac{1}{\sqrt{\epsilon_0 \mu_0}} \left(\frac{\partial H_y}{\partial x} - \frac{\partial H_x}{\partial y} \right) \quad (39.c)$$

$$\frac{\partial H_x}{\partial t} = \frac{1}{\sqrt{\epsilon_0 \mu_0}} \left(\frac{\partial E_y}{\partial z} - \frac{\partial E_z}{\partial y} \right) \quad (39.d)$$

$$\frac{\partial H_y}{\partial t} = \frac{1}{\sqrt{\epsilon_0 \mu_0}} \left(\frac{\partial E_z}{\partial x} - \frac{\partial E_x}{\partial z} \right) \quad (39.e)$$

$$\frac{\partial H_z}{\partial t} = \frac{1}{\sqrt{\epsilon_0 \mu_0}} \left(\frac{\partial E_x}{\partial y} - \frac{\partial E_y}{\partial x} \right) \quad (39.f)$$

The development of the PML for three dimensions closely follows the two dimensional version. The only difference is that we have to deal with three directions instead of two.

For instance (36.a) becomes

$$j\omega \left(1 + \frac{\sigma_x(x)}{j\omega\epsilon} \right) \left(1 + \frac{\sigma_y(y)}{j\omega\epsilon_0} \right) \left(1 + \frac{\sigma_z(z)}{j\omega\epsilon_0} \right)^{-1} D_z = c_0 \left(\frac{\partial H_x}{\partial x} - \frac{\partial H_x}{\partial y} \right) \quad (40)$$

Implementing it will closely follow the two dimensional development. Start by rewriting Eq. 40 as,

$$j\omega \left(1 + \frac{\sigma_x(x)}{j\omega\epsilon}\right) \left(1 + \frac{\sigma_y(y)}{j\omega\epsilon_0}\right) D_z = c_0 \left(1 + \frac{\sigma_z(z)}{j\omega\epsilon_0}\right) \left(\frac{\partial H_y}{\partial x} - \frac{\partial H_x}{\partial y}\right) \quad (41)$$

$$= c_0 \text{curl}_z h + c_0 \frac{\sigma_z(z)}{\epsilon_0} \frac{1}{j\omega} \text{curl}_z h$$

$$\text{Let } I_{Dz} = \frac{1}{j\omega} \text{curl}_z h$$

Which is an integration when it goes to the time domain. Thus above Eq. becomes

$$j\omega \left(1 + \frac{\sigma_x(x)}{j\omega\epsilon}\right) \left(1 + \frac{\sigma_y(y)}{j\omega\epsilon_0}\right) D_z = c_0 \left(\text{curl}_z h + \frac{\sigma_z(z)}{\epsilon_0} I_{Dz}\right) \quad (42)$$

The implementation of this into FDTD parallels that of the two dimensional PML, except the right side contains the integration term I_{Dz} . Therefore following the previous procedure we get,

$$\text{curl}_z h = \begin{bmatrix} H_y^n(i+1/2, j, k+1/2) - H_y^n(i-1/2, j, k+1/2) \\ H_x^n(i, j+1/2, k+1/2) + H_x^n(i, j-1/2, k+1/2) \end{bmatrix} \quad (43.a)$$

$$I_{Dz}^n(i, j, k+1/2) = I_{Dz}^{n-1}(i, j, k+1/2) + \text{curl}_z h \quad (43.b)$$

$$D_z^{n+1/2}(i, j, k+1/2) = g13(i)g3(j)D_z^{n-1/2}(i, j, k+1/2) + g12(i)g2(j)0.5(\text{curl}_z h + gk1(k)I_{Dz}^n(i, j, k+1/2)) \quad (43.c)$$

The I_{Dz} is a three dimensional array that is dimensioned throughout the problem space, but used only at two edges. The three dimensional implementation will have a total of six such arrays, which clearly is a waste of computer resources. For this reason, I_{Dz} will be broken up into small three-dimensional arrays, defined at the low values of k and one defined at the high values of k . Similarly equations for D_x , D_y , H_x , H_y , H_z can

be derived. In the iterative FDTD algorithm, values of D are computed first and then E is computed as,

$$E_x = g_{ax} D_x$$

$$E_y = g_{ay} D_y$$

$$E_z = g_{az} D_z$$

$$\text{Where } g_{ax} = g_{ay} = g_{az} = 1 / (\epsilon_r + (\sigma^* dt / \epsilon_0))$$

This is a medium dependent parameter. In the case of PECs (Perfect Electric Conductor), one can easily define it by making g_{ax} , g_{ay} and g_{az} as zero so that the respective field components of E becomes zero, thus the boundary conditions for PEC are automatically assigned in the computation. The components of H are computed from the computed E values.

4.5 Lubbers feed model for fast FDTD convergence

With the transient excitation in FDTD, impedance and scattering parameters over a wide frequency band can be calculated. One difficulty with FDTD is that for some applications, few thousands of time steps may be required for the transient fields to decay. This difficulty is common in the case of circuits having very high quality factor. One method to reduce the time steps required is to apply signal processing methods to predict the voltages and currents at later times from the results computed for early times. Instead of making FDTD calculations for the full number of time steps required for transients to dissipate, one might make actual FDTD calculations for some fraction of this total number of time steps, and use these results to predict those for the later times [9].

Applying the various prediction methods adds additional complexity to the FDTD calculation process. The prediction methods are complicated, and may require care and skill to obtain accurate results. Most of the methods described require the use to determine the order of the prediction process, related to the number of terms of whatever expansion function is used to approximate the FDTD time signal. A poor choice for the order of the prediction model can result in larger precision errors.

Another simple approach is to include a source resistance in the excitation signal source. This can considerably reduce the large time steps required in the simulation. The source resistance value which is equal to the characteristic impedance of the system is usually employed.

4.5.1 Resistive source model

FDTD transient calculations are often excited by a hard voltage source, whose internal source resistance is zero ohms. These sources are very easy to implement in an FDTD code. The electric field at the mesh edge where the source is located is determined by some function of time rather than by the FDTD update equations. A common choice is a Gaussian pulse, but other functions may also be used. The Gaussian pulse is significantly greater than zero amplitude for only a very short fraction of the total computation time, especially for resonant geometries such as many antennas and microstrip circuits.

Once the pulse amplitude drops the source voltage becomes essentially zero, the source effectively becoming a short circuit. Thus, any reflections from the antenna or circuit which return to the source are totally reflected. The only way the energy introduced into the calculation space can be dissipated is through radiation or by absorption by lossy media or lumped loads. For resonant structures, there are frequencies for which this radiation or absorption process requires a relatively long time to dissipate the excitation energy. Using a source with an internal resistance to excite the FDTD calculation provides an additional loss mechanism for the calculations.

Consider that it is desired to excite an FDTD calculation with a voltage source that corresponds to an electric field E in the z direction at a certain mesh location $i_s \Delta x, j_s \Delta y, k_s \Delta z$, described using the usual Yee notation. The corresponding equivalent circuit for a voltage source which includes an internal source resistance R_s is illustrated in Fig. 4.3. If the source resistance R_s is set to zero then the usual FDTD electric field at the source location is simply given by

$$E_s''(i_s, j_s, k_s) = \frac{V_s(n\Delta t)}{\Delta z} \quad (44)$$

V_s is any function of time, often a Gaussian pulse.

However, with the source resistance included, the calculation of the source field $E_s''(i_s, j_s, k_s)$ at each time step is complicated slightly. To determine the terminal voltage V of Fig. 4.3 and, thus, the FDTD electric source field $E_s''(i_s, j_s, k_s)$, the current through the source must be determined. This can be done by Ampere's circuital

law, taking the line integral of the magnetic field around the electric field source location.

The current through the source is then given by

$$I_s^{n-1/2} = (H_x^{n-1/2}(i_s, j_{s-1}, k_s) - H_x^{n-1/2}(i_s, j_s, k_s))\Delta x + (H_y^{n-1/2}(i_s, j_s, k_s) - H_y^{n-1/2}(i_{s-1}, j_s, k_s))\Delta y \quad (45)$$

so that by applying Ohm's law to the circuit of Fig. 4.3 the electric source field is given by

$$E_s^n(i_s, j_s, k_s) = \frac{V_s(n\Delta t)}{\Delta z} + \frac{I_s^{n-1/2} R_s}{\Delta z} \quad (46)$$

If $R_s=0$, in this equation, then the usual hard-voltage source results. The value of the internal resistance does not appear to be critical. A reasonable choice for R_s is to use the value of the characteristic impedance of the transmission line.

4.5.2 Staircase transition for microstrip line feed

The antenna discussed in thesis uses a microstrip line as the feed. In order to model the microstrip line, the substrate thickness is discretized as more than one Yee cell. The excitation field is to be applied to the cell between the top PEC of the strip line and the PEC ground plane. In order to obtain a gap feed model, a staircased mesh transition as shown in the Fig. 4.4 is used in FDTD.

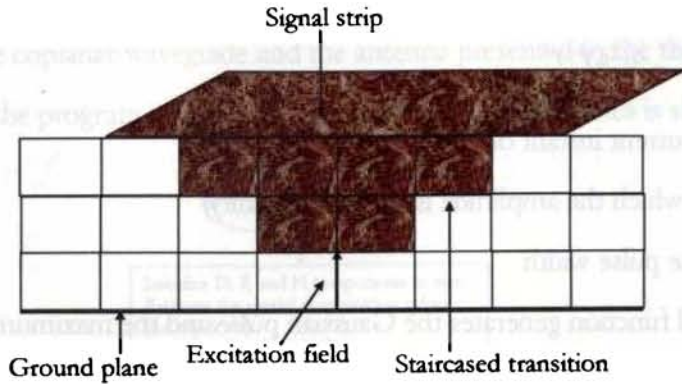


Fig. 4.4 FDTD Staircased feed model for microstrip line in FDTD

In the figure the darkened portions are treated as PEC. This staircased configuration results a gap model between the top strip and ground plane. The excitation field is shown as arrow in the figure. The stair case model transition from the electric field feed to the microstrip line at the top is used to provide a relatively smooth connection from the single feed location to the microstrip.

4.6 Excitation functions

A variety of excitation functions such as Gaussian pulse, sinusoidal, sine modulated by a Gaussian can be used to excite a system in FDTD computation. Gaussian pulse and sinusoidal functions are used in the thesis to analyze the problem. Gaussian pulse excitation gives a broadband response of the problem. But sinusoidal function provides a single frequency response, and thus a frequency sweep has to be used for broadband frequency response.

4.6.1 Gaussian pulse function

A Gaussian pulse can be expressed as,

$$E(t) = e^{-(t-t_0)^2/T^2}$$

Where t is the current instant of time

t_0 is the time at which the amplitude is maximum (unity)

T determines the pulse width

The exponential function generates the Gaussian pulse and the maximum of the pulse reaches at the instance when $t = t_0$.

The parameter T is very significant in the FDTD simulation. Because the pulse width determines the frequency up to which the simulation is accurate. When the pulse width is narrow, broad band simulation can be attained.

4.6.2 Sine function

Sinusoidal excitations are important while computing the E/H field values for a particular frequency of interest. A function of the following form is termed as sine function.

$$E(t) = E_0 \sin(2\pi ft)$$

Where E_0 determines the peak amplitude (usually unity)

' t ' is the current instant of time and ' f ' is the frequency of operation

4.7 General flow chart of FDTD algorithm

The MATLAB based computer codes were developed to study the resonant behavior of the coplanar waveguide and the antenna presented in the thesis. The general flow chart for the program to calculate the return loss characteristics is shown in Fig. 4.5.

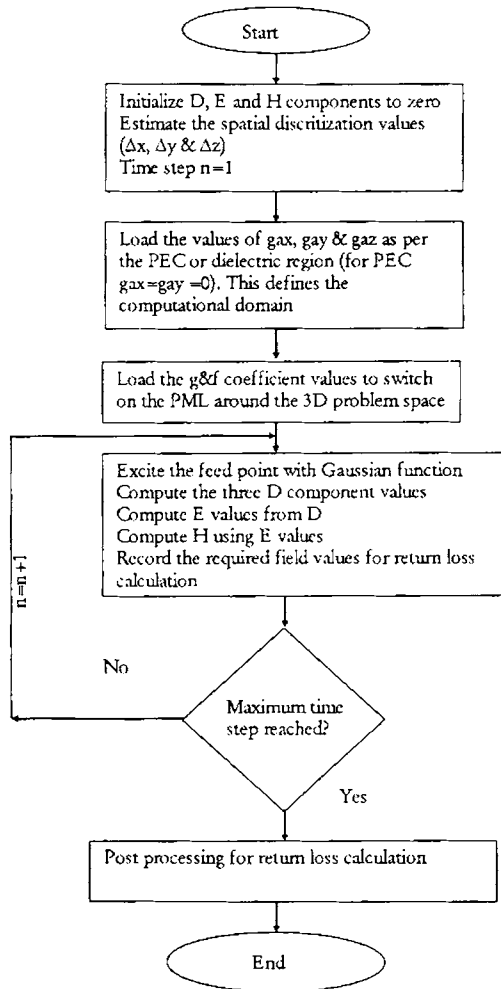


Fig. 4.5 FDTD Flow chart

4.8 Return loss calculation

To obtain the return loss at the feed point, the incident and reflected waveforms must be known. The FDTD simulation calculates the sum of incident and reflected waveforms. To obtain the actual value of reflected waveform, the computed waveform at the feed point is recorded, and is now subtracted from the incident pulse to obtain the reflected value. All the two waveforms are in time domain. The return loss value can be obtained as,

$$\text{Returnloss}(dB) = 20 \log \frac{FFT(\text{Reflected wave})}{FFT(\text{Incident wave})}$$

Usually the excitation is given as the E field component in the computation. Thus the reflected and incident waveforms are the time domain values of E field component.

4.9 References

- 1 K. S. Yee, "Numerical solution of initial boundary value problems involving Maxwell's equations in isotropic media," *IEEE Transactions on Antennas and Propagation*, AP-14, 4, pp. 302-307, 1966.
- 2 X. Zhang and K. K. Mei, "Time domain finite difference approach to the calculation of the frequency dependent characteristics of microstrip discontinuities," *IEEE Trans. Microwave Theory Tech.*, vol. 36, pp. 1775-1787, Dec. 1988.
- 3 Hallond, R, and J. W. Williams, Total field versus scattered field finite difference codes: A comparative Assessment, *IEEE Transactions*, Vol. 30, 1983, pp. 4583-4588.
- 4 Enquist and Majada, Absorbing Boundary Conditions for the Numerical simulation of waves, *Mathematics of computation*, Vol. 31, 1977, pp. 629-651.
- 5 Mur G, Absorbing boundary conditions for the Finite Difference Approximation of the Time domain Electromagnetic field equations, *IEEE Transactions EMC-23*, 1981, pp. 377-382.
- 6 J.P. Berenger, A perfectly matched layer for the absorption of EM waves, *J. Computational Physics*, Vol. 114, 1994, pp. 185-200
- 7 Sullivan Dennis M, *Electromagnetic simulation using the FDTD method*, IEEE press series on RF and Microwave Technology, USA
- 8 Z. S Sacks, D. M. Kingsland, R. Lee, and J.F. Lee, A perfectly matched anisotropic absorber for use as an absorbing boundary condition, *IEEE Transactions on Antennas and Propagation*, Vol. 43. December 1995, pp. 1460-1463.
- 9 V. Jandhyala, E. Michielssen, and R. Mittra, FDTD signal extrapolation using the forward-backward autoregressive model, *IEEE Microwave and guide wae letters*, Vol. 4, June 1994, pp. 163-165.

Investigations on Coplanar Waveguides (CPW)

The fundamental investigations towards the development of a coplanar antenna are described in this chapter. An open circuit coplanar waveguide is rigorously analyzed theoretically and experimentally to bring out certain important conclusions regarding the excitation of resonant/radiation phenomena in offset fed open circuit coplanar waveguides. This chapter is the foundation of the ‘coplanar antenna’ described in the succeeding chapter.

5.1 Introduction

Any transmission line can be configured as a radiating system by properly modifying its structural parameters and feed point, to obtain radiation from large discontinuities. The structural and feed point modifications can change the transmission line properties to a great extent. The system then becomes a pure radiating system rather than an energy guiding device. The mode excited and the impedance characteristics may change. This idea is applied to a Coplanar Waveguide to radiate electromagnetic energy. At resonance the input impedance conjugately matched to the impedance of the excitation source, maximum power is delivered to the device and hence improve the reflection efficiency. This chapter presents the results of the investigations carried out to find the resonance/radiation phenomena in coplanar waveguides (CPW) catering to the need of compact antennas. Investigations on open circuit CPW with finite ground conductor show that it excites a spurious resonant mode due to the length and width of the finite lateral ground strips and centre strip. But this resonant system is not compact compared to the operating wave length, resulting a bulky radiating system. More over, the radiation efficiency, gain and radiation pattern are very poor. Theoretical investigations on an open circuit CPW with feed offset delivered an interesting result. The device excites a resonant mode, which offers a highly compact radiating structure compared to the operating wavelength. The excellent radiation characteristics assure that the CPW with offset feed is a suitable configuration as a radiating system for compact microwave systems, where size of the antenna is a major concern. The FDTD computation results of the electric field in the structure give more insight into the radiation mechanism of the problem. Parametric analysis is also presented to confirm the phenomenon. Finally the equivalent circuit representation of the offset fed CPW structure is presented to explain the resonance behavior.

5.2 Resonance and radiation from finite ground open circuit CPW

Consider a CPW printed on a dielectric substrate of relative permittivity ϵ_r and thickness h . The CPW is excited at one end, and the other end is open circuited. The top view and crosssectional view of the CPW geometry are shown in Fig. 5.1.

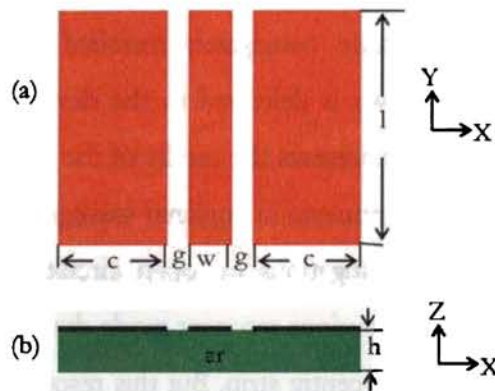


Fig. 5.1 Geometry of open circuit CPW
 a) Top view
 b) Cross sectional view

The device is excited with a Sub Miniature Amphenol (SMA) connector. This is a bound mode, and no radiation is expected to come out of the structure. When an open circuited CPW is excited, standing wave pattern is formed in the structure. The reflection coefficient is nearly 1 for this case. This is not the case for all frequencies. At higher frequencies the device exhibit low values of reflection coefficient. That is the input impedance of the device approaches the source impedance (50Ω). Resonance/radiation phenomena at higher microwave bands due to the influence of the

centre strip and ground strip dimensions are observed. The radiation characteristics of the device and parametric analysis results are also performed to confirm the radiation/resonance on the CPW.

5.2.1 Return loss characteristics

A typical CPW of length $l=20$ mm designed for $50\ \Omega$ characteristic impedance has the dimensions $w=3$ mm, $g=0.5$ mm, $c=15$ mm when printed on FR₄ substrate of $\epsilon_r=4.7$ and thickness $h=1.6$ mm. Measured and FDTD calculated return loss characteristics of open circuited CPW is shown in Fig. 5.2.

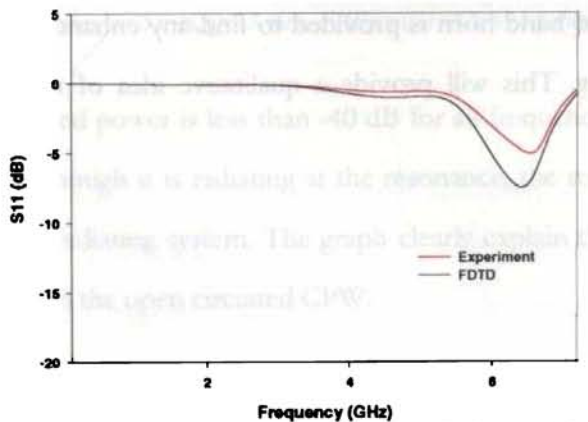


Fig. 5.2 Return loss characteristics of CPW designed for $50\ \Omega$ characteristics impedances $l=20$ mm, $w=3$ mm, $g=0.5$ mm, $c=15$ mm, $\epsilon_r=4.7$, $h=1.6$ mm.

The return loss characteristics shown in the figure indicates that the device behaves as a pure transmission line up to 5.5 GHz. The characteristics are akin to an open circuited transmission line. Above 5.5 GHz, return loss characteristics of the device changes slightly. The return loss value of -5 dB is observed at 6.5 GHz. This indicates that there is a tendency of resonance on the structure even when the other port of the

device is open circuited. So there is a possibility of power radiation from this type of structure. Note that the device dimensions are large compared to the wavelength at the resonant frequency. That is why this behavior is not suitable for compact antenna applications.

5.2.2 Far field radiation

The far field radiation characteristic of the antenna is analyzed to study more details of afore said resonance and is shown in Fig5.3. The received power at the resonance along the maximum radiation direction is shown in the figure. The far field received power by a broad band horn is provided to find any enhanced received power at the resonant frequency. This will provide a qualitative idea of radiation from the system.

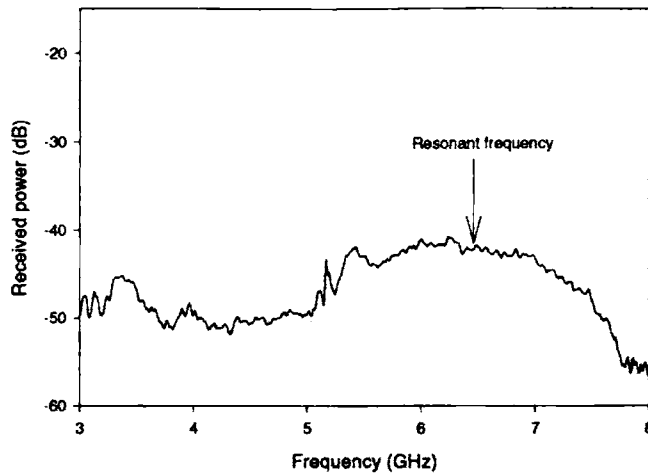


Fig. 5.3 Far field radiation received from CPW using standard horn antenna $l=20$ mm, $w=3$ mm, $g=0.5$ mm, $c=15$ mm, $\epsilon_r=4.7$, $h=1.6$ mm.

The received power is less than -40 dB for all frequencies except at the resonant frequency. Even though it is radiating at the resonance, the received power is very low, exhibiting a poor radiating system. The graph clearly explain that there is little radiation around 6GHz from the open circuited CPW.

5.2.3 3D radiation pattern

The computed 3D gain radiation pattern obtained from IE3D simulation is shown in Fig. 5.4.

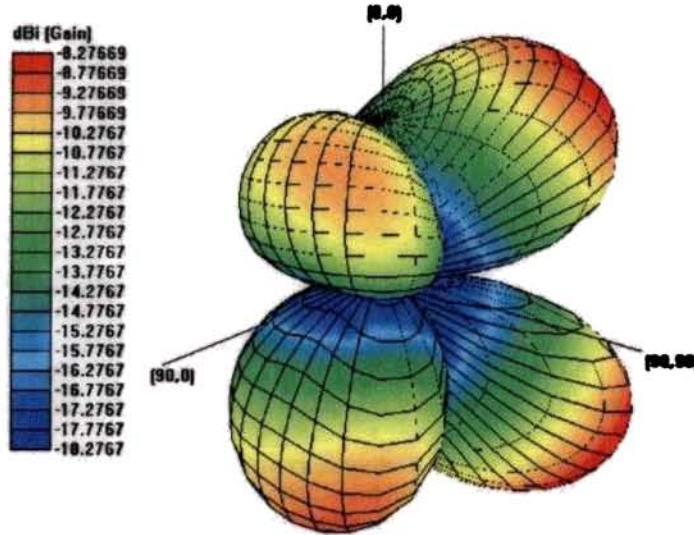


Fig. 5.4 Computed 3D radiation pattern of the CPW at the resonance (5.5 GHz) $l= 20 \text{ mm}$, $w=3 \text{ mm}$, $g=0.5 \text{ mm}$, $c=15 \text{ mm}$, $\epsilon_r=4.7$, $h=1.6 \text{ mm}$.

The radiation pattern is found to have four lobes and not radiating along the broad side direction (ie, $\theta=0$, $\Phi=0$) . The distorted radiation pattern indicates that the device as such is not suitable for mobile terminal applications, where omni direction radiation coverage is very important. This shows that we have to manipulate the antenna geometry to achieve the omni directional radiation coverage.

5.2.4 Gain and Efficiency

The return loss value at the resonance indicates that the device does not matched to the source. The estimated gain of the system is only -8.2 dBi at the resonant frequency, and not suitable as a radiator. The computed efficiency is only 20% at the resonance. The estimated gain and efficiency of the antenna indicates that the device is

not suitable as a radiator in its present form. The effect of structural parameters on the efficiency and gain should be investigated in order to confirm the resonant characteristics completely.

It is found from the parametric analysis that length 'l' has influence on the resonant frequency. The resonant condition is more pronounced only when the finite ground width CPW is considered. Width of the centre strip is also influencing the resonance. Impedance matching at the resonance becoming worse as 'g' increases. Since the fields in the structure are not completely interacting with dielectric material, appreciable change in the resonant frequency is not observed with change in the substrate dielectric constant.

5.2.5 Conclusions

The investigations to find out an efficient, compact radiating structure revealed a possibility of radiation phenomena in CPWs. The conclusions from the study are as follows;

1. When the frequency of operation is sufficiently high, open circuited CPWs excites a resonant mode.
2. The resonant frequency is more influenced by the structural parameters such as l, w, and c.
3. The dimension 'g' affects the impedance matching at resonance
4. The efficiency of the system is very low (nearly 20%)
5. Maximum gain observed is -2.1 dBi when the centre strip width is large.
6. Radiation pattern is highly distorted.

5.3 Resonance and radiation in offset fed open circuit CPW

In conventional coplanar waveguide design width of the center strip is always kept small and thus surface current orthogonal to the direction of power flow is negligible. It is also well known that the field distributions in the two slots of the conventional CPWs are out of phase when excited by an SMA connector. They cancel at the far field and thus no radiation along the bore sight direction is expected from the device. On the other hand if both the slots are having in phase field distribution then there may be radiation from the structure. This is not possible with the conventional CPW feeding schemes. But when a conventional open circuited CPW is excited with a feed offset, then a new resonant mode is excited in the structure, at lower microwave bands. In this case the dimensions are very small compared to the operating wavelength of the new resonance.

The device works purely as a resonant system other than an open circuited transmission line at this frequency. That is resonance formed in the structure may bring down the input impedance, even though the other end of the structure is open circuit. In other words the CPW transmission line is transformed to a CPW antenna. FDTD method is employed to study the resonant and radiation characteristics of the device numerically. FDTD method provides a complete understanding of the field at the two slots of the device. Odd mode and even mode excitation schemes are separately employed to explain the behavior of the device completely.

A CPW having 50Ω characteristics impedance printed on FR4 substrate with $\epsilon_r=4.7$ and thickness 1.6 mm, having the structural parameters $w=3$ mm, $g=0.5$ mm, $c=15$ mm and $l=20$ mm is used for FDTD computation. The behavior of the system is then confirmed with parametric analysis. The radiation characteristics, equivalent circuit representation and radiation mechanism are finally explained.

5.3.1 FDTD analysis of offset fed open circuit CPW

This section explains the numerical results obtained from FDTD computation of the corner fed CPW structure. The resonance phenomenon is explained from the return loss and input impedance characteristics of the device. Radiation mechanism of the device is explained from the E field in the structure at the resonance.

5.3.1.1 Description of the problem and excitation schemes

An offset fed CPW is shown in Fig. 5.6. The structure is open circuited at the other end. The feed point is selected at the corner along the width of the signal strip.

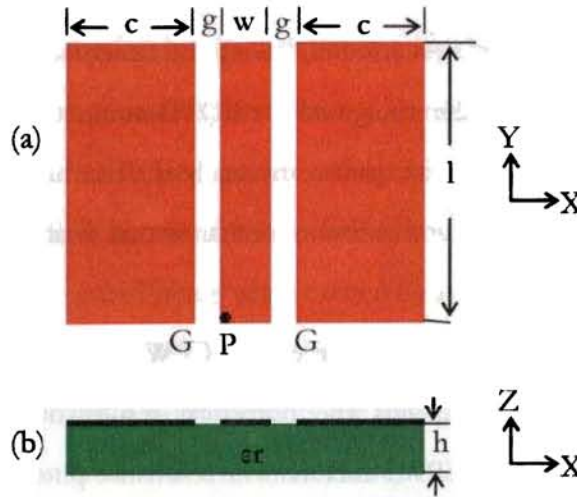


Fig.5.6 Offset fed open circuited CPW.

- a) Top view
b) Cross sectional view

The CPW designed for 50Ω characteristic impedance has the structural parameter values as described in Section 5.3. The device is designed on FR4 substrate of dielectric constant 4.7 and thickness 1.6 mm. In conventional CPWs the E-field distribution established in the two slots resembles the ‘odd modes’ in coupled slot lines. Another possibility is that the two slots establish an in phase field distribution. This is similar to ‘even mode’ E-field distribution.

The FDTD analysis computes the characteristics of the offset fed CPW for odd mode and even mode excitation separately. Note that the ‘odd mode’ and ‘even mode’ doesn’t refer to the odd and even modes in coupled slot lines. But the electric field

distributions in the slots are similar to that established in coupled slot lines. Fig. 5.7 represents the odd mode and even mode excitation schemes employed in FDTD.

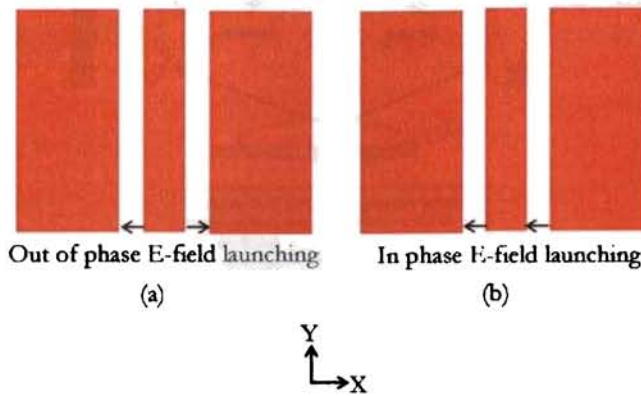


Fig.5.7 Odd mode and Even mode field launching in FDTD analysis
(a) Odd mode (b) Even mode

In FDTD the excitation source is modeled based on Luebber's feed model. The source currents are first calculated. From the currents corresponding values of 'E' component at the feeding cell is calculated. The value of 'E' is then converted to 'D' by using the relation, $D = \epsilon E$.

According to the coordinate system mentioned in Fig. 5.7, the Dx component value at the two cells of the slots are assigned with excitation signal. In the case of odd mode excitation, the two signals are out of phase. Where as in even mode the two source signals are in phase. The source currents for the two feeding locations are obtained in FDTD by applying Ampere's circuital law using right hand thumb rule. The schematic representations for both the cases are shown in Fig. 5.8.

The CPW is excited at the two locations using Gaussian pulse function. The return loss value and E and H field values are separately calculated for both the schemes.

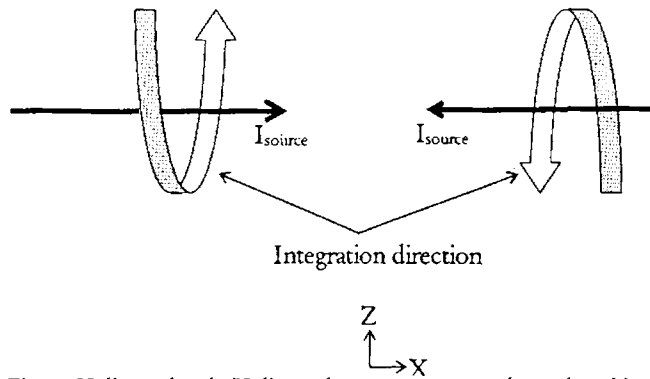


Fig.5.8 X directed and $-X$ directed source current path employed in FDTD computation

5.3.1.2 FDTD flow chart

Flow chart for the FDTD program employed to calculate the CPW characteristics such as resonant mode and E field distribution, to explain the resonance/radiation phenomena in offset fed CPW is shown in Fig. 5.9. MATLAB was used to realize the iterative algorithm of FDTD concept. The built in FFT function in MATLAB is used to compute the frequency domain characteristics of the device.

Δx , Δy and Δz in the computation domain is taken as 0.5 mm. Maximum frequency of the simulation is set as 8 GHz. So the spatial discretization is less than $\lambda/20$ of the maximum frequency of the computation. The substrate is discretized as 3 cells in the Z-direction. 10 air cells are assigned at each side of the CPW structure to simulate the practical condition in which the device is in contact with surrounding air. A layer of cells just above the strips are assigned with effective dielectric constant value as the average value of substrate dielectric constant and air to facilitate fringing field effect at the two guiding slots in the computation. 10 cells are assigned for PML ABC at each side

of the problem space. This is sufficient to effectively absorb the power at the boundary. According to the stability criteria, the calculated time step is $\Delta t=0.83$ picoseconds.

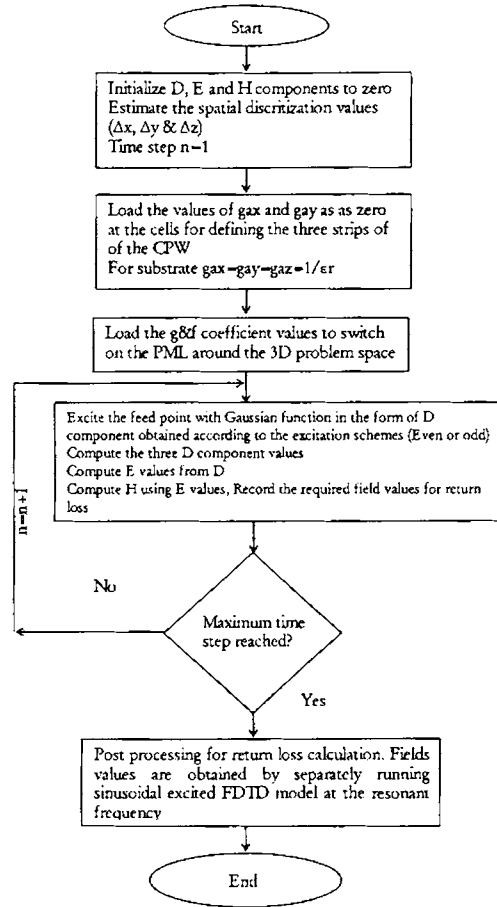


Fig. 5.9 FDTD Flow chart for the computation of offset fed CPW return loss and field distribution

The FDTD computation domain consists of a total of 108 cells in the X-direction, 80 cells in Y-direction and 43 cells in the Z-direction.

5.3.1.3 Input Gaussian pulse

FDTD computes the wideband response of the CPW by energizing it using Gaussian pulse function with pulse width of 15 picoseconds. The two slots are energized separately in order to facilitate the odd mode and even mode excitation. The time domain Gaussian pulse used to excite the CPW at the two slots, for even mode and odd mode are shown in Fig. 5.10 and 5.11.

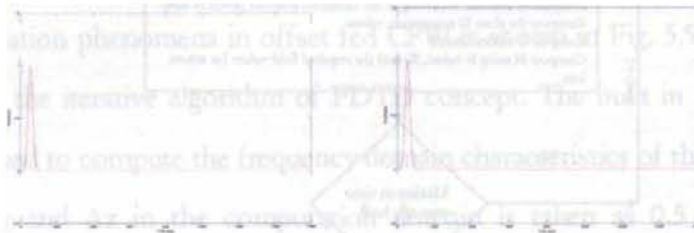


Fig.5.10 Gaussian pulse used in FDTD to excite the CPW slots for Even mode excitation scheme

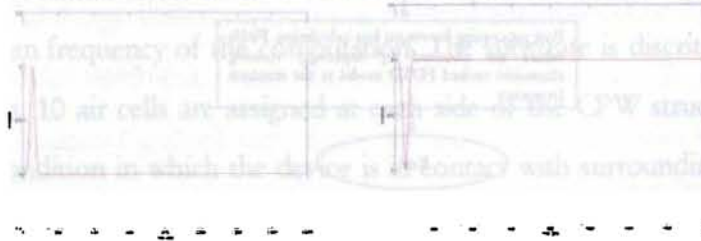


Fig.5.11 Gaussian pulse used in FDTD to excite the CPW slots for Odd mode excitation scheme

In the case of odd mode, the excitations signals are 180° out of phase with each other. The pulse width is 15 picoseconds, which is sufficient to analyze the structure up to 8 GHz. But even mode excitation is obtained by energizing CPW with in phase Gaussian pulse at the two slots. The pulse width in this case is also 15 picoseconds.

5.3.1.4. PML coefficients

The PML based D and H field FDTD equations use 18 coefficients, namely f & g coefficients. The f coefficients are used to compute H fields, where as g coefficients are used for computing D. Note the g and f values are gradually varied in such a way that the Electric and Magnetic field values at the boundary are vanishing. The g_{i1} , g_{j1} , g_{k1} and f_{i1} , f_{j1} , f_{k1} are set to zero at the computation domain except at the boundary.

In this analysis 10 cells are assigned for PML. The reflection from the boundary is very low for this value. . When PML is larger than this number, the computation slows down to a great extent. Fig. 5.12 and 5.13 depicts the f and g coefficients.

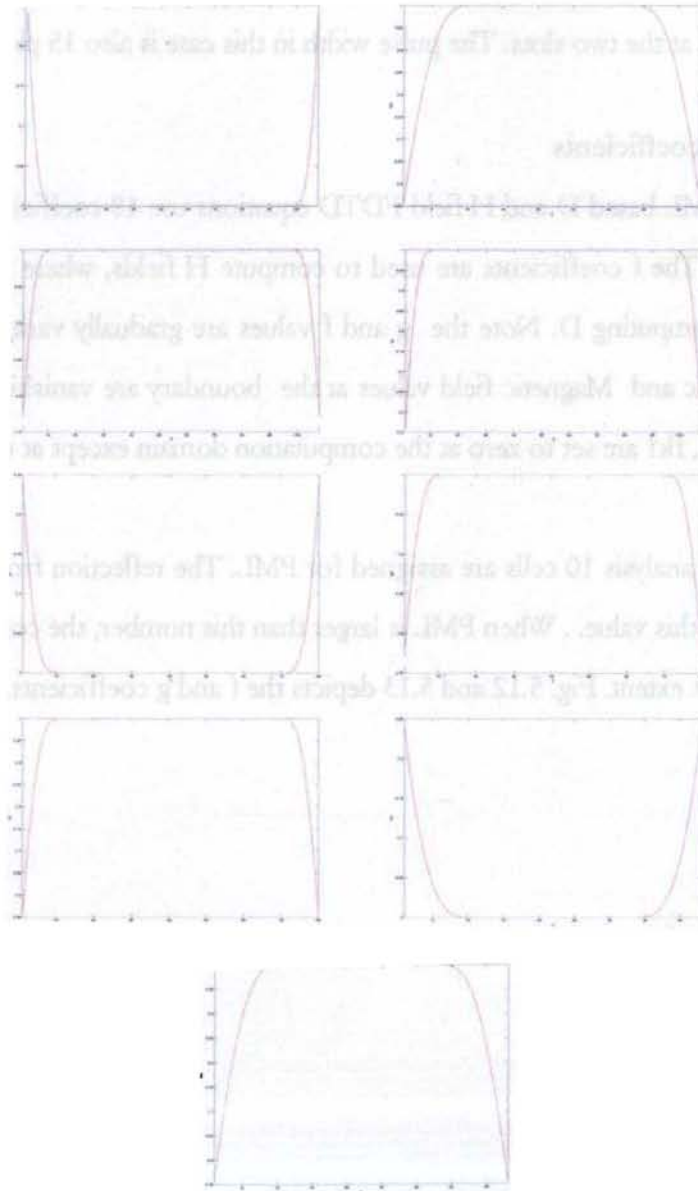


Fig.5.12 Different PML coefficients (f) used in the 3D FDTD computation

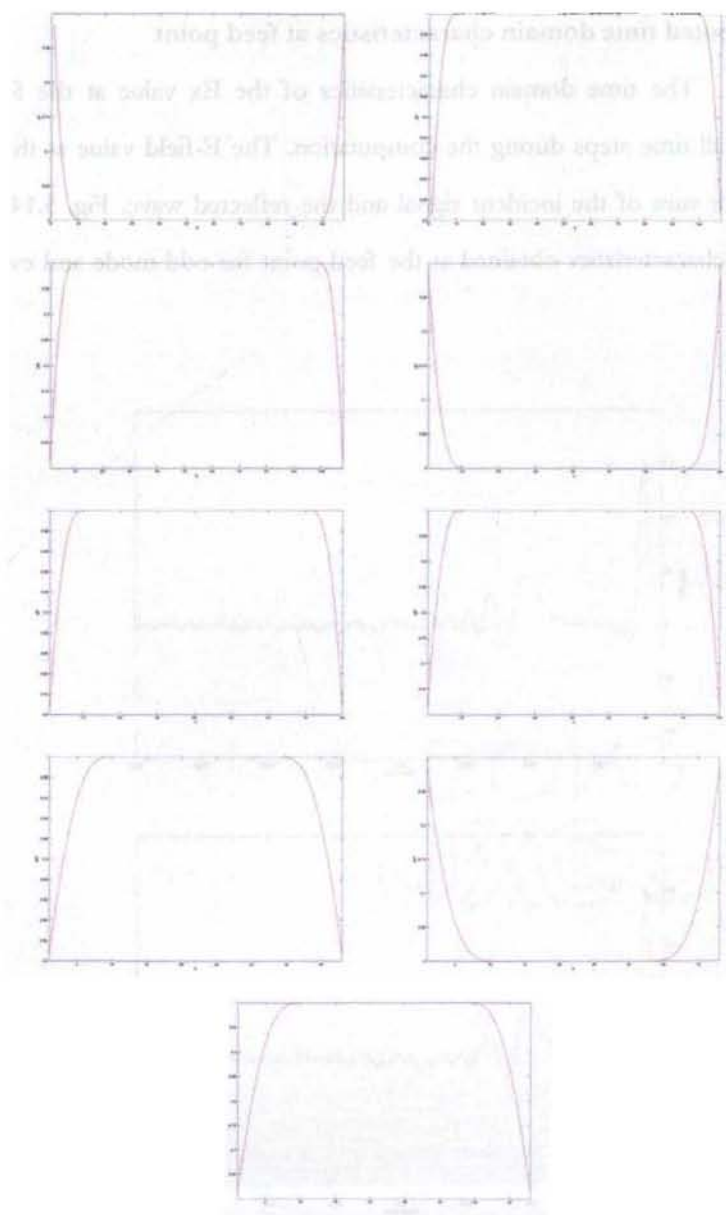


Fig.5.13 Different PML coefficients (g) used in the 3D FDTD computation

5.3.1.5 Computed time domain characteristics at feed point

The time domain characteristics of the E_x value at the feed point is recorded for all time steps during the computation. The E -field value at the feed point cell is a vector sum of the incident signal and the reflected wave. Fig. 5.14 depicts the time domain characteristics obtained at the feed point for odd mode and even mode of excitations.

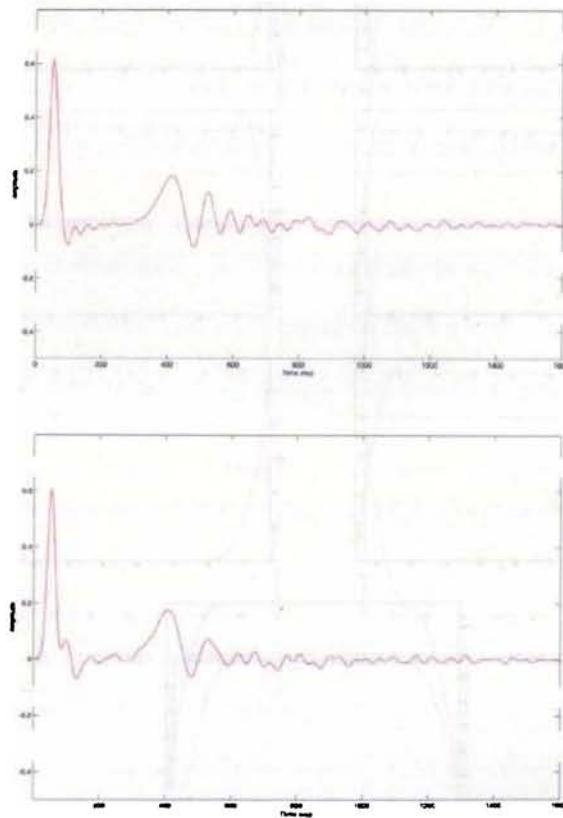


Fig.5.14 Computed time domain characteristics at the feed point for odd mode and even mode excitation

Total time steps taken to converge the computation is 1600 with 0.83 picoseconds as discretization time. Once the field value is perfectly settled down, the return loss can be computed.

The numerical results obtained from FDTD is discussed in the next sections to explain the new resonance behavior on offset fed CPWs. Experimental results are also provided in order to substantiate the theoretical findings. A CPW with offset feed analyzed using FDTD method is fabricated and tested using HP 8510C vector network analyzer. A photograph of the fabricated prototype is shown in Fig. 5.15.



Fig.5.15 Photograph of the open circuited CPW with offset feed scheme.

The device is excited using an SMA connector at one port. Offset feeding is clear from the photograph. Feed point selected is at the corner of the centre strip along 'w'. Outer conductor of SMA is soldered to the ground strips of the CPW. Measured return loss characteristics are described in the following section to explain the resonance behavior.

5.3.1.6 Return loss characteristics and input impedance

The CPW modeled using FDTD computation shows a low return loss value well below -10dB, at 2.55 GHz. The computed and measured return loss characteristics of the device are shown in Fig. 5.15.

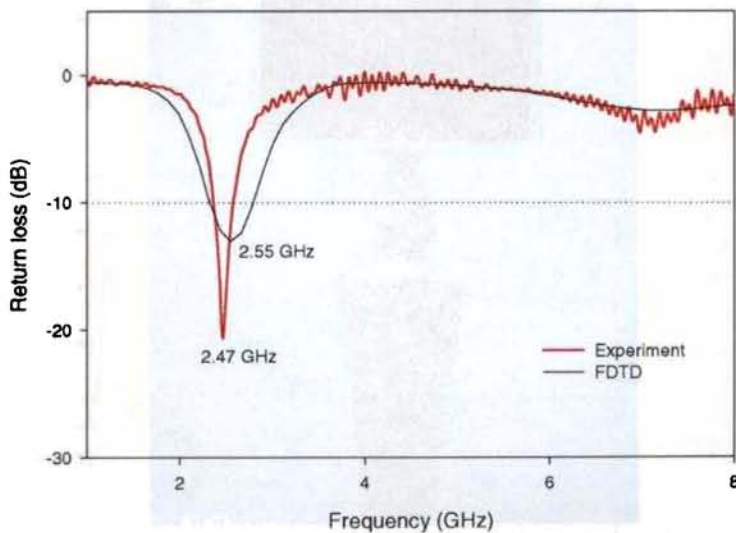


Fig.5.15 Computed and measured return loss characteristics of the open circuit CPW with offset feeding

The -10dB return loss band width is 8% ($f_c=2.47$ GHz, 2.371 to 2.572 GHz). It is worth noting that return loss value doesn't imply that the device is radiating at this frequency, but the device is accepting energy at this frequency. The spurious resonance observed in section 5.1 is also present at ~ 7 GHz with return loss value of -5 dB. The computed value differs by 3.1 % from measured values. The discrepancy in the -10 dB band width between measured and computed value is mainly due to the modeling error occurred at the gaps, and the coupling of the connector which is not considered in FDTD. The new dip in the return loss thus formed is the area of our interest because at this frequency the device is very small compared to its operating wavelength, and thus suitable for compact antenna applications. Note that the computed return loss value presented is for the even mode excitation scheme. A similar characteristic with poor return loss value (RL = -11.8 dB) is observed for odd mode excitation scheme also.

The simplest way to explain the resonant characteristics of a radiating system is to analyze the impedance characteristics of the problem at the feed point. In any resonant system the reactive components are zero at resonant frequency and the system behaves purely as resistive. But at the either sides of the resonant frequency, the reactive part of the impedance increases. One side dominates with capacitive reactance and other with inductive reactance. Fig. 5.16 shows the input impedance characteristics of the device. This is the impedance offered by the structure and thus it implies the resonant behavior of the system

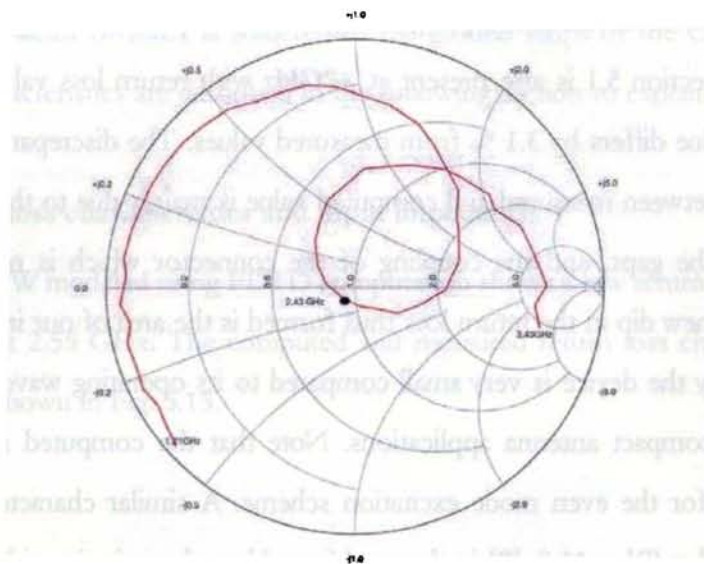


Fig.5.16 Input impedance of the open circuit CPW with feed offset

The input impedance at 2.47 GHz is approximately 50Ω with negligible value of reactive part, and it moves to either sides of the smith chart as the frequency deviates from the resonant frequency. Obviously, this behavior is similar to the resonance explained in any RLC resonant circuit. Thus it is concluded that the device works as a resonant structure other than a transmission line.

5.3.1.7 Computed fringing electric fields at the gaps

The three dimensional FDTD algorithm gives the electric and magnetic field component values at each cells. Once these values are obtained, one can explain the working of the device very easily. Because the electric and magnetic fields are responsible

for radiation of EM energy. In this study the field component values at the two gaps of the device is very important. If the device is radiating the field components in the two slots should be approximately equal in magnitude and direction. The calculated field components at the two slots (at the top layer of the substrate) are discussed below.

A. Ex component

Computed E_x components on the top layer of the CPW structure obtained for even and odd mode excitation schemes are shown in Fig. 5.17 (a) & (b). The E_x field is zero in the PEC regions. But strong E-fields exist at the two guiding slots. Note that the two slots are equally excited in the case of Even excitation scheme. Where as the amplitude of the field at the two guiding slots are slightly different in the case of Odd excitation scheme. Both the slots excite a field distribution having approximately quarter wavelength variation.

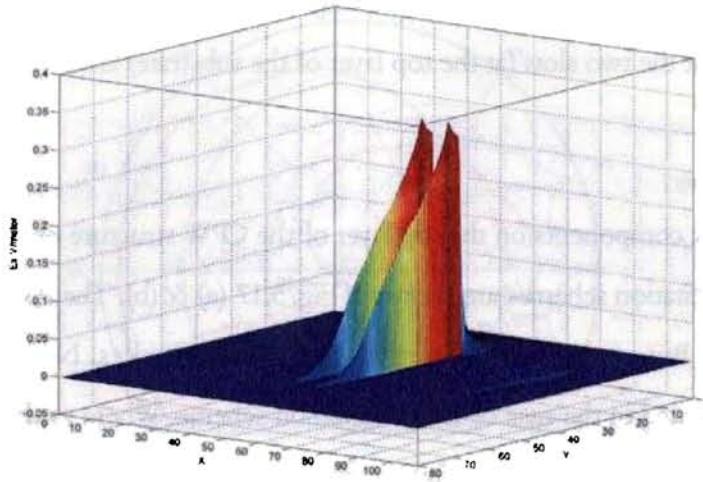


Fig.5.17 (a) Computed E_x value on the top layer of the CPW structure (Even excitation)

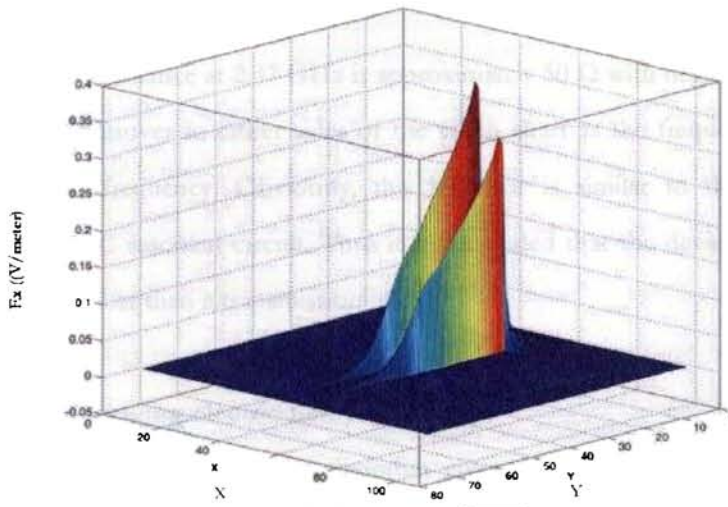


Fig.5.17 (b) Computed E_x value on the top layer of the CPW structure (Odd excitation)

B. Ey component

The E_y component obtained from FDTD computation is shown in Fig. 5.18 (a) & (b). It is observed from the two figures that there is no significant variation of electric field value along the length of the structure for both the excitation schemes. The amplitude of E_y is less than 0.05 Volts/meter in the two slots of the CPW. The longitudinal field component value at the two slots should be absent if the radiation from the device is due to the fringing fields established at the slots due to the coupling between centre strip and the lateral strips.

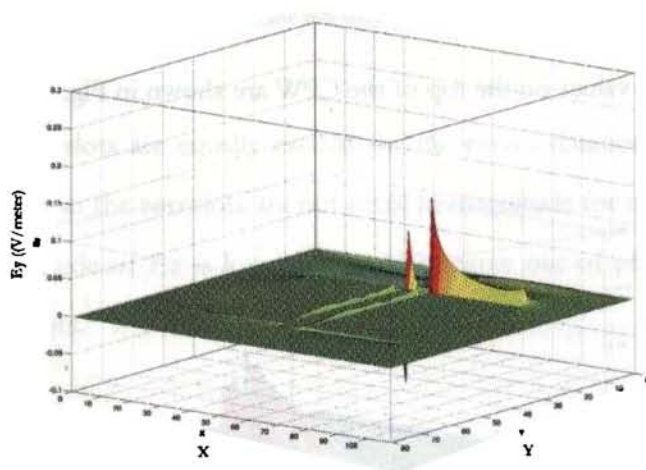


Fig.5.18 (a) Computed E_y value on the top layer of the CPW structure (Even excitation)

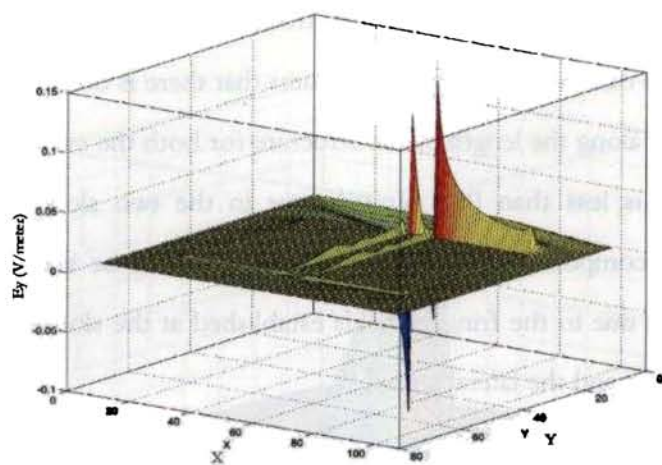


Fig.5.18 (b) Computed E_y value on the top layer of the CPW structure (Odd excitation)

E_z component

The E_z component values on the top of the CPW are shown in Fig. 5.19 (a) & (b).

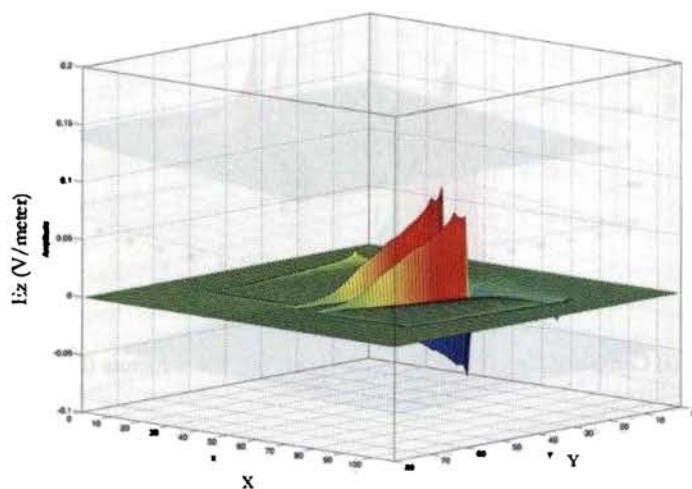


Fig.5.19 (a) Computed E_z value on the top layer of the CPW structure (Even excitation)

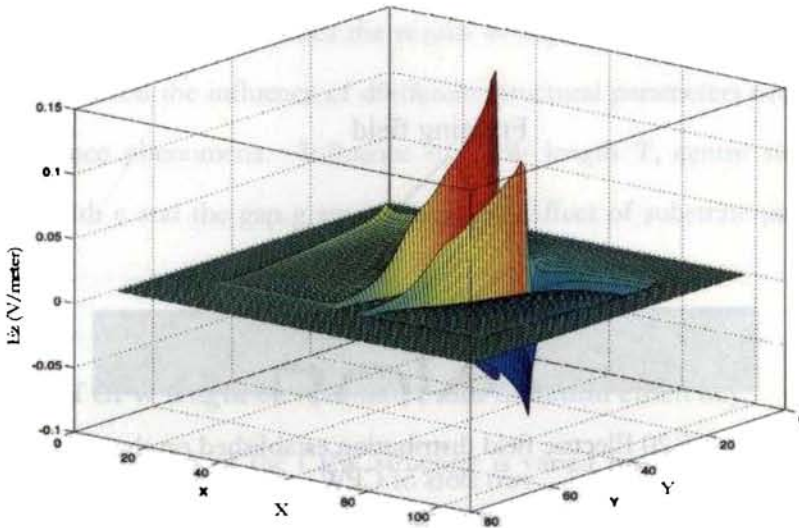
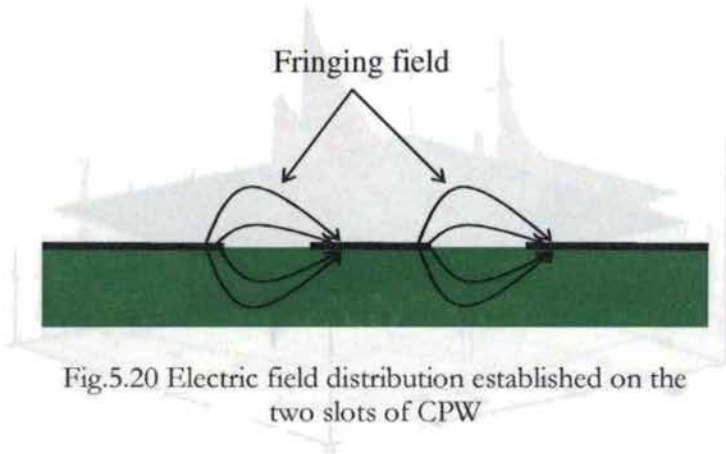


Fig.5.19 (b) Computed E_z value on the top layer of the CPW structure (Odd excitation)

The slots are equally excited for the even excitation scheme, where as the field distribution at the two slots are not equal in magnitude for the other case. It can be seen that magnitude of E_z is low and are 180 degree out of phase at the identical points in the two slots.

The inferences obtained from the E-field distribution indicates that there are only E_x and E_z field components existing at the two slots during both the excitation schemes. The E_y value is significantly low. The 180 degree out of phase E_z values will be cancelled at the far field. This strongly indicates that the radiation from CPW structure at the resonance will be due to the fringing fields from the centre strip to the lateral ground strips. The pictorial representation of the E-field distribution established on the two slots is shown in Fig. 5.20.



5.3.1.8 Conclusion

The FDTD analysis and the measured values of return loss concludes that a resonance phenomena is observed on an open circuit conventional CPW with offset feeding mechanism. The input impedance behavior strongly supports the argument that the impedance matching obtained at the lower microwave band is due to resonance excited on the structure. The return loss observed has -10 dB band width of 8%. The detailed investigations on E_x , E_y and E_z field components revealed that the two slots excites an in phase E - field distribution. Following section explains the parametric analysis of the offset fed CPW structure to reveal the resonant phenomena very clearly.

5.4 Parametric analysis

This section describes the results of experimental as well as theoretical investigations to reveal the influence of different structural parameters of the CPW on the new resonance phenomena. Influence of CPW length l , centre strip width w , ground strip width c and the gap g are investigated. Effect of substrate parameters are also presented.

5.4.1 Effect of CPW length on resonance and radiation efficiency

The length of the CPW structure is varied from 14 mm to 20 mm to study its effect on the resonant frequency and radiation efficiency of the structure. The variation of the resonant frequency and the radiation efficiency with different CPW length are depicted in Fig. 5.21.

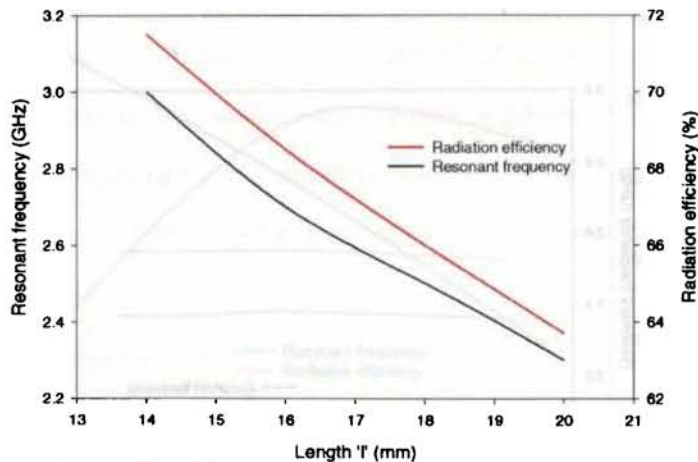


Fig. 5.21 Effect of CPW length on resonant frequency radiation efficiency

The resonant frequency is varying almost linearly with ℓ . As ℓ increases, resonant frequency decreases. It can be seen that a 130 MHz frequency change is observed for 1 mm change in ℓ . This is a drastic variation. The radiation efficiency of the system is also varying with ℓ . The variation is almost linear. As ℓ increases radiation efficiency decreases. The FDTD computation reveals the fact that large variation in magnitude of E-field is observed at the two slots when ℓ is increased sufficiently large. This will slightly bring down the radiation efficiency. Note that ℓ is varied symmetrically for the three strips.

5.4.2 Effect of ground strip width on resonance and radiation efficiency

Influence of the ground strip width on the new resonant phenomena is presented in this section. The width ' c ' is varied from 10 mm to 16 mm to study its effect on resonant frequency and the radiation efficiency of the device. Fig. 5.22 shows the influence of ' c ' on these parameters.

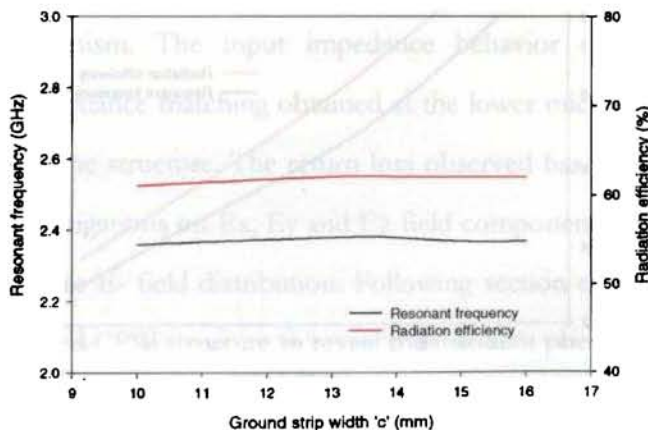


Fig. 5.22 Effect of ground strip width on resonant frequency radiation efficiency

It is clear from the graph that variation of resonant frequency with 'c' is negligible. When 'c' varies from 10 mm to 16 mm the resonance shifts slightly from 2.36 GHz to 2.37 GHz. This is a very small change and it can be concluded that effect of 'c' on the resonant frequency is negligible. The radiation efficiency remains constant through out this observation. The FDTD analysis indicates that radiation of the resonant mode is only due to the length of the equally excited two gaps of the CPW. The variation of 'c' is not affecting the length of the two slots. Thus the radiation efficiency remains almost constant.

5.4.3 Effect of centre strip width on resonance and radiation efficiency

Effect of CPW centre strip width 'w' on the resonance and radiation efficiency is depicted in Fig. 5.23.

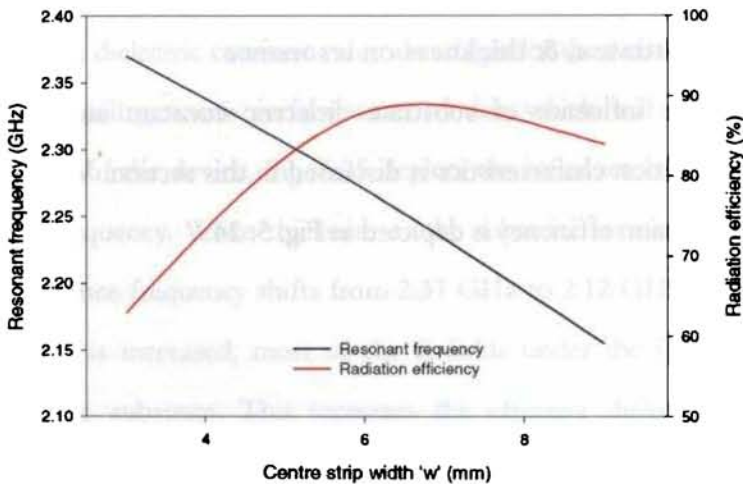


Fig. 5.23 Effect of centre strip width on the resonant frequency and radiation efficiency

Resonant frequency depends on the width 'w' of centre strip. When 'w' changes from 3 mm to 9 mm the resonant frequency decreases from 2.37 GHz to 2.16 GHz. A 35 MHz frequency shift is observed for 1 mm change in 'w'. Radiation efficiency of the structure is also varying drastically with 'w'. Radiation efficiency is found to be increasing as 'w' increases and reaches a saturation level. When $w = 6$ mm, the radiation efficiency is 88%. After 6 mm radiation efficiency is slightly decreasing. But the decline is not drastic. When 'w' increases, separation between two slots is increasing. This modifies the radiation pattern slightly.

Gap 'g' doesn't produce much effect on the resonance. But the return loss value at the resonance becoming worse as 'g' is increased above 1 mm. As 'g' increases the coupling between the ground strips and centre strip decreases. This will adversely affect the impedance matching. So 'g' is selected as 0.5 mm for all the study.

5.4.4 Effect of substrate ϵ_r & thickness on resonance

The influence of substrate dielectric constant and thickness on the resonance and radiation characteristics is discussed in this section. Variation of resonant frequency and radiation efficiency is depicted in Fig. 5. 24.

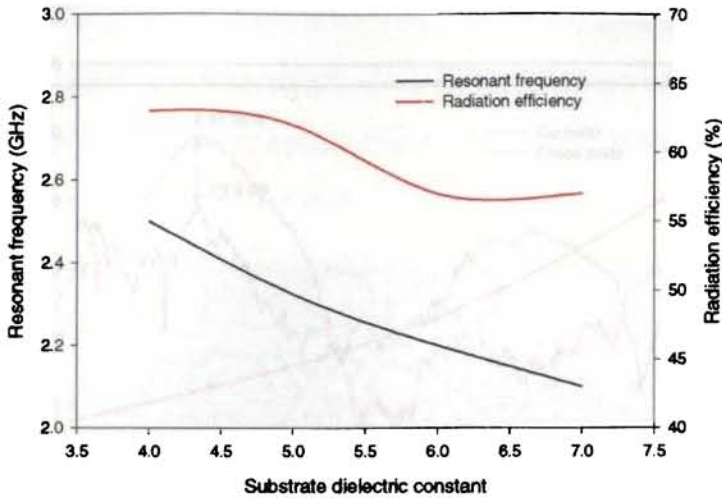


Fig. 5.24 Effect of substrate dielectric constant on resonant frequency radiation efficiency

As the relative permittivity increases the resonant frequency decreases. FDTD results reveal that the E-field components are strong in the substrate material also, especially underneath the gaps. The calculation of resonant frequency should account the effective permittivity of the medium other than the relative permittivity alone. The substrate dielectric constant value also degrades the radiation efficiency. High dielectric constant will generate surface wave modes, which will adversely affect the radiation efficiency of the device. Fig. 5.25 depicts the influence of substrate thickness on the resonant frequency. When thickness of the substrate increases from 1.6 mm to 4.6 mm, the resonance frequency shifts from 2.37 GHz to 2.12 GHz (250 MHz). When dielectric thickness is increased, most of the E-fields under the CPW structure traps inside the dielectric substrate. This increases the effective dielectric constant value slightly, and decreasing resonant frequency.

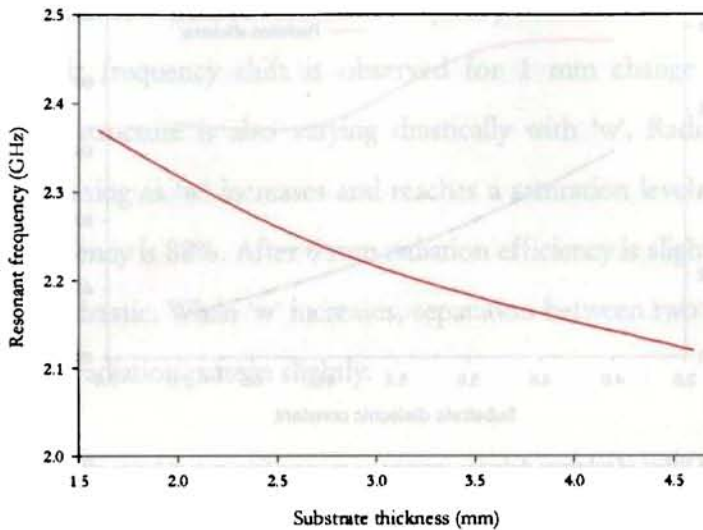


Fig. 5.25 Effect of substrate thickness on resonant frequency

5.5 Far field radiation and Polarization

The co-polar and cross polar received power from the offset fed CPW at the far field region is shown in Fig. 5.26. A standard horn antenna is used as the receiving antenna. The horn antenna is highly linearly polarized. Aim of the experiment is to study the polarization and the signal strength of electromagnetic radiation at the resonant frequency. The offset fed CPW is placed on a turn table with its feed parallel to the axis of the turn table and rotated to receive maximum power at the horn antenna. The experimental arrangement is similar to one used for gain measurement. Network analyzer is operating in S21 mode with the offset fed CPW in the transmitting mode.

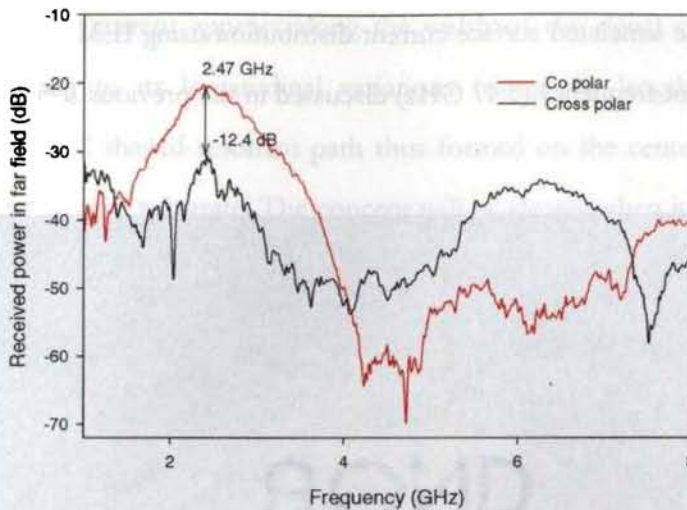


Fig. 5.26 Far field radiation received by a standard linearly polarized horn antenna Dimensions: $w=3$ mm, $g=0.5$ mm, $c=15$ mm and $l=20$ mm on FR4 substrate of $\epsilon_r=4.7$ and thickness $h=1.6$ mm

The horn antenna received maximum power in its E-plane. That is the device is radiating horizontally polarized signals. The polarization direction confirms the validity of the FDTD analysis also. The FDTD computation already explained that the fringing field is the radiating field. Moreover the tangential component of the fringing field at the two slots will be in phase. But the resolved normal component will be out of phase. Thus the normal components cancel at the far field, where as the tangential components reinforced to form the radiation. It is observed from the figure that ~ 12 dB polarization discrimination is observed. At higher frequencies the received power is feeble. When the frequency of operation is ~ 6 GHz, radiated power is slightly less. This behavior is already discussed in section 5.2 of this chapter.

5.6 Current distribution

The simulated surface current distribution using IE3D on the offset fed CPW at the resonant frequency (2.47 GHz) discussed in the previous section is shown in Fig. 5.27.

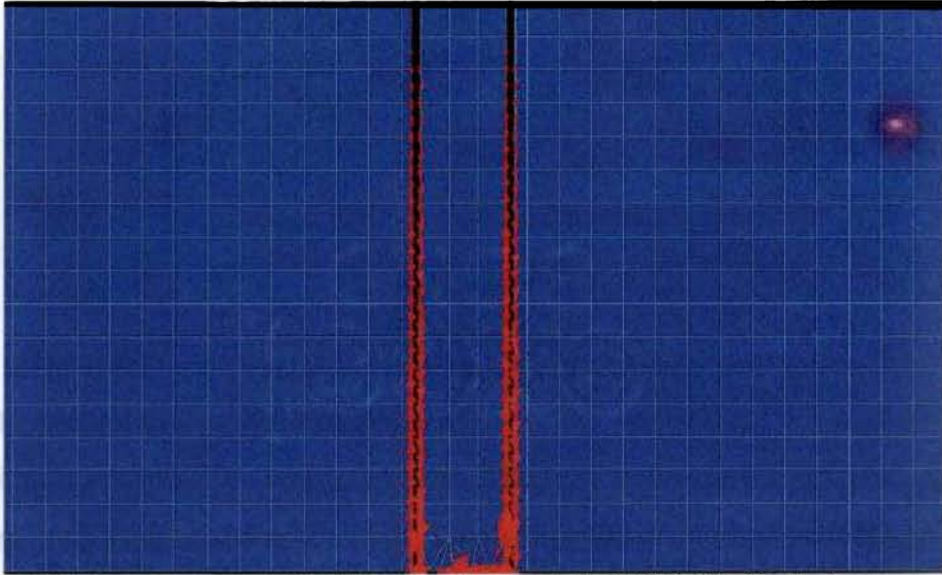


Fig. 5.27 2D vector current density variation on the open circuited CPW with offset feed at resonance frequency. Dimensions: $w=3$ mm, $g=0.5$ mm, $c=15$ mm and $l= 20$ mm on FR4 substrate of $\epsilon_r=4.7$ and thickness $h=1.6$ mm

Arrows in the figure shows the direction of current flow and the thickness indicates the magnitude of current vector. Naturally surface current will be concentrated more at the edges of the strips due to the attraction of opposite charges induced on the lateral strips through the gaps. Thus the surface current on the middle part of the centre strip is zero. In order to maintain this current distribution the gaps should be very small in terms of its operating wavelength.

Figure clearly shows that when feed point is moved to the corner, a transverse surface current appears along the width of the signal strip (at the feeding edge) in addition to its longitudinal variations (along the length) on the coplanar structure. The “U” shaped resonant path thus formed on the center strip is half wave length in the dielectric substrate. The concept will be clearer when it is compared to the surface current distribution on a conventional coplanar waveguide of same dimension operating at the same frequency, and is shown in Fig. 2.28.

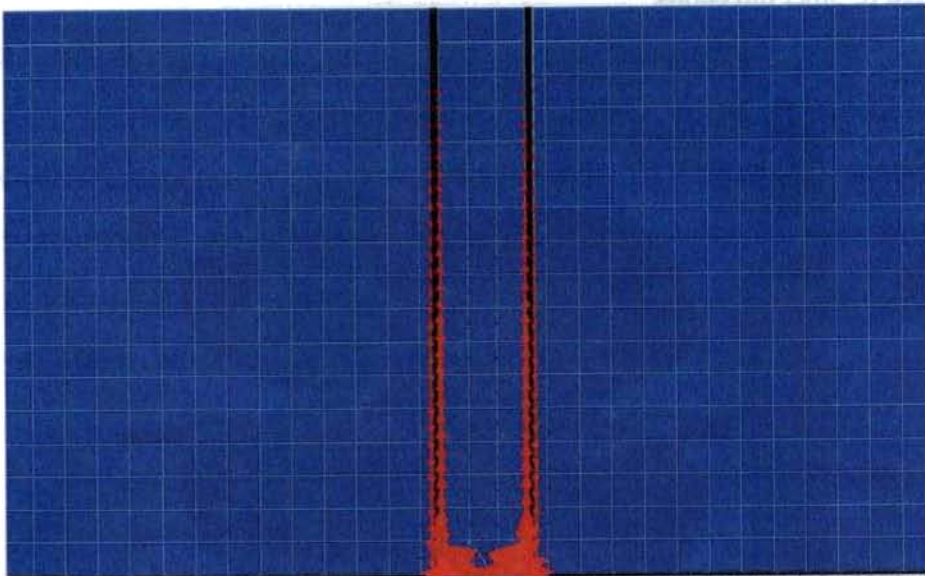


Fig. 5.28 2D vector current density variation on a conventional open circuited CPW. Dimensions: $w=3$ mm, $g=0.5$ mm, $c=15$ mm and $l=20$ mm on FR4 substrate of $\epsilon_r=4.7$ and thickness $h=1.6$ mm

A balanced current distribution is established at the edges of the signal strip when a conventional CPW is excited by the feed point at the middle of the signal strip width. Thus the magnitude and phase of the current distribution at any two symmetrical points along the length on the CPW signal strip will be equal. In other

words, the E-field distribution at the guiding slots is due to the strong coupling of centre strip with the lateral strips through the gaps. The balanced current distribution is also clear from in the figure.

5.7 Radiation pattern and gain

The estimated 3D radiation pattern at the resonant frequency using IE3D is shown in Fig. 5.30. The broadside power ($\theta=0, \Phi=0$ direction) is very low compared to other directions.

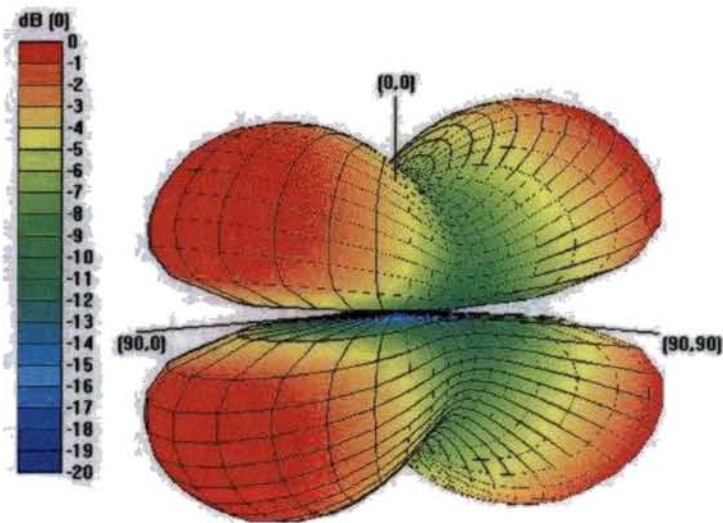


Fig. 5.30 3D radiation pattern of open circuited CPW with offset feeding
Dimensions: $w=3$ mm, $g=0.5$ mm, $c=15$ mm and $l=20$ mm on FR4 substrate of $\epsilon_r=4.7$ and thickness $h=1.6$ mm

The figure shows 4 lobes in the radiation pattern. This produce sharp nulls in the two principal plane patterns. When the centre strip width is increased, the maxima in the radiation pattern comes to the broadside directions ($\theta=0, \Phi=0$ & $\theta=180,$

$\Phi=0$ directions), producing a figure of eight radiation pattern in the E-plane and omnidirectional radiation pattern in H-plane.

Gain of the device is measured using gain transfer method. Measured gain of the device is 1.8 dBi at 2.47 GHz. This also indicates that the device is radiating electromagnetic energy when the feed offset scheme is employed. The estimated gain of the device is 2.1 dBi at the resonant frequency.

5.8 Equivalent circuit representation and radiation mechanism

The FDTD computation, parametric analysis and the current distribution studies clearly gives an insight into the resonance mechanism of the structure when it is excited with an offset feed. Consider a case in which the CPW is excited with a corner feed. The equivalent circuit representation incorporating the offset feed of CPW is shown in Fig. 5. 29.

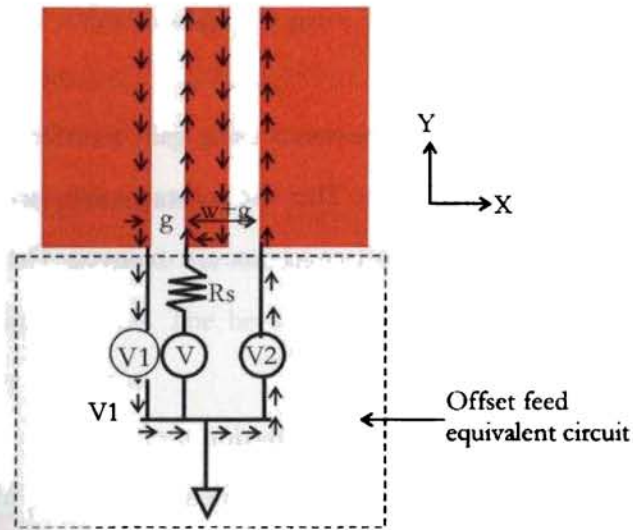


Fig. 5.29 Equivalent circuit and current path of CPW excited with a corner feed

Owing to the corner feeding, the potential at the two ground points (V_1 and V_2) will not be exactly equal. The imbalance in the potential ($V_1 \neq V_2$) is due to the additional length ' w ' in the ground connection for the RF current to reach the right lateral strip. A small offset ' w ' can produce slight change in V_2 with respect to V_1 (say more positive or negative). The microwave signal source is represented as a voltage source ' V ' with an internal resistance ' R_s '. The R_s will be the impedance of the signal source (usually 50Ω). Left lateral strip is connected to the outer conductor of SMA connector directly. Let the RF potential at a particular instant is $V_1=0$ at the feed point on left lateral strip. But the additional path length ' w ' introduced at the right side due to the central strip width ' w ' (' g ' is common for both the sides) force the potential at feed point connected to the right

lateral strip to 'V2'. Note that V2 is represented in the equivalent circuit using a voltage source without any internal resistance. This is only a virtual source.

The current from the source coming to the feed point at the centre strip must flow to left lateral strip through the gap and reaches the virtual source $V1=0$. In the gap displacement current plays similar role of conduction current in the conducting strip. This will produce a dominant E_x component at the left gap as per the coordinates mentioned in figure. But in actual case the gap is an air dielectric interface and the E-field has a fringing effect than a straight link to the ground strip. This is the only possible current path for this case since current always flows to minimum potential ($V1=0$). The virtual source V2 is slightly at higher potential (very small) than V1. The excess charges thus reaching ground flows through the source V2 and reaches the feed point at the centre strip by the electromagnetic coupling at the right gap, as shown in the figure. The ground connection offered by the signal source is not introducing zero impedance for the RF current due to its inherent inductance property. Note that the current is not flowing through the signal source due to the relatively high potential of 'V' than V2. The current path thus completes through the right lateral strip. In the right lateral strip the displacement current launches a dominant value for E_x component. The in phase Electric field values at the slots are then progressing along the length of the CPW. Finally it reaches the end of the line and reflected back to the source, producing a standing wave pattern.

The above explanation indicates a serious problem that the feeding arrangement (usually outer conductor of the SMA) will radiate some electromagnetic energy due to

the transverse variation of surface current flow to sustain this resonance. The final antenna configuration derived from these discussions will take this point into consideration. As described in Chapter 1, Section 1.6 the radiation in coplanar antenna is solely due to radiation from the two big discontinuities offered by coplanar waveguide gaps. The offset feeding arrangement is used only for exciting a novel resonance on CPW for obtaining an in phase field distribution at the two gaps supporting radiation. Note that the new resonance produces impedance variation along the width of the centre strip.

FDTD analysis clearly shows the electric field is existing in the slots and the fields are in phase for the offset feeding. The radiation from the device at resonance is due to the tangential component of fringing fields along the length at the two gaps separating center strips from the two lateral strips. This field is due to the electromagnetic coupling between the center strip and the two lateral strips. The radiation mechanism is depicted in Fig. 5.31.

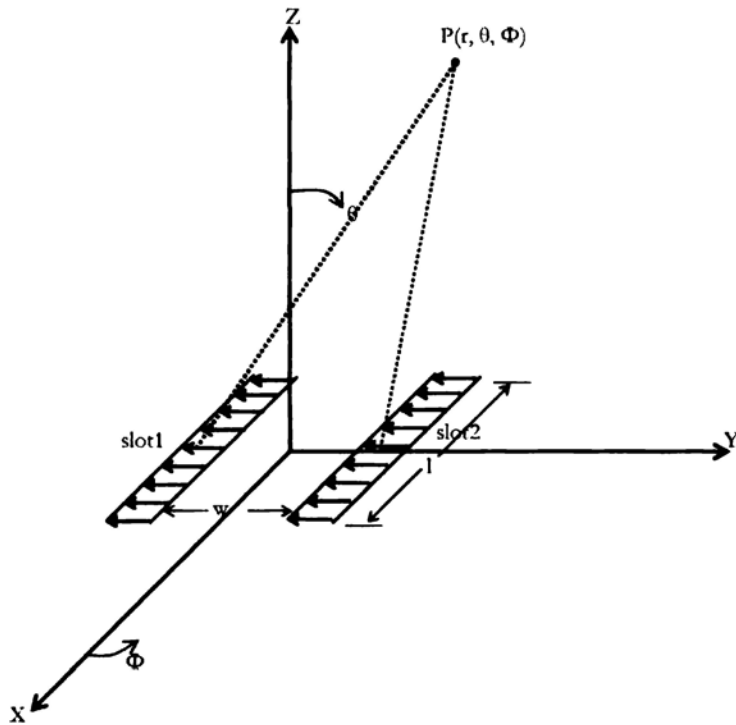


Fig. 5.31 Radiation mechanism of open circuited coplanar waveguide with offset feed

The device at resonance can be considered as two slot radiators of length 'l' placed in the XY plane, and separated by a distance 'w'. The total radiation at point $P(r, \theta, \Phi)$ is the vector sum of fields at the point, radiated from the two sources. This will produce a broad side radiation if the distance 'w' is half wave length of the radiating frequency. In order to maintain a nearly constant phase of the electric field at the two gaps, the dimension 'l' should be less than $\lambda_d/4$.

5.9 Conclusions

The conclusions of the chapter are summarized below. These conclusions are used to design the dual-band antenna element in the next chapter of the thesis.

1. An open circuit CPW with conventional feeding excite spurious resonance at higher microwave bands.
2. The mode thus excited at higher bands is not radiating EM energy efficiently. The radiation pattern, gain and efficiency are not enough to consider it as an efficient compact radiator.
3. A coplanar waveguide structure is able to excite a resonant mode at a lower frequency band when the feed point is away from the center of the signal strip, along the width (usually at the corner).
4. The new resonance is influenced mainly by the length l , signal strip width ' w ', and substrate parameters.
5. The resonance is due to the 'U' shaped resonant path excited on the centre strip and the coupling between centre strip and the two lateral strips.
6. FDTD analysis and measured far field radiation shows that the tangential component of the fringing fields radiates and produce a horizontally polarized EM radiation.
7. FDTD analysis shows that the corner feeding excites in phase field distribution.
8. The width ' w ' should be sufficiently large in terms of the operating wave length to obtain broad side radiation.
9. The measured gain of the device is ~ 1.8 dBi

10. Length 'l' of the waveguide should be less than $\lambda_d/4$, to obtain a distortion less radiation pattern, where λ_d is the wave length in the dielectric corresponding to the desired resonance. This reduces the phase variation of the electric fields in the slots.

CHAPTER 6

Development and Analysis of a Compact Microstrip line-fed Dual-band Coplanar Antenna

Development and analysis of the Compact Dual-band Coplanar Antenna is presented in this chapter. The device is developed based on the conclusions arrived in the previous chapter. The coplanar geometry is excited with a microstrip line at the corner of its wide centre strip for dual band operation. The resulting compact antenna has dimension of $\lambda/5 \times \lambda/14$, where λ is the free space wavelength at the fundamental resonance.

6.1 Introduction

The conclusions of the investigations on coplanar waveguide presented in the previous chapter obviously indicate that a resonant mode can be easily achieved on a coplanar waveguide by exciting it with an offset feed scheme. The device exhibit good radiation characteristics. Moreover the device dimensions are very small compared to the operating wavelength. The compactness together with the excellent radiation characteristics suggests its application as an ideal antenna for compact devices like mobile phone, wireless LAN cards in laptops etc. Antennas for mobile terminals should meet certain criteria such as small size compared to the wavelength of operation, nearly omni-direction radiation coverage, reasonable gain, good efficiency etc. This novel design exhibits all the above criteria.

Previous discussions conclude that there exists a lateral current variation on the outer conductor of the SMA connector when the coplanar transmission line is excited with an offset feed scheme. It should be noted that this current variation is very important in order to sustain the resonance. A current path (a conducting path) between the two ground points should exist to excite the so called resonance. The radiation pattern study and the radiation mechanism at the fundamental resonance of the device indicate that a wide centre strip width is essentially required to obtain a broadside radiation with omni directional coverage. In order to proceed, a study with wide centre strip width is to be carried out. More over, a wide centre strip may give rise to an additional resonance on the structure. This chapter discusses the design and analysis of a compact antenna system by taking all these points into consideration. Resulting radiating configuration is an ideal candidate for compact mobile terminal applications. The

theoretical investigations, parametrical analysis and finally simple design equations are discussed in this chapter.

6.2 Offset fed coplanar geometry with wide centre strip width

A Coplanar waveguide geometry with wide centre strip width is analyzed in this section. The parametric analysis presented in the previous chapter concluded that the resonant frequency is decreasing as the centre strip width is increasing. In this section a wide centre strip width 'w' is employed for the study. Note that one should expect the same resonance and radiation characteristics presented in the previous chapter for this case also. Otherwise, the working of the device may not be same as that of coplanar waveguide geometry with offset feed.

When wide centre strip is employed, the device no longer behaves as a transmission line. The offset fed coplanar structure along with the parameters are depicted in Fig.6.1. The structure consists of a wide centre strip of $l=9$ mm, $w=12.5$ mm, $g=0.5$ mm and $c=5$ mm printed on an FR4 substrate of $\epsilon_r=4.7$ and thickness $h=1.6$ mm.

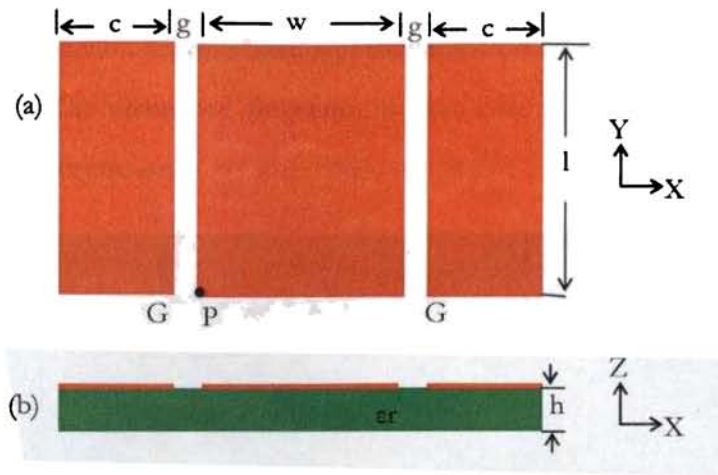


Fig.6.1 Offset fed coplanar geometry with wide centre strip width
 (a) Top view
 (b) Cross sectional view

The device is excited at the corner of the centre strip (P) and the two lateral ground strips are grounded. The 'port for edge group' scheme in IE3D is employed to excite the structure. According to the equivalent circuit representation of the offset feed explained in section 5.8 of chapter 5, a resonance should exist in this structure also, due to the potential difference between the two ground points. This potential difference is due to the asymmetry in the feeding, as explained in section 5.8. Figure 6.1 clearly shows the offset feed point P and the ground points G.

Fig. 6.2 depicts the simulated return loss characteristics of the device. The device resonates at 3.655 GHz with 7.6% return loss bandwidth.

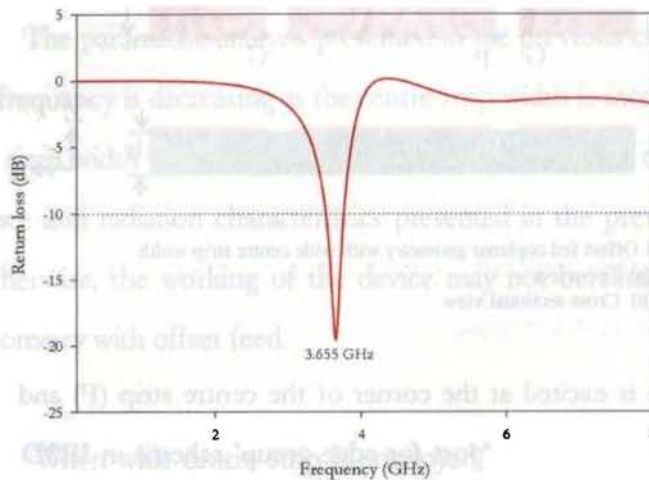


Fig. 6.2 Return loss characteristics of offset fed coplanar geometry with wide centre strip width, with dimensions $l=9$ mm, $w=12.5$ mm, $g=0.5$ mm and $c=5$ mm printed on an FR4 substrate of $\epsilon_r=4.7$ and thickness $h=1.6$ mm

Return loss value at the resonance is ~ -19 dB. The -10 dB return loss band width for this case is 280 MHz. The resonant mode thus obtained for this case strongly indicates that the offset fed coplanar waveguide structure can excite the so called resonance by widening the centre strip. Here, the attempt to widen the centre strip is done purposefully in order to modify the radiation pattern to cater the need of mobile wireless gadget applications. Equivalent circuit representation presented in the previous chapter holds good for this case also.

Fig. 6.3 depicts the current distribution obtained from IE3D for this case. It can be seen that the wide centre strip width excites the same 'U' shaped resonant path on the coplanar structure. The resonance frequency in this case is due to the 'U' shaped resonant path on the centre strip.



Fig. 6.3 Surface current distribution obtained on the offset fed coplanar waveguide structure with wide centre strip width, dimensions $l=9$ mm, $w=12.5$ mm, $g=0.5$ mm and $c=5$ mm printed on an FR4 substrate of $\epsilon_r=4.7$ and thickness $h=1.6$ mm.

It is observed from the figure that there is only negligible current variation on the middle parts of the three strips. Current densities are more intense at the edges of the strips. The 'U' shaped current path is very clear from the structure. The 'U' shaped resonant path on the centre strip is approximately equal to the half wavelength in the substrate at the resonant frequency. The 'U' shaped current distribution induces an oppositely flowing currents at the edges of the ground strips due to the strong coupling with centre strip and the two ground strips. Thus a horizontally polarized electromagnetic radiation is expected for this case. Width of the ground strips and the gaps has no significant influence on the resonant frequency, where as length of the waveguide and substrate materials strongly affect the resonant frequency.

Fig. 6.4 shows the 3D radiation pattern of the antenna at the resonant frequency. The radiation pattern is to be viewed according to the coordinate system mentioned in Fig. 6.1.

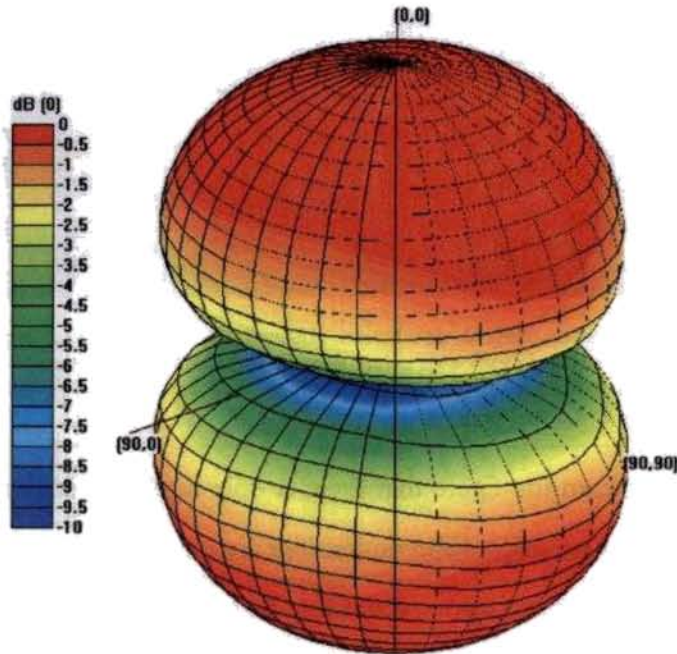


Fig. 6.4 3D radiation pattern of the offset fed coplanar geometry with wide centre strip width. Dimensions are dimensions $l=9$ mm, $w=12.5$ mm, $g=0.5$ mm and $c=5$ mm printed on an FR4 substrate of $\epsilon_r=4.7$ and thickness $h=1.6$ mm

The 3D radiation pattern shows that the maxima of the radiation pattern is along broad side directions. When the width 'w' is increased, the two radiating slots becomes far apart. This should produce a broad side radiation according to the discussions in Chapter 5, section 5.8.

The estimated gain of the antenna at the resonant frequency is 2.1 dBi. In this case the length 'l' of the structure is small compared to the operating wavelength. This will reduce the phase variation in the slots, producing good directive gain at resonance. The estimated radiation efficiency is 79% at the resonance.

During the above studies the two grounds are excited near the two slots. That means the current excitation on the ground strips are negligible at resonance. In order to attain maximum compactness for the final radiating structure an attempt was done to excite a current distribution on the ground strips along with the so called resonance due to the 'U' shaped resonant path on the centre strip, resulting a coplanar configuration as shown in Fig. 6.5.

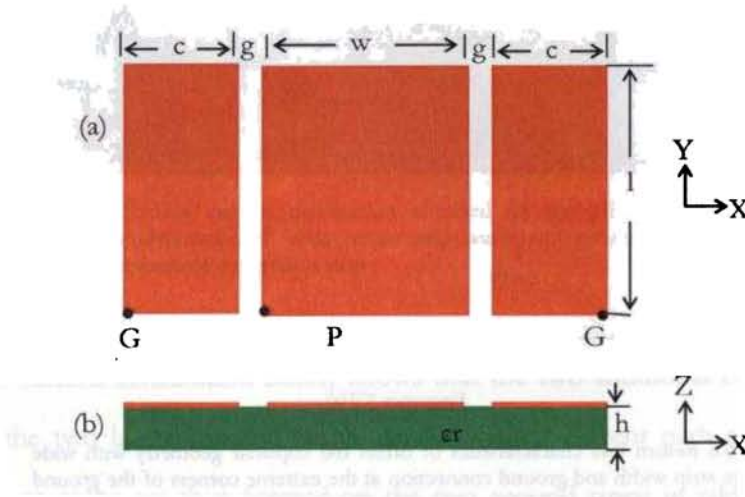


Fig.6.5 Offset fed coplanar geometry with wide centre strip and ground connections at the extreme corners of the ground strips
 (a)Top view
 (b)Cross sectional view

The dimension of the coplanar geometry is same as that used in the previous study. It should be noted that both the ground points are shifted symmetrically to the extreme ends of the ground strips. In compact antennas the only way to excite a low

frequency with in the small volume is to increase the current path on the structure by the meandering techniques.

The idea behind this attempt is the same current meandering technique applied in compact antenna designs. But the fundamental mode of the structure should remain as it is, other wise this technique may results in new radiating modes. Fig. 6.6 depicts the estimated return loss characteristics of the device using IE3D for this case.

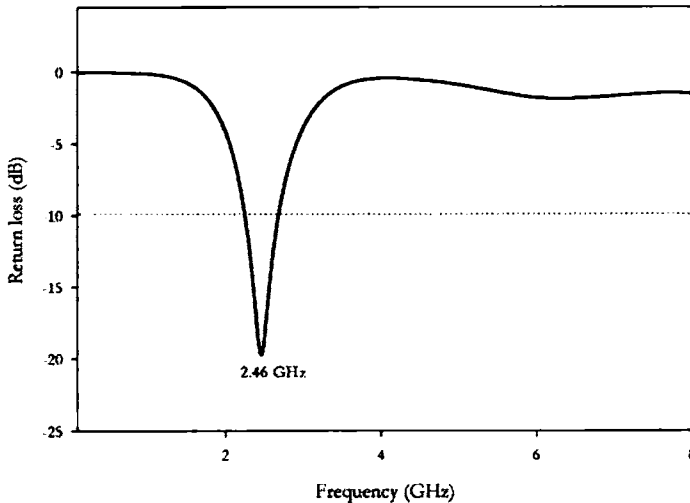


Fig. 6.6 Return loss characteristics of offset fed coplanar geometry with wide centre strip width and ground connection at the extreme corners of the ground strip

The structure resonates at 2.46 GHz with 16% return loss bandwidth. The bandwidth obtained from -10dB points is 400MHz. It should be noted that the resonant frequency has shifted to the lower side for this case. The return loss value at resonance is ~ -19 dB. This structure is very compact in terms of the wavelength at resonance. A

compact dimension of $\lambda/13 \times \lambda/5$ is achieved. The bandwidth is also higher than that obtained in the previous sections.

Analysis of surface current distribution and radiation pattern has to be carried out to confirm that the radiation mechanism at resonance is same as that of the fundamental mode of the coplanar wave guide structure with offset feeding scheme. Fig. 6.7 depicts the surface current distribution on the coplanar patches at the resonant frequency.

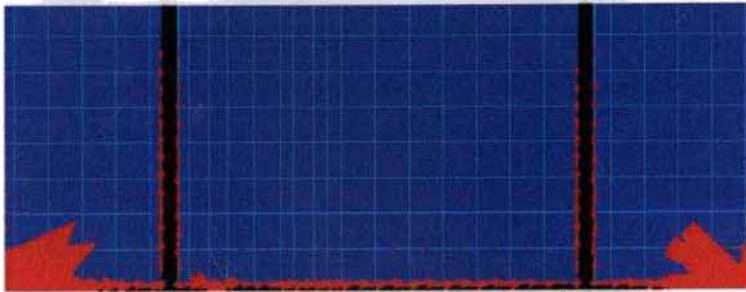


Fig. 6.7 Surface current distribution obtained on the offset fed coplanar waveguide structure with wide centre strip width and ground points at the extreme corners of the ground strip

The current distribution clearly shows that the two additional current paths are excited on the two lateral ground strips. An 'I,' shaped current path and 'reflected L' shaped current paths are thus formed on the two ground strips in addition to the 'U' shaped current path on the centre strip ('reflected I,' shaped current path does not refer to the current reflections from discontinuities). It can be seen that the 'U' shaped current path is approximately half wavelength in the substrate and 'I,' and 'reflected I,' current paths are quarter wavelength each in the substrate. Thus the total current variation on the surface of the structure is approximately full cycle variation in the dielectric. The

current distribution shown in figure indicates that a strong coupling still exists between the centre strip and the two lateral ground strips. The fringing fields at the two slots are the cause of radiation for this configuration. The effect of substrate and other structural parameters are also similar to the characteristics presented in chapter 5, section 5.4. Since the feed asymmetry exists for this case, the equivalent circuit representation discussed in section 5.8 of chapter 5 holds good for this case also. Thus it can be concluded that the feeding asymmetry in coplanar structures can be used effectively to design an antenna. The feed point asymmetry is the only crucial point to excite resonance on the coplanar waveguide structure. The other parameters only govern its resonance and radiation characteristics.

Fig. 6.8 shows the 3D radiation pattern of the device at the resonant frequency. Maximum radiation is found to be at the broad side directions.

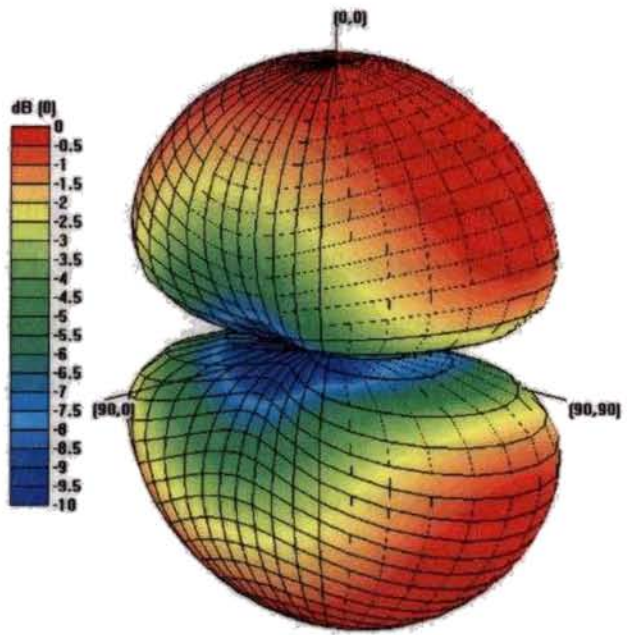


Fig. 6.8 3D radiation pattern of the offset fed coplanar geometry with wide centre strip width and ground points at the extreme corners of the ground strip

The maxima at the broadside direction strongly support the fact that the radiation mechanism of this configuration is same as that explained in chapter 5, section 5.8. The two slots are the source of radiation for this case also. The only difference is that unused metallic strip is used by the surface current for more compactness. The estimated gain and efficiency of the device are 1.8dBi and 76% respectively at resonance.

6.3 Dual-band coplanar antenna configuration

The above investigations on coplanar waveguide structure concludes that a coplanar waveguide structure can excite a resonant mode in the structure if an offset feed scheme is employed, resulting a compact radiating structure with good radiation characteristics. More compactness can be achieved by feeding the ground potential to the lateral ground strips at the extreme ends.

In chapter 5 an SMA connector was used to excite the structure. The centre strip width of the coplanar waveguide was small for that case. Moreover there was a lateral variation of surface current on the outer conductor of the SMA connector. One can say that this current variation may result in an imperfect transition from the mode excited in offset fed coplanar waveguide structure to the transverse electromagnetic mode (TEM) of SMA connector. A lateral variation of surface current on the outer conductor of the SMA connector is to be avoided. Moreover when the width of the centre strip is large, the SMA connector cannot be used to excite the system. Thus a new feeding system is required to excite the coplanar geometry. A microstrip line is employed as the feed for this configuration. The microstrip line feed, importance of the ground plane in the present design, conducting pins for providing grounds to the ground strips etc. are described in this section.

6.3.1 Microstrip line feed

The microstrip line consists of a small printed strip called signal strip on the top layer of a substrate with a ground plane on the bottom layer. Width of the signal strip, substrate dielectric constant and the thickness of the substrate govern its characteristic impedance. A microstrip line feed is selected purposefully to excite the coplanar antenna. Since the width of the centre strip is wider than conventional signal strips in coplanar wave guides, there is a possibility to obtain a new resonant mode from the same structure with same feeding arrangement. Thus the microstrip feed line is placed at the extreme corner on the centre strip of the coplanar geometry. Fig. 6.9 shows the top view and cross sectional view of the microstrip line employed in the design.

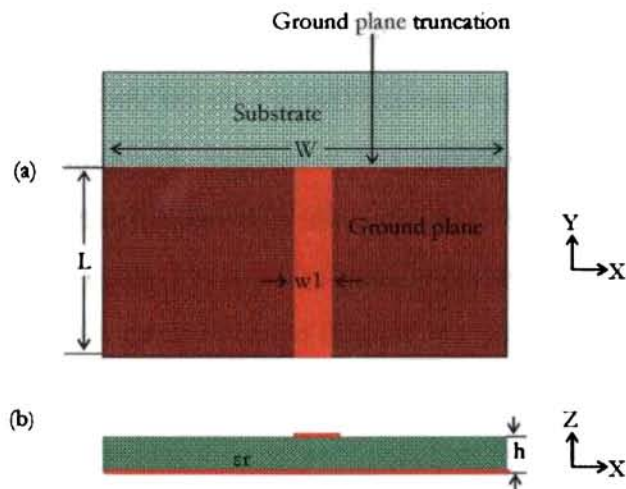


Fig.6.9 Microstrip line feed used to excite the coplanar antenna

- (a) Top view
 (b) Cross sectional view

The ground plane of the microstrip line has length ' L ' and width ' W ' printed on the bottom layer of the substrate. A signal strip of width ' w_1 ' designed for 50Ω characteristic impedance is printed on the top layer of the substrate. Length of the signal

strip is also '1.'. The ground plane truncation is clearly shown in the figure. Typical values of the microstrip line parameters are $L=40\text{mm}$, $W=53\text{mm}$, $w_1=3\text{mm}$ on FR4 substrate of thickness $h=1.6\text{ mm}$ and dielectric constant $\epsilon_r=4.7$. The microstrip line is excited using a $50\ \Omega$ SMA connector. The proximity of the ground truncation to the coplanar geometry is very critical to excite the two resonant bands of the antenna. More explanations on the effect of ground plane on the final antenna configuration will be discussed in the parametric analysis section later in this chapter.

6.3.2 Ground plane and its importance in the present design

The ground plane of the microstrip line has another important job other than working as the ground plane of microstrip line feed. In order to sustain the resonance on the coplanar geometry a common conducting path between both the ground points (G) are very essential. This is achieved through the ground plane at the truncation edge. Two conducting pins or vias extending from the corners of the lateral strips to the ground plane truncation set up a current path between the two ground points. The current path on the resulting structure is depicted in Fig. 6.10.

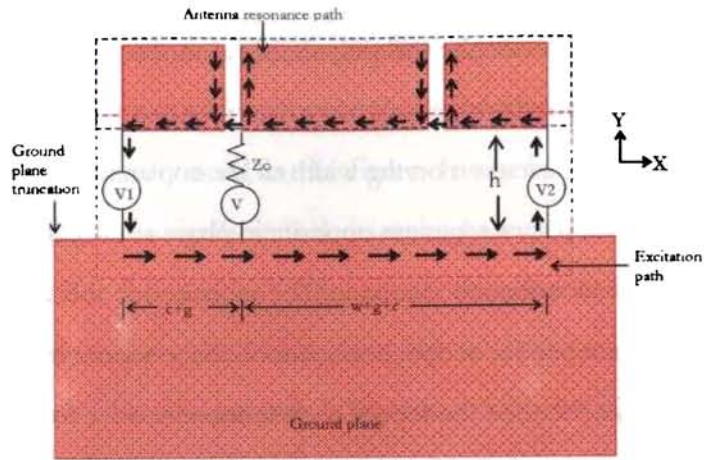


Fig.6.10 Current path at the fundamental resonance on the coplanar antenna geometry when excited by a microstrip line at the corner of the centre strip

The coplanar geometry is at the top layer of the substrate. But for the simplicity of understanding the operation they are placed on the same plane (XY plane) with the ground plane. The current path on the coplanar antenna structure can be split into two categories. One is called excitation path and other one the antenna resonance path. The excitation path is highly required to establish the antenna resonance path. It should be noted that the current on the ground plane is flowing through the ground plane edge at the ground truncation. The virtual voltage sources V1 and V2 due to the path difference 'w' between the two ground points of the vias are slightly at different potentials. V is the excitation signal at the tip of the microstrip line truncation and the internal resistance Z_0 is equal to the characteristic impedance of the feed line. As explained in section 5.8 of chapter 5, an excitation path is established in the structure. The E_x component of the electric field launched in the two slots produce the antenna resonant path and finally the radiation from the antenna structure. It is clear from the figure that the current path on

the ground plane is extremely important to sustain this mode of operation. But the current variation on the ground plane is only confined at the ground truncation edge, thus it does not alter the fundamental job of ground plane as the ground of the microstrip line. Since the current variation on the width of the coplanar strips near the ground truncation and on ground planes edges are opposite in phase at the excitation path of the antenna, there will not be radiation due to it. The radiation, at the lower resonance is solely due to the fringing fields at the two gaps of the coplanar structure. This will enhance the polarization purity of the excited electromagnetic wave from the antenna.

Since the thickness of the substrate is very small compared to the operating wavelength, there will be a strong coupling between the centre strip and ground plane at some frequencies. At a higher frequency, when the width of the centre strip is approximately equal to half of the wavelength in the dielectric a new mode will be excited on the structure. The pictorial representation of this case is shown in Fig. 6.11.

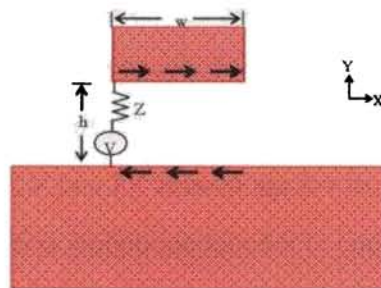


Fig.6.11 Current path at the second resonance on the coplanar antenna geometry when excited by a microstrip line at the corner of the centre strip

The fringing fields from the edge of the centre strip to the ground plane is the cause of radiation at this frequency. This will produce a vertically polarized

electromagnetic radiation (along Y direction) from the structure. That means the radiation at the second resonance of the coplanar antenna can be approximated to the radiation from a slot excited with half wave sinusoidal distribution, lying on XY plane of the coordinate system mentioned in the figure. It can be concluded that the ground plane of the feed line has a significant role in exciting the two resonant frequencies in the coplanar antenna. But the current distribution on the ground plane for the two modes are confined mostly to the ground truncation edge only, and it will not affect the entire circuit performance when the antenna is integrated with RF circuits, where the same ground plane is shared by the circuit.

6.3.3 Conducting pins or vias

Two conducting pins made of copper are used to connect the two ground strips to the truncated edge of the ground plane. Diameters of the conducting pins are 1 mm throughout the study. The conducting pin has a height exactly equal to the height of the substrate and the ends of the pins are soldered to the ground strip and the ground plane respectively. Instead of conducting pins via holes can be used. Performance of the via holes are almost similar to the conducting pins. This has been confirmed through simulation studies.

6.3.4 Antenna configuration

The final microstrip line excited dual-band coplanar antenna configuration is depicted in Fig. 6.12.

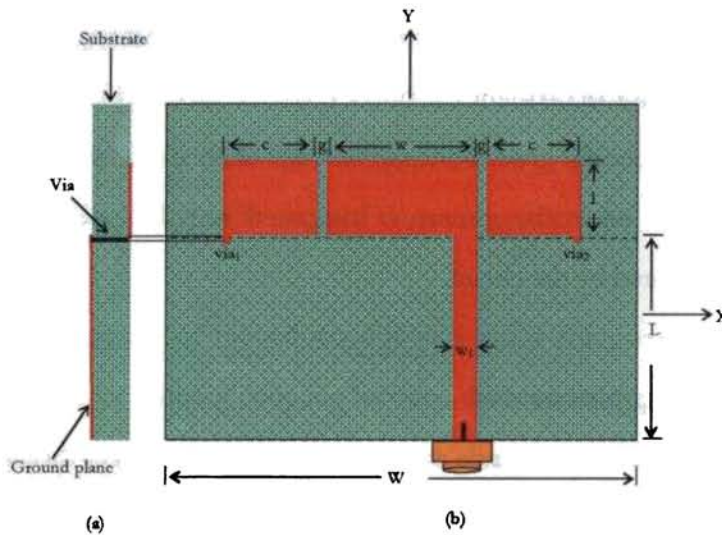


Fig.6.12 Geometry of the dual-band microstrip line fed coplanar antenna printed on a dielectric substrate

- (a) Cross section view
(b) Top view

It consists of the three coplanar strips and the corner fed microstrip line signal strip of 50Ω characteristic impedance on the top layer, a truncated ground plane near the feed line end and two conducting pins for connecting ground strips to the ground. The device is printed on a standard substrate material. Substrate materials with low dielectric constants are preferred for the design in order to avoid surface wave excitations, which will reduce the antenna efficiency and distort the radiation patterns.

The centre strip of the coplanar geometry has length ' l ' and width ' w ' excited by the microstrip line of length ' L ' and width ' w_1 '. The two lateral strips are separated from the centre strips by the gap ' g '. Width of the each lateral strip is ' c '. The cross-sectional view clearly shows the via connecting the top lateral strips to the ground through the substrate. The top view of the antenna is in the XY plane of the coordinate system. Position of the feed line is fixed at the extreme corner of the centre strip to excite the first two modes of the antenna. The antenna should exhibit good impedance matching for the two resonances, when the feed line is placed at this location. The ground truncation is represented by dotted lines in the figure. A 50Ω SMA connector is used to excite the system. When the antenna is excited, two distinct resonant modes are excited, which generate two wide bands with orthogonal polarizations. The gap ' g ' should be small compared to the wavelength corresponding to the lower resonance to obtain good electromagnetic coupling between the centre conductor and the lateral strips.

Fabrication of the antenna was done using standard photolithographic techniques. Care should be taken while doing photolithography for obtaining a uniform and exact ground truncation as shown in the figure, other wise the impedance bandwidth and matching at the two resonant frequencies may be degraded. Exact aligning of the top layer and bottom layer masks is the crucial part to be considered during fabrication for achieving good accuracy. The conducting pins should be perfectly soldered to the structure. A dry soldering or imperfect connection of conducting pins result spurious resonances in the structure, other than the two expected bands. The characteristics of the device will be explained in the forthcoming sections of the chapter.

6.4 FDTD analysis of coplanar antenna

The theoretical analysis of the antenna is carried out using FDTD method. MATLAB based in-house codes were developed for analyzing the antenna. Perfect Matched Layer ABC is employed in FDTD. Return loss characteristics of the antenna and the field distribution in the structure are computed using FDTD.

6.4.1 Description of the problem

The 2D view of the FDTD computation domain defined for the microstrip line fed dual-band coplanar antenna is depicted in Fig. 6.13.

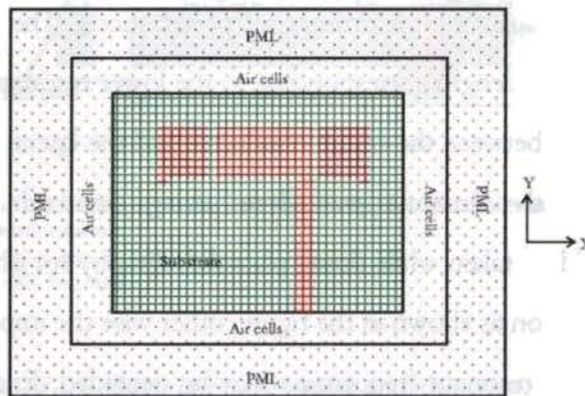


Fig.6.13 2D view of FDTD computation domain of microstrip line fed coplanar antenna

Consider a microstrip fed dual-band coplanar antenna with the structural dimensions as $l=9$ mm, $w=12.5$ mm, $c=5$ mm, $g=0.8$ mm, $L=40$ mm, $W=53$ mm when printed on FR4 substrate of $\epsilon_r=4.7$, and thickness $h=1.6$ mm. Width of the signal strip is 3 mm for 50Ω characteristic impedance. The FDTD analysis will compute the

frequency response of the antenna by exciting it with a Gaussian pulse. The return loss characteristic of the antenna was first calculated. The E-field distributions on the top, middle and bottom layers of the antenna structure are then computed using sinusoidal excitation at the centre frequencies of the two resonant bands. In the figure the antenna geometry is surrounded by few cells of air to simulate the real condition in which the antenna is placed in air. The antenna geometry and air cells are surrounded by the PMI layer.

Luebber’s feed model was employed to excite the microstrip line feed of the antenna. Dz component value is assigned as excitation signal at the port. Ez value is automatically computed from Dz value in the FDTD loop. Using the Hx and Hy components in the Yee cells around the excitation field the source current is calculated. Return loss of the antenna is calculated at the excitation point. The feed model employed to simulate the system is shown in Fig. 6.14.

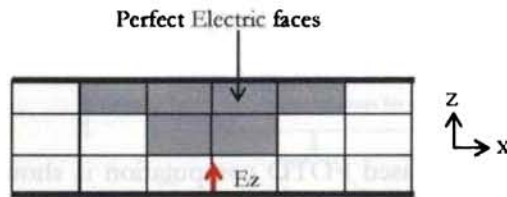


Fig.6.14 Luebbbers feed model employed in the FDTD computation of coplanar antenna.

In the figure the darkened portions are PEC regions in order to obtain a gradual transition from the field excitation point to the signal strip. The PEC condition is

achieved by assigning E_z and E_x values of the corresponding Yee cell faces are as zeros. In this computation the substrate layer is discretized as 3 cells in the Z-direction.

The conducting pins used to realize the prototype of the antenna is of cylindrical in shape. Fig. 6.15 shows the modeling of conducting pins in FDTD.

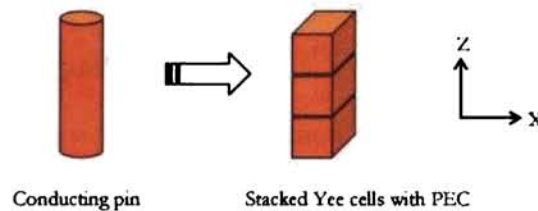


Fig.6.15 Modeling of conducting pin in FDTD computation

In order to make the computation efficient in terms of time the two conducting pins are modeled as stacked Yee cells in the Z direction by assigning with PEC at all the faces ($E_x=E_y=E_z=0$). This will not affect the accuracy of the computation since the frequency of operation of the device is not very high.

6.4.2 FDTD flow chart

The flow chart of PMI based FDTD computation is shown in Fig. 6.16. The Δx , and Δz in the computation domain are taken as 0.5 mm. Δy is 1mm in the computation, this will bring down the total number of Yee cells to a great extent. These values are less than $\lambda/20$ at the maximum frequency of the computation, and gives good accuracy for the computed values. Five air cells are assigned at each side of the CPW structure to simulate the practical condition in which the antenna is in contact with

surrounding air. A layer of cells just above the three coplanar strips and underneath the bottom layer are assigned with effective dielectric constant value as the average value of substrate dielectric constant and air to facilitate fringing field effect at the three radiating slots for lower and higher resonances in the computation. 10 cells are assigned for PML ABC at each side of the problem space. This is sufficient to effectively absorb the power at the boundary. According to the stability criteria, the calculated time step is $\Delta t=0.83$ picoseconds.

There are 142 cells in the X direction, 87 cells in Y direction and 33 cells in Z direction of the 3D FDTD computational domain.

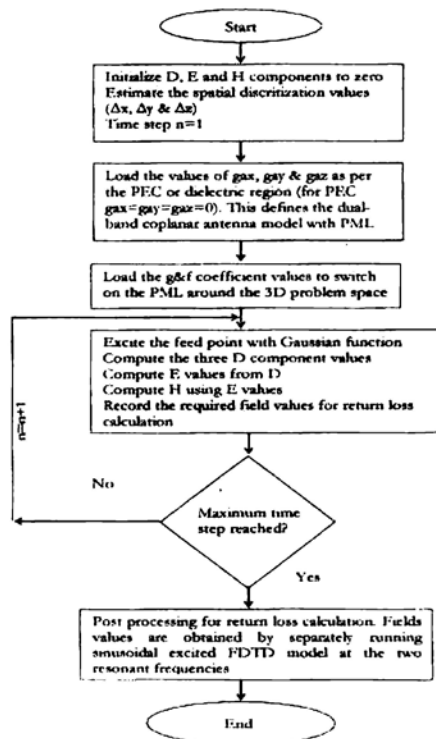


Fig. 6.16 FDTD Flow chart for the analysis of coplanar antenna

6.4.3 Input Gaussian pulse

The Gaussian pulse used to excite the computation domain is shown in Fig. 6.17. A narrow pulse of 10 picoseconds duration is used to excite the structure.



Fig.6.17Gaussian pulse used in the FDTD computation

The Gaussian pulse value is employed as the voltage source for calculating the source 'dz', which is assigned as the excitation signal derived using Krichoff's voltage law.

6.4.4 Computed time domain characteristics at feed point

The computed time domain response of the E_z component at the feed point is depicted in Fig. 6.18.

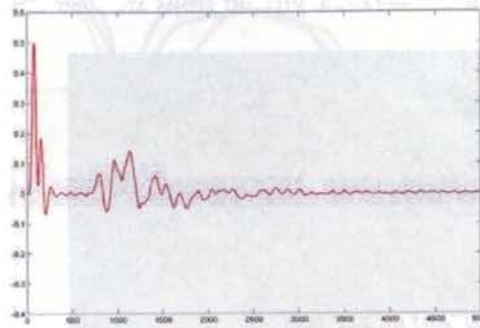


Fig.6.18 Time domain response of the E_z field at the port

The electric field component has settled down at around 5000 time steps. The Luebbers feed model employed in the computation effectively brings down the computation time steps. Note that the E_z value at any instant of time in the port is the mixture of reflected as well as incident excitation field. The time domain response of the electric field E_z is proportional to the voltage at the port.

A prototype of the same device used in FDTD computation is fabricated using standard photolithography process. A standard 3.5 mm SMA is connected to the feed line to excite the device. The antenna was tested using HP8510C vector network analyzer. Photograph of the device is shown in Fig. 6.19. The two conducting pins connected to the extreme ends of the lateral ground strips are clear in the figure.

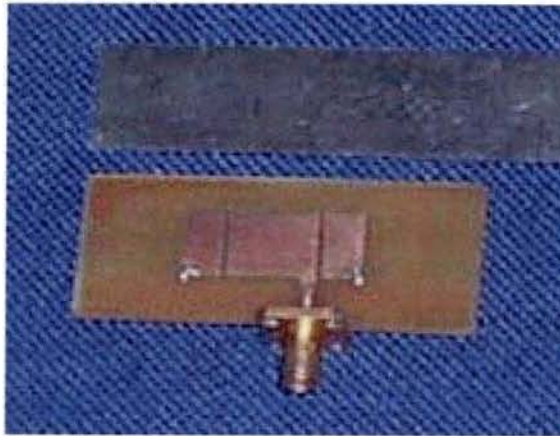


Fig. 6.19. Photograph of the compact microstrip-fed dual-band coplanar antenna for 2.4/5 GHz bands

The following section describes the results obtained using FDTD computation. Experimental results are also provided in order to substantiate the computed results.

6.4.5 Return loss characteristics

When the launched Gaussian pulse is complexly settled down in the computation domain the return loss value of the device is calculated. Incident voltage is the time domain Gaussian pulse, where as reflected voltage at the port is the difference of time domain values of E_z field at the port and the Gaussian pulse. The time domain values are first converted to frequency domain by taking FFT of the values and then

return loss is calculated. The computed, measured as well as HFSS simulation results are shown in Fig. 6.20.

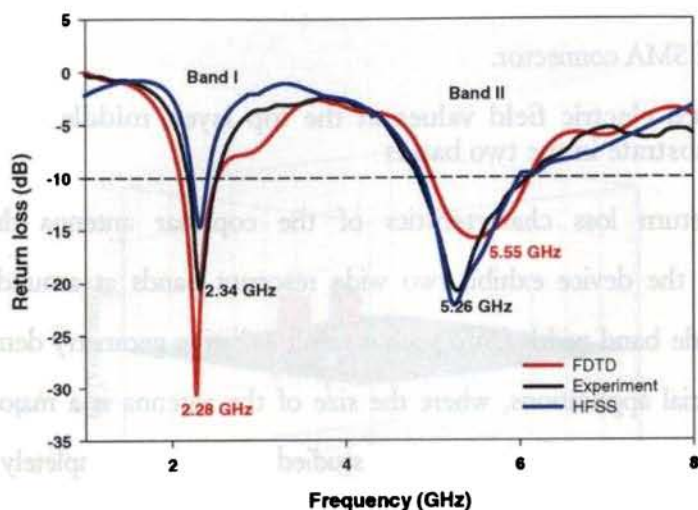


Fig. 6.20 Computed, measured and HFSS simulated return loss characteristics of the dual-band microstrip line fed coplanar antenna when $l=9$ mm, $w=12.5$ mm, $c=5$ mm, $g=0.8$ mm, $L=40$ mm, $W=53$ mm when printed on FR4 substrate of $\epsilon_r=4.7$, and thickness $h=1.6$ mm.

The computed return loss characteristics are almost in agreement with the measured values. The return loss characteristics computed using FDTD shows that the antenna resonates at 2.28 GHz and 5.55 GHz with -30.5 dB and -16 dB return loss for lower and higher resonances respectively. The antenna has 17% band width (-10dB bandwidth: 410 MHz) in the lower band and 20% band width (-10dB bandwidth: 1.1 GHz) in the higher band. The measured curve shows that the antenna resonates at 2.34 GHz and 5.26 GHz respectively. The measured bandwidth is 14% in the lower band (2.19-2.52 GHz) and 22% (4.84-6.07 GHz) in the higher band. The FDTD results differ from the measured values by 2.6% in the lower band and 4.3% in the higher band. More accurate results may be obtained by incorporating the effect of SMA connector.

Return loss characteristics of the antenna is simulated using Ansoft HFSS. The validity of the results obtained from FDTD computation and measurement are thus confirmed. It can be seen that HFSS results are almost same as measured values. This again confirms that the error in the FDTD and measured results are due to the contribution of SMA connector.

6.4.6 Computed electric field values at the top layer, middle layer and bottom layer of the substrate in the two bands

The return loss characteristics of the coplanar antenna discussed above concludes that the device exhibit two wide resonant bands at around 2.4 GHz and 5GHz. The wide band width from such a small radiating geometry demands its use in many commercial applications, where the size of the antenna is a major concern. The gain, radiation pattern, efficiency are to be studied in order to completely accept this as a new efficient radiating system. Following section gives more insight into the radiation mechanism of the device at the two resonant bands. The computed E-field distribution at the two resonant frequencies, at the three layers of the antenna are presented to confirm that the radiation from the device at the lower band is from the two gaps of the coplanar geometry, where as the radiation at the higher band is due to the fringing fields at the gap separating the width of the centre strip and the truncated ground plane.

The computed E-fields at top layer, middle layer and bottom layer of the substrate obtained by giving the sinusoidal excitations at the two resonant frequencies are presented to confirm it.

E-field components at the first resonance

The E_x , E_y and E_z components at 2.28 GHz are shown in Fig. 6.21 (a)-(i). This is the first resonant frequency of the antenna obtained using FDTD computation.

A. Top layer

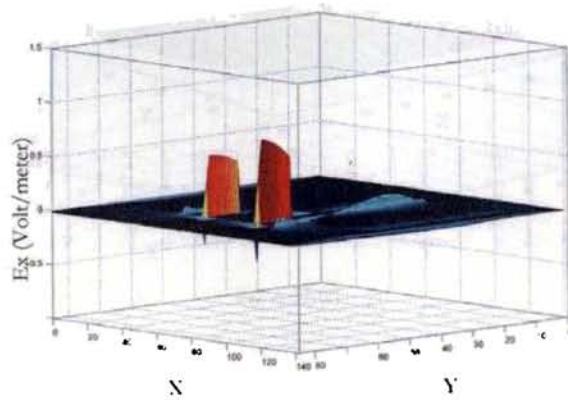


Fig 6.21 (a)

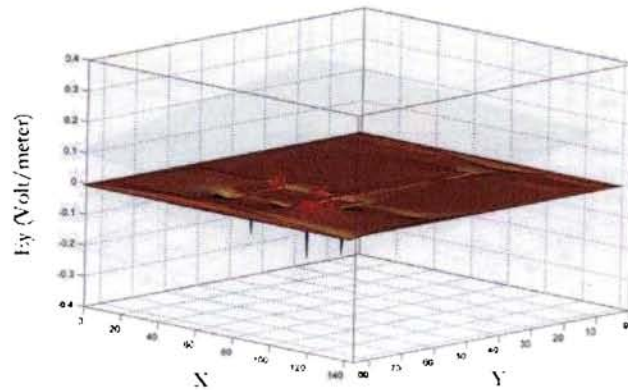


Fig 6.21 (b)

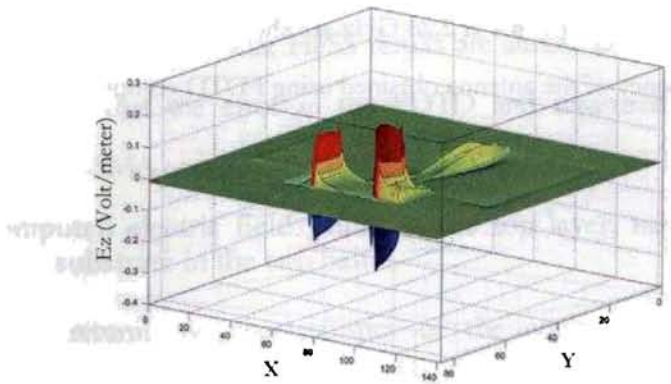


Fig. 6.21 (c)

B. Middle layer

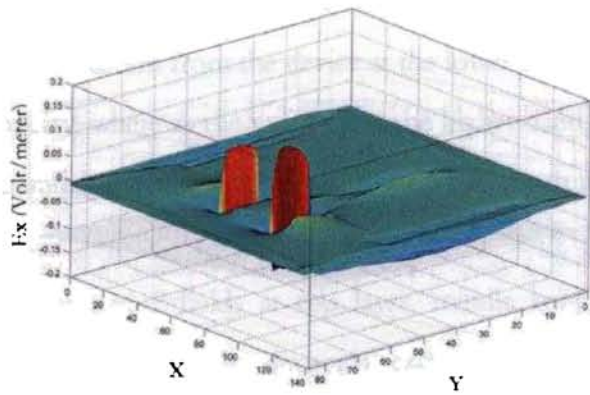


Fig. 6.21 (d)

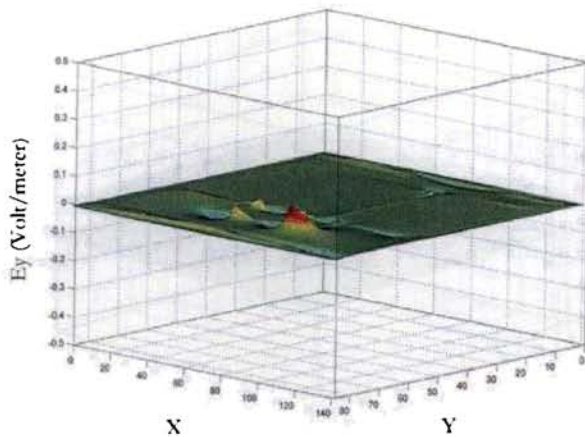


Fig. 6.21 (e)

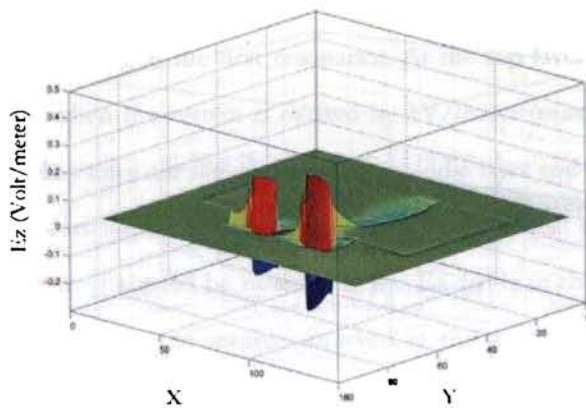


Fig. 6.21 (f)

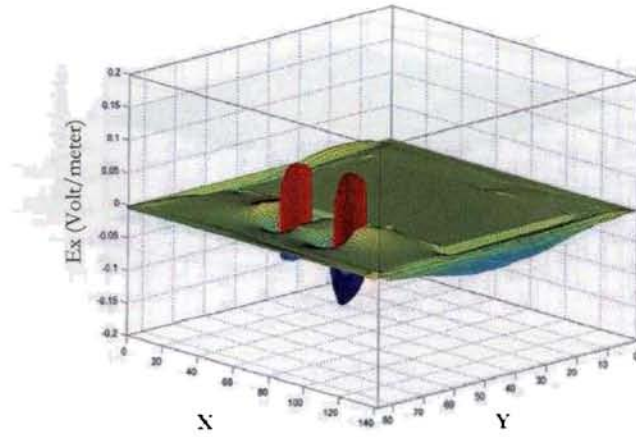
C. Bottom layer

Fig. 6.21 (g)

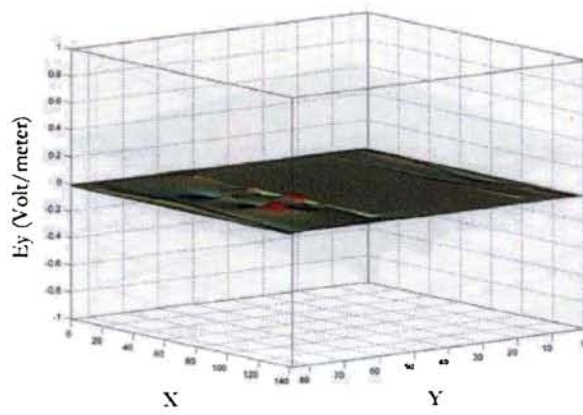


Fig. 6.21 (h)

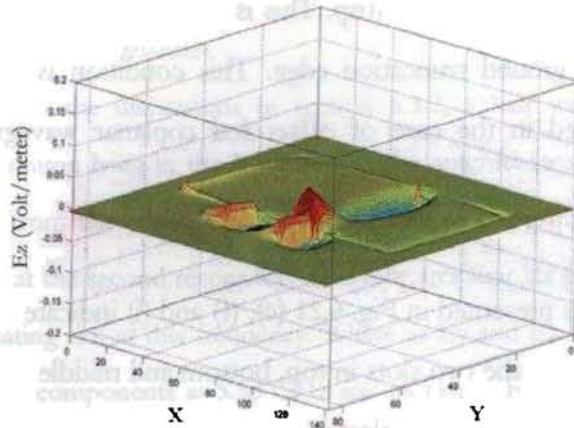


Fig. 6.21 (i)

Fig. 6.21 (a), (d) and (g) shows the computed E_x -fields at the top, middle and bottom layers of the antenna. The FDTD computed results shows that E_x values at the two slots are dominating at the first resonance. At the top layer a maximum of 0.5 V/meter is observed when the system is excited by 1V/meter (maximum amplitude of the gaussian pulse). E_x values are slightly less at the middle layer and bottom layer of the structure at locations corresponding to the slots. The E_x values at middle and bottom layers are ~ 0.1 V/meter. It should be noted that the E_x fields in the slots are in phase components. This is same as the results observed in the case of offset fed coplanar waveguide discussed in chapter 5.

The computed E_y components presented in Fig. 6.21 (b),(e) and (h) clearly shows that there is only negligible E_y component in the structure at the first resonance. In the top layer of the antenna $-0.05\text{V}/\text{meter}$ is observed at the gap separating ground truncation and the right lateral ground strip. This is due to a weak coupling between the right lateral strip and ground truncation edge. This condition is also similar to the FDTD results observed in the case of offset fed coplanar waveguide presented in chapter 5.

E_z components presented in Fig. 6.21 (c), (f) and (i) indicate that the E_z value is 180 degree out of phase in the two slots in top, bottom and middle layers of the structure at the first resonance. $0.1\text{V}/\text{meter}$ of electric field is observed on top and middle layers. But the E_z field is very feeble in the bottom layer of the substrate. The 180 degree out of phase E_z values will be cancelled at the far field and does not contribute to the radiated field from the structure.

The interpretation of field values presented above concludes with two important points. Radiation at the lower resonance is mainly due to the contribution of in phase E_x components at the two slots. This inference is exactly similar to the results obtained for the electric field distribution in the case of a coplanar waveguide excited with corner feed. Owing to the similarity of radiation mechanism of coplanar antenna at the fundamental resonance to the radiation mechanism of an offset fed coplanar waveguide, the present design is not a wide monopole element with two shorted parasitic strips. In

the case of monopoles the radiation should be due to the current distribution on the top patch and its image on the ground plane (ground plane of the microstrip line in this case).

E-field components at the second resonance

According to the discussions in section 6.3.2, a half wave length slot with sinusoidal field variation lying in the XY plane of the antenna structure, approximating the fringing field from the edge of centre strip width to the ground truncation is the cause of radiation at the second resonance. This indicates that E_x field values should be absent in the radiating slot at this frequency. Where as E_y and E_z field values can exist. The E_x , E_y and E_z components at 5.55 GHz are shown in Fig. 6.22 (a)-(i). This is the second resonant frequency of the antenna obtained using FDTD computation. The field components at the three layers of the substrate are presented. The field components are computed by exciting the antenna using sinusoidal excitation function with $f=5.5$ GHz.

A. Top layer

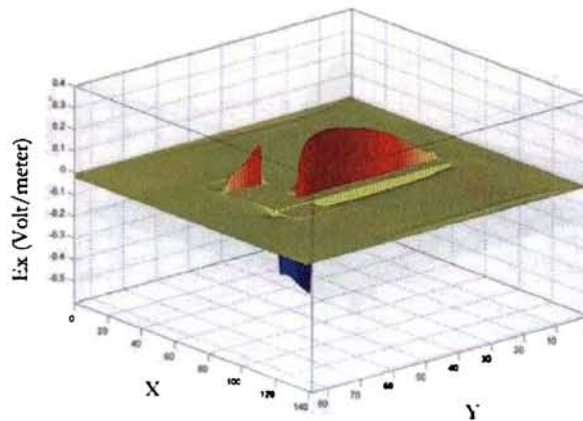


Fig. 6.22 (a)

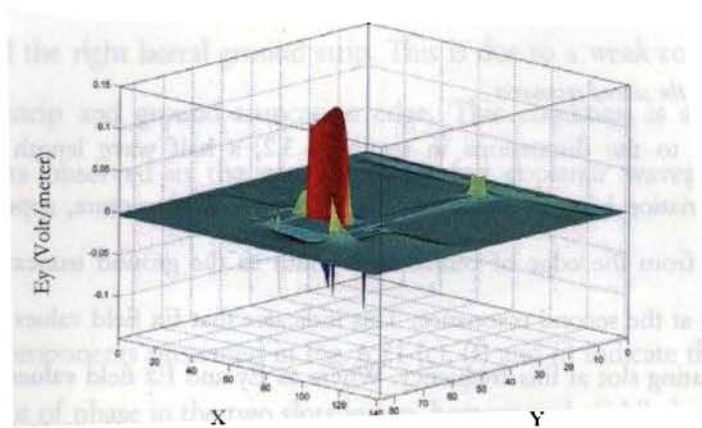


Fig. 6.22 (b)

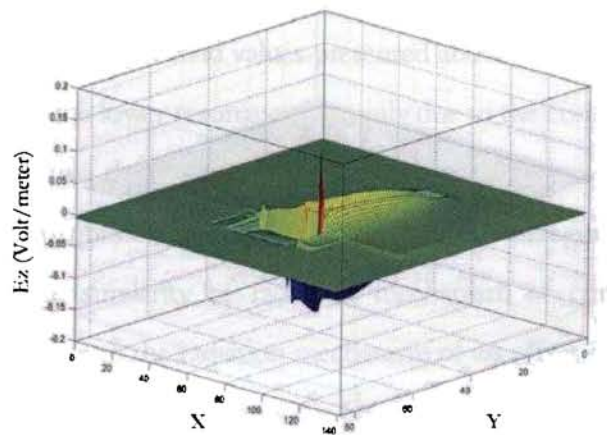


Fig. 6.22 (c)

Middle layer

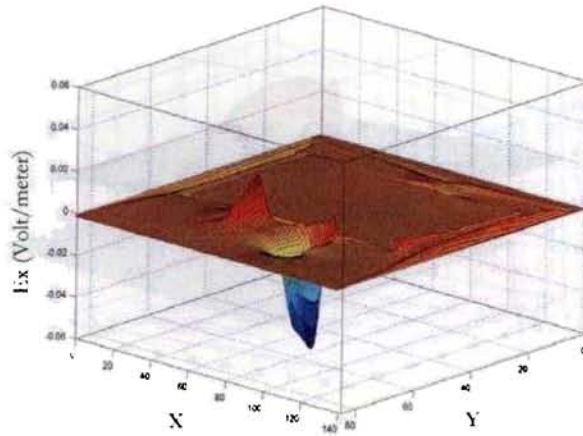


Fig 6 22 (d)

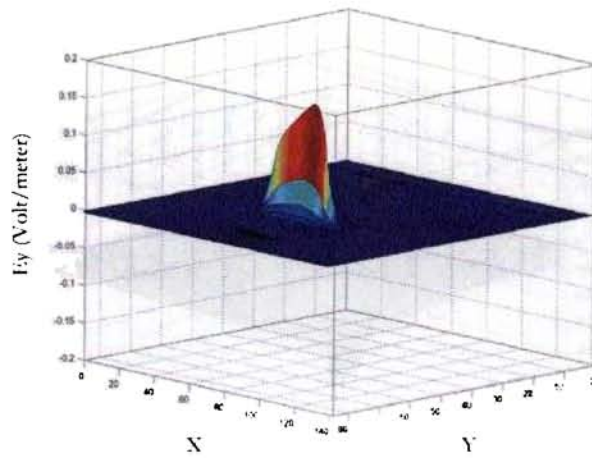


Fig 6 22 (c)

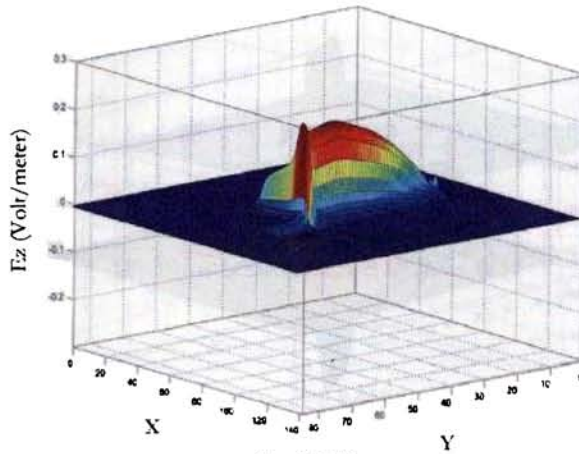


Fig. 6.22 (f)

C. Bottom layer

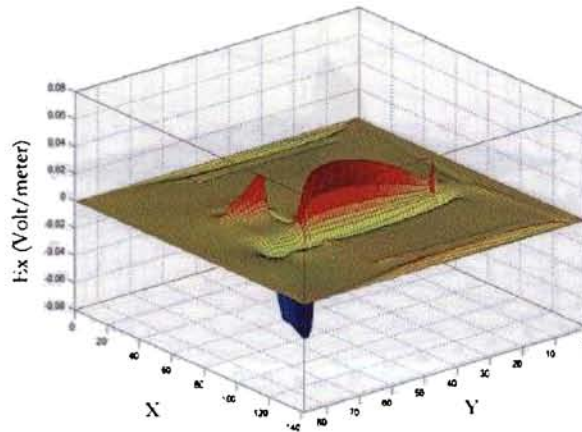


Fig. 6.22 (g)

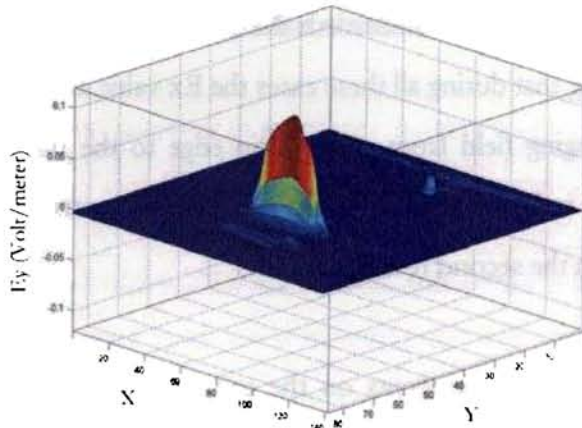


Fig 6.22 (h)

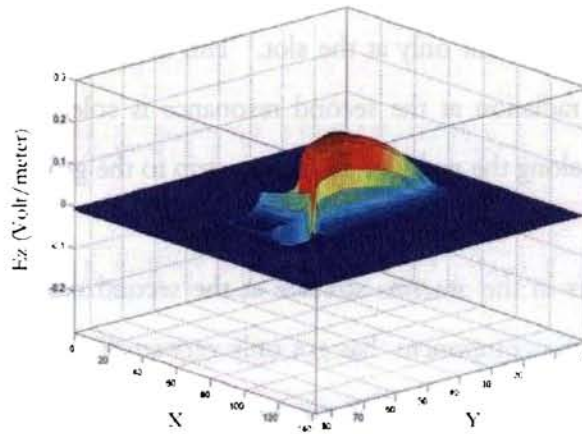


Fig 6.22 (i)

Fig. 6.22 (a), (d) and (g) shows the E_x component of electric fields present in the top, middle and bottom layers of the antenna structure at the second resonance. It is clear from the figure that E_x component has $\sim 0.2\text{V}/\text{meter}$ amplitude in the two slots of the coplanar geometry at the top layer. But they are out of phase components and cancel at the far field, resulting no radiation. In the middle and bottom layer E_x component has only a feeble value at the location underneath the two slots and are out of phase each other. It is worth noting that during all these cases the E_x value at the location of the slot approximating the fringing field from centre strip edge to the microstrip line ground truncation is zero. This indicates that E_x component is not contributing radiation from the coplanar antenna in the second resonant band.

The computed E_y components on the top, middle and bottom layer of the antenna structure at the second resonance is presented in Fig. 6.22 (b),(e) and (h). A half wave variation of E_y field component is observed at the second resonance. A peak amplitude of $0.15\text{ V}/\text{meter}$ is observed at the top layer. E_y component on the radiating structure is found to be present only at the slot. This supports the concept present in section 6.3.2 that the radiation at the second resonance is solely due to the radiation from the fringing field along the width of the centre strip to the ground plane edge.

E_z components in the antenna structure at the second resonance is depicted in Fig. 6.22 (c),(f) and (i). E_z component has got only very small value on top, middle and bottom layers. It is worth noting that E_y component is the only strong field component present in the structure on the three layers at the second resonance. Moreover, the electric

field components present in feed lines are mutually opposite during all the cases and no radiation is expected from the feed structure. That is the antenna at the second resonance will produce a vertically polarized electromagnetic radiation due to the E_y component of the fringing field along the width of the centre strip edge to the ground plane edge. Since the field variation in the radiating slot is approximately $\lambda d/2$, the radiation behavior will not be same as that obtained for the first resonance.

6.4.7 Conclusions

This part of the chapter describes the important points brought out from the theoretical investigation of the dual-band coplanar antenna using FDTD method.

- The returnloss characteristics in the two bands indicate that the antenna excites two resonant bands with wide impedance band width.
- The proposed dual-band antenna supports the concept of resonance due to the offset feeding in coplanar waveguides
- Microstrip line fed coplanar antenna configuration looks similar to a wide monopole antenna with shorted parasitic patches. But according to the FDTD results this apprehension is no longer valid. The computed E-field values at the fundamental resonance are not same as that usually present in the monopoles
- The computed E-field at the second resonance on the antenna shows that E_y component is very strong at the slot approximating fringing field from width of the centre strip to the bottom ground plane truncation.
- A half wave length variation of E-field is observed at the radiating slot in the second resonance
- The electromagnetic field is horizontally polarized(X direction) in the lower band of the antenna.
- The electromagnetic field is vertically polarized(Y direction) in the second band

- Since top layer and bottom layer of the antenna structure are supporting the same E-field distribution for the radiating field components in both the bands, a bidirectional radiation pattern is expected from the structure in the two operating bands.

PML based FDTD approach have given a clear insight into the problem. The return loss characteristics, radiation mechanism and the polarization of the EM energy radiated from the structure at the two resonances are clearly understood from the FDTD analysis.

6.5 Parametric analysis

In this section the parametric analysis of the device is discussed in detail. The structural parameters of the antenna are varied in order to study its effect on the two resonant frequencies and thus to confirm the two modes of the proposed antenna. The resonant frequency and impedance band width are the main parameters studied. Parametric analysis also leads to the formulation of simple equations to design the proposed antenna for any two bands of operation. In order to perform the parametric analysis the coplanar antenna with structural parameters as $l=9$ mm, $w=12.5$ mm, $c=5$ mm, $g=0.8$ mm, $L=40$ mm, $W=53$ mm when printed on FR4 substrate of $\epsilon_r=4.7$, loss tangent 0.02 and thickness $h=1.6$ mm is used. Width of the signal strip is 3 mm for 50 Ω characteristic impedance.

6.5.1 Effect of length 'l' on resonant frequencies and bandwidth

Fig. 6.23 shows the effect of length 'l' of the coplanar antenna on the return loss characteristics.

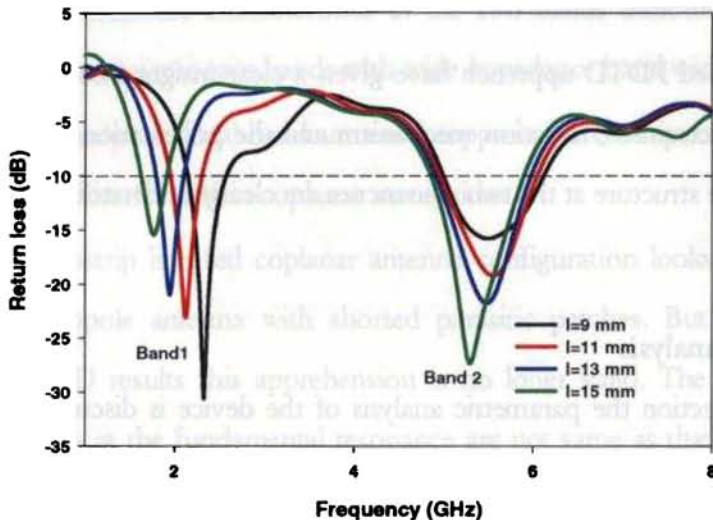


Fig. 6.23 Effect of dimension 'l' on the return loss characteristics of the microstrip line fed dual-band coplanar antenna

The length 'l' is varied from 9 mm to 15 mm. In this case, the resonant frequency in the lower band changes from 2.33 GHz to 1.77 GHz, whereas higher resonance varies from 5.2 GHz to 5.18 GHz only. Here, all other parameters of the antenna are kept constant. It can be concluded that the lower resonance decreases as l increases and the upper resonance remains unchanged. Because as l increases symmetrically for the three strips, the resonant length for the first band increases four times and thus the resonant frequency in the first band decreases more rapidly. Since width of the centre strip is kept

constant during this study the second resonance remains almost unchanged. Second resonance is solely due to the width 'w' of the centre strip.

Influence of 'l' on the bandwidth performance is also very important. Return loss characteristics of the fabricated antenna shows that the two bands are wide. The influence of length 'l' on the -10dB return loss bandwidth at the two resonant bands are shown in Fig. 6.24.

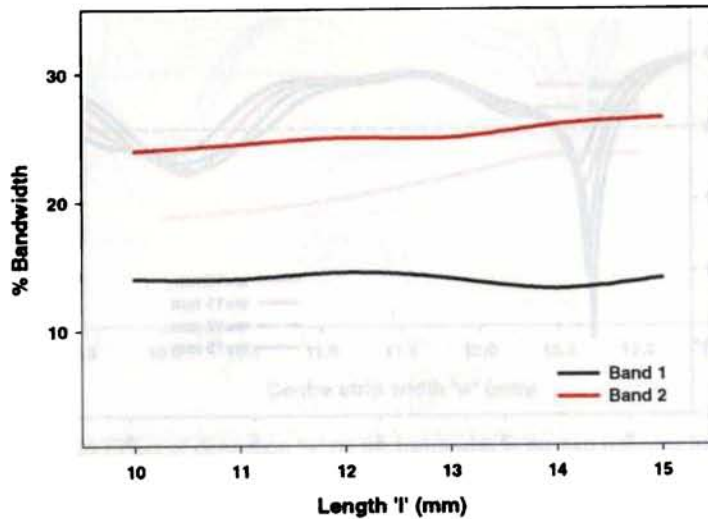


Fig. 6.24 Effect of dimension 'l' on the bandwidth at the two resonant bands of the microstrip line fed dual-band coplanar antenna

It is noted that bandwidth of the antenna's second resonant band increases slightly as l increases. When 'l' changes from 9 mm to 15 mm the band width in the lower band remains unchanged, but in the second band it varies from 19% to 23 %. This is due to the increase in surface area of the centre strip as l increases. It is a well proved fact that thick dipole elements yield more band width. The principle holds good for this case also.

6.5.2 Effect of centre strip width 'w' on resonant frequencies and band width

The centre strip width 'w' is a common dimension for the two resonances. The 'U' shaped current path in the lower band uses 'w' to sustain the resonance. In the higher band width 'w' is the sole cause of resonance in the structure. Influence of dimension 'w' on the two resonant frequencies are depicted in Fig. 6.25.

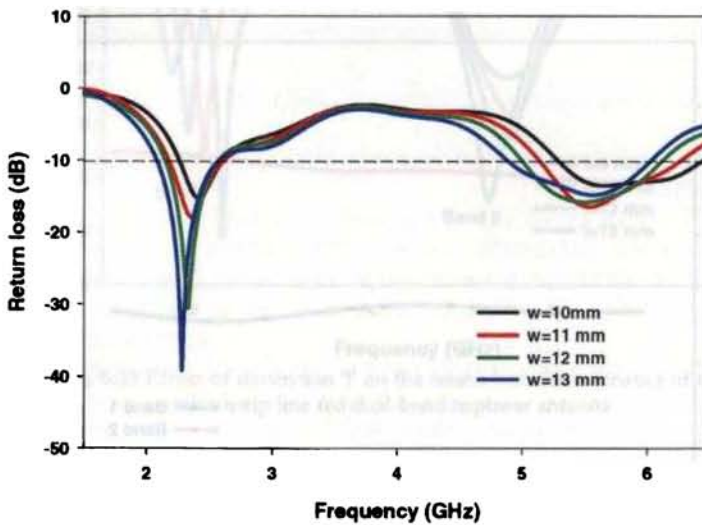


Fig. 6.25 Effect of dimension 'w' on the return loss characteristics of the microstrip line fed dual-band coplanar antenna

Figure shows that when 'w' increases from 10 mm to 13 mm the lower resonance changes from 2.41 GHz to 2.32 GHz and the upper resonance changes from 5.5 GHz to 5.32 GHz. That is the higher resonance is more rapidly varying than the lower resonance due to the change in 'w'. Because as 'w' increases, as explained, the resonant path for lower resonance increases and thus first resonance decreases. The 'w' contributes a small part in the total resonant length in the lower resonance, where as 'w'

is the sole part of resonance in the higher band and thus influences more at the higher band.

The variation of bandwidth in the two bands with the change in 'w' is depicted in Fig. 6.26.

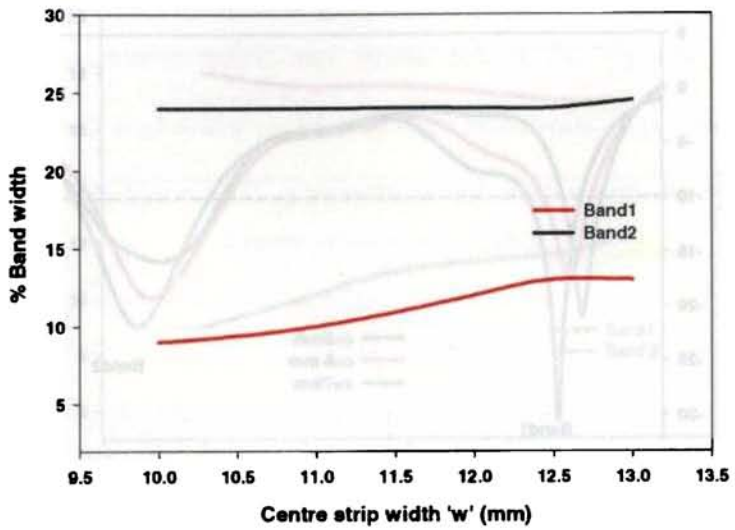


Fig. 6.26 Effect of dimension 'w' on the bandwidth at the two resonant bands of the microstrip line fed dual-band coplanar antenna

When 'w' changes from 10 mm to 13 mm return loss bandwidth in the first band increases as shown in the figure, where as the bandwidth in the second band remain unchanged. Because the increase in 'w' increases the surface area for the surface current on the centre strip at the lower resonant frequency, where as it doesn't increase the surface area for the current on the strip corresponding to upper resonance, and thus the bandwidth remains unchanged in the second band.

6.5.3 Effect of lateral strip width 'c' on resonant frequencies and band width

The effect of the lateral strip width 'c' on the two resonant frequencies are depicted in Fig. 6.27. In order to facilitate the imbalance in the feed the two lateral ground strips are varied equally.

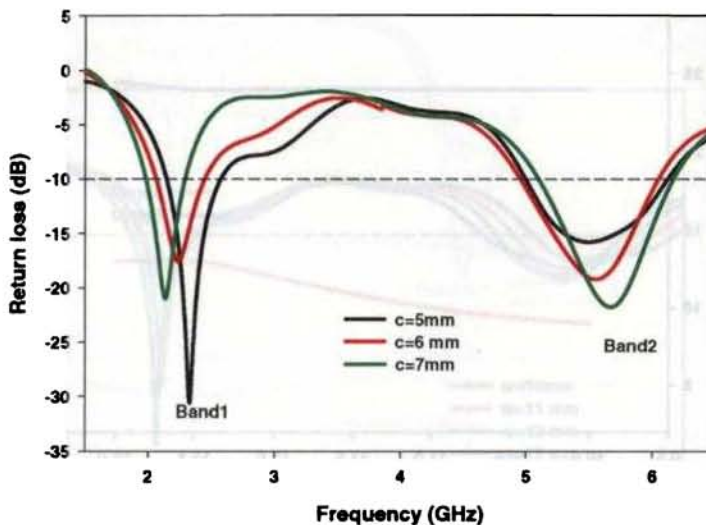


Fig. 6.27 Effect of antenna length 'c' on the return loss characteristics of the microstrip line fed dual-band coplanar antenna

The lateral strip width affects the first resonance very much, where as the second resonant frequency remains almost same. When 'c' varies from 5 mm to 7 mm the resonant frequency in the first band has changed from 2.39 GHz to 2.1 GHz. When 'c' increases symmetrically for the two strips, the resonant length for the first band increases two times, and thus the resonant frequency for the first band decreases. Since resonant length 'w' is not changed, the resonant frequency in the second band remains almost

constant. The resonant frequency has only very small change when 'c' changes from 5 mm to 7 mm.

Influence of the lateral strip width on the band width performance of the antenna in the two bands are depicted in Fig. 6.28.

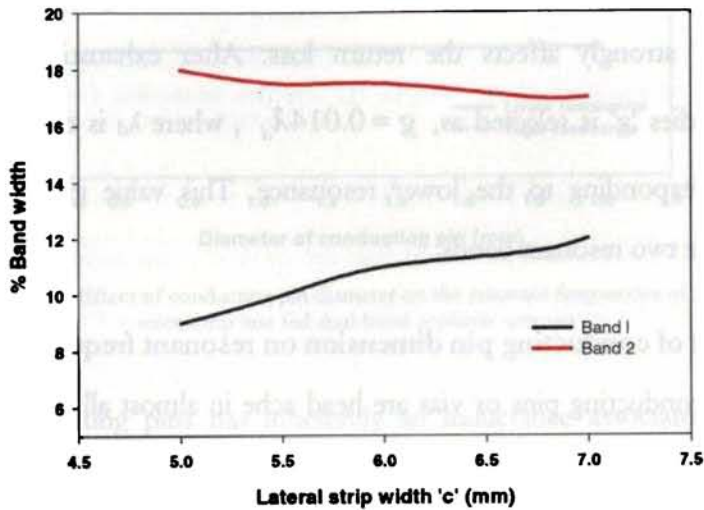


Fig. 6.28 Effect of dimension 'c' on the bandwidth at the two resonant bands of the microstrip line fed dual-band coplanar antenna

The impedance bandwidth in the two resonant bands are slightly affected when width of the two lateral strips are changed. When the width changes from 5 mm to 7 mm the bandwidth in the lower resonance changes from 9% to 12 %, where as the bandwidth in the higher resonance degrades slightly. When the lateral strip width is increased the surface current along the length of the lateral strips has got more surface area, which in turn will increase the band width in the lower band slightly. Since the surface current at the lateral strips have only negligible value at the higher resonance the effect is negligible for this case.

6.5.4 Effect of gap 'g' on resonant frequencies and band width

Gaps 'g' in the structure is the discontinuity forming radiation at the lower resonance of the structure. The 'g' determines the coupling between the centre strip and the two lateral strips. In order to achieve strong coupling the gap 'g' should be very small compared to the operating wavelength at the lower resonance. In the same time close proximity of 'g' may affect the resonant property of the higher band. Moreover the change in 'g' strongly affects the return loss. After exhaustive experimental and simulation studies 'g' is selected as, $g = 0.014\lambda_d$, where λ_d is the wave length in the dielectric corresponding to the lower resonance. This value gives good return loss response in the two resonant bands.

6.5.5 Effect of conducting pin dimension on resonant frequencies

The conducting pins or vias are head ache in almost all microwave circuits. Its length and diameter affects the performance of the circuit. The effect of conducting pin diameter on the two resonant frequencies is depicted in Fig. 6.29.

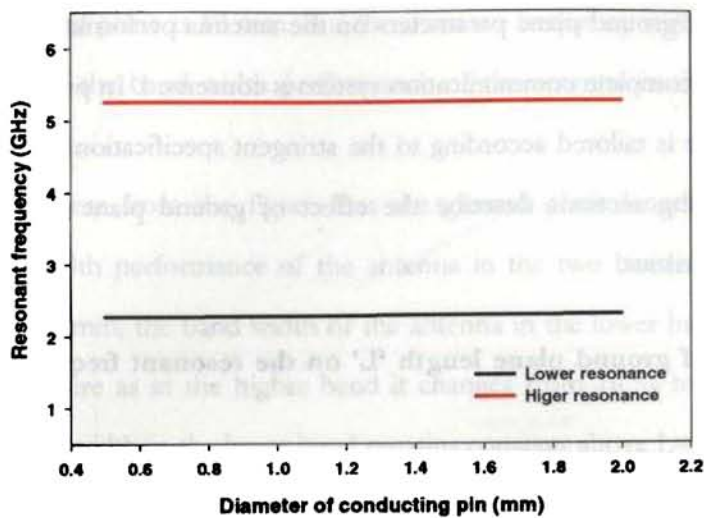


Fig. 6.29 Effect of conducting pin diameter on the resonant frequencies of the microstrip line fed dual-band coplanar antenna

Conducting pins has inherently an inductance associated with it. The inductance increases as its length increase. But in this context the length of the conducting pin is equal to the substrate height, and is very small compared to the operating wave length at the lower resonant frequency. Length of the conducting pins is to be considered while calculating the lower resonance of the antenna. Variation study is done using HFSS simulation package. When the diameter of the conducting pin is increased from .5 mm to 2 mm, the resonant frequency is increased by only 20 MHz, at the lower band. Where as, at the higher band the resonant frequency is almost remains constant. The increased pin diameter reduces the resonant length, which in turn increases the resonant frequency in the lower resonance. Since the higher resonance is due to the width of the centre strip the conducting pin dimension has not affected the resonance.

Effect of ground plane parameters on the antenna performance is an important study as far as a complete communication system is concerned. In practice dimension of the ground plane is tailored according to the stringent specifications of communication systems. Following sections describe the effect of ground plane dimensions on the antenna characteristics.

6.5.6 Effect of ground plane length 'L' on the resonant frequencies and band width

The effect of ground plane length 'L' on the resonant frequencies of the antenna are depicted in Fig. 6.30. It is observed that the ground plane dimension is not affecting the two resonant frequencies significantly. The lower resonance has increased by 50 MHz when the ground plane length is reduced from 40 mm to 10 mm.

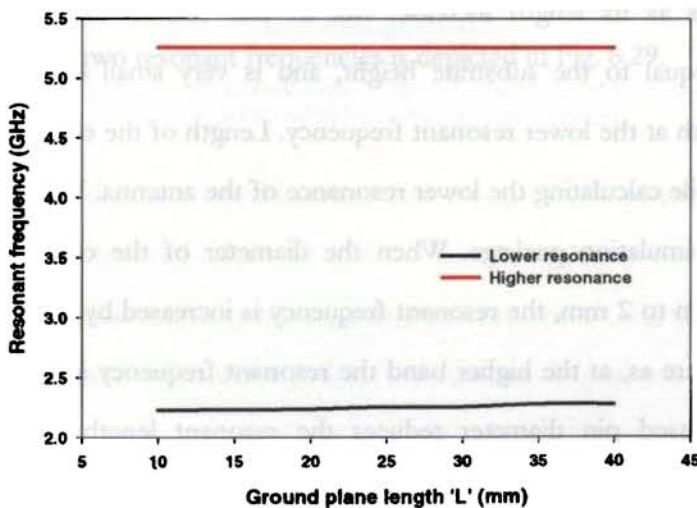


Fig. 6.30 Influence of ground plane length 'L' on the dual band coplanar antenna resonant frequencies

The return loss value is found to be very poor at the higher resonance when length of the ground plane is 10 mm. But the resonant frequency is remains same. The influence of 'L' on the band width performance of the antenna in the two bands are depicted in Fig. 6.31.

It clear from the figure that the ground plane length 'L' significantly affects the bandwidth performance of the antenna in the two bands. When 'L' varies from 10 mm to 40 mm, the band width of the antenna in the lower band changes from 10 % to 14 %, where as in the higher band it changes from 16 % to 22 %. It is also noted that the bandwidth in the lower band remains constant above L=30 mm. It can be concluded that the ground plane is not affecting the resonant frequencies of the antenna significantly, but the impedance bandwidth characteristics in the two bands are affected. The worst case bandwidth (when L=10 mm) is 10% in the lower band and 16 % in the higher band.

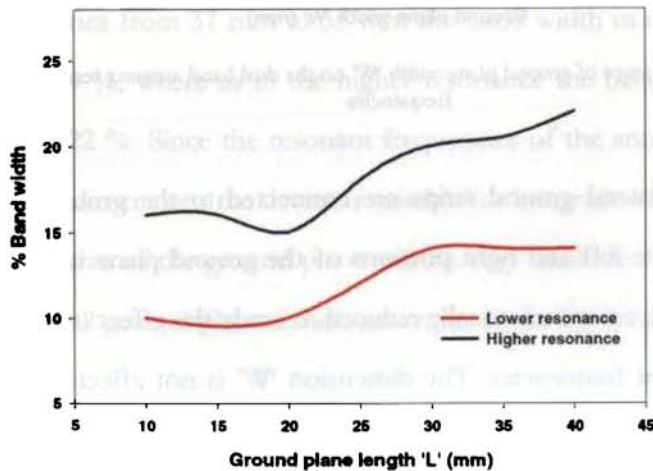


Fig. 6.31 Influence of ground plane length 'L' on the band width characteristics of the dual band antenna

6.5.7 Effect of ground plane length 'w' on the two resonant frequencies and band width

The influence of ground plane width 'W' on the two resonant frequencies of the antenna is depicted in Fig. 6.32. Width of the ground plane cannot be reduced below the total width of the coplanar radiating structure.

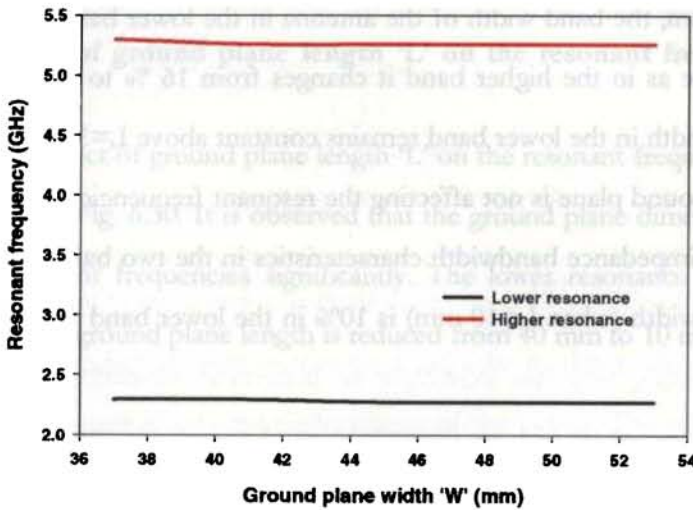


Fig. 6.32 Influence of ground plane width 'W' on the dual band antenna resonant frequencies

Since the lateral ground strips are connected to the ground truncation at the extreme corners, the left and right portions of the ground plane width extending from the conducting pins are symmetrically reduced to study the effect of ground plane width 'W' on the resonant frequencies. The dimension 'W' is not affecting the two resonant frequencies.

The band width performance of the antenna in the two resonant bands with the various ground plane width is depicted in Fig. 6.33.

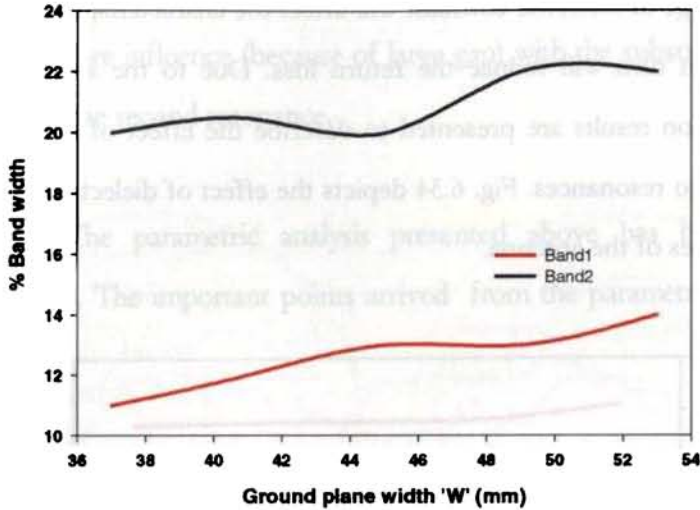


Fig. 6.33 Influence of ground plane width 'W' on the band width performance of the dual band antenna

When W varies from 37 mm to 53 mm the band width in the lower resonance varies from 11 to 14 %, where as in the higher resonance the band width has a small shift from 20 % to 22 %. Since the resonant frequencies of the antenna is not affected by the ground plane dimensions the device is suitable for integration in compact wireless modules where the size of the ground plane will be very small. It should be noted that the antenna with small ground plane dimensions reduces the band width performance of the antenna.

6.5.8 Effect of dielectric constant ϵ_r on resonant frequencies

The dielectric constant of the substrate material has influence on the resonant frequencies. When the antenna including the feed structure is fabricated on a dielectric substrate, the change in dielectric constant will affect the characteristic impedance of the feed line, which in turn will reduce the return loss. Due to the scarcity of different laminates, simulation results are presented to describe the effect of substrate dielectric constant on the two resonances. Fig. 6.34 depicts the effect of dielectric constant on the resonant frequencies of the antenna.

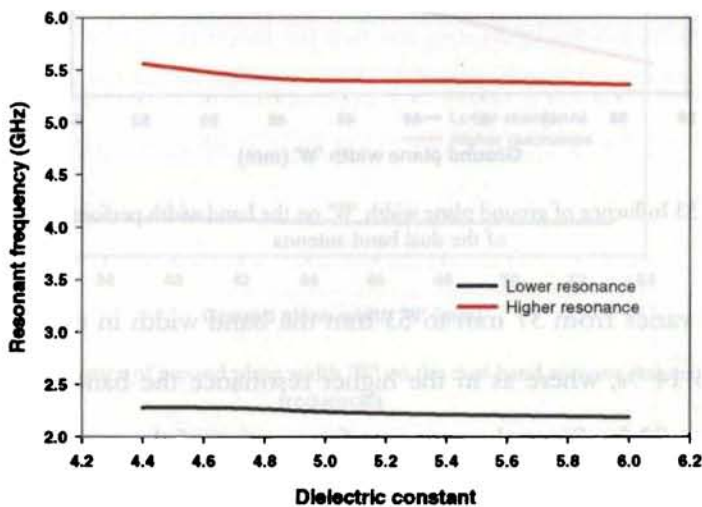


Fig. 6.34 Influence of substrate dielectric constant on the two resonant frequencies of the antenna

When ϵ_r varies from 4.7 to 6 the lower resonant frequency reduces by 90 MHz, where as the higher resonance reduces by 200 MHz. In the case of lower resonance the electric field components are not confined with in the substrate. The average dielectric

constant of air and substrate material has to be considered while calculating the resonant frequency in the lower band. Since the gap 'g' is very small, the small variation in the substrate dielectric constant will not affect the lower resonance very much. At the second resonance the fringing field from width of the centre strip to the ground truncation has more influence (because of large gap) with the substrate material. This in turn will change the second resonance.

The parametric analysis presented above has brought out certain important points. The important points arrived from the parametric analysis are given below.

- The lower resonant frequency is influenced by length and width of the centre strip and the two lateral ground strips.
- The higher resonance is solely due to the width of the centre strip
- The conducting pin length should be accounted while calculating the resonant frequency in the lower band
- The rectangular geometry effectively increases the surface area for the meandered surface current on the three strips, and thereby exhibiting wide band width in the lower band
- Length of the centre strip increases the band width in the higher band
- The ground plane dimensions of the antenna has no significant effect on the antenna resonant frequency. But the impedance band width in the two bands are greatly affected by the length and width of the ground plane.

- Effective dielectric constant value is to be used for calculating the lower and higher resonant frequencies of the antenna

6.6 Far field radiation and polarization

The far field radiation measured using a standard horn antenna is depicted in Fig. 6.35.

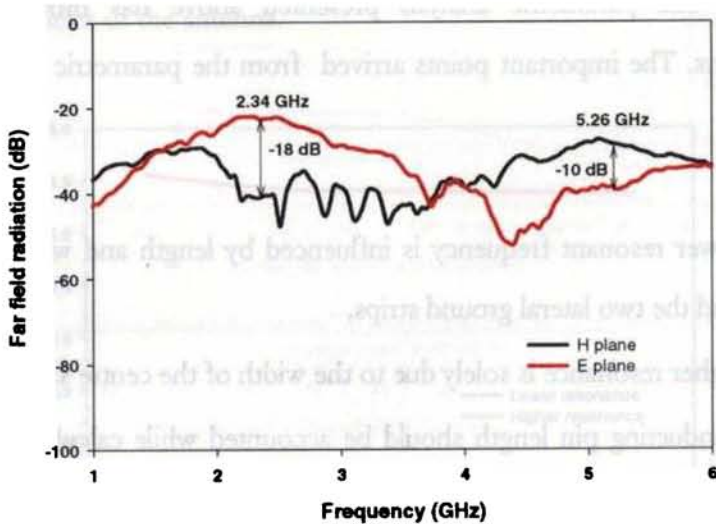


Fig. 6.35 Far field radiation of dual-band coplanar antenna received by a standard horn antenna

When the two slots of the coplanar antenna are perpendicular to the E-plane (Horizontal polarization) of the horn antenna, the horn antenna receives maximum power. Thus horizontally polarized EM energy is received. \sim 18 dB polarization discrimination is achieved at the lower resonant frequency. In the higher band, the antenna produces a vertically polarized EM energy. In this case the slot separating the

centre strip to the ground truncation is parallel to the H-plane of the horn antenna. Polarization discrimination for this case is only -10dB.

6.7 Principal plane radiation patterns

The principal plane radiation pattern of the typical antenna at 2.19, 2.34 and 2.52 GHz are shown in Fig.6.36.

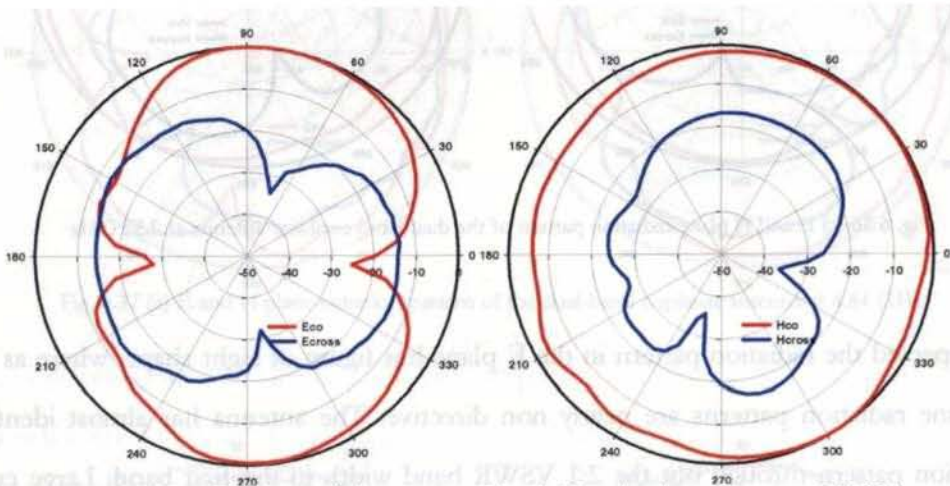


Fig. 6.36 (a) E and H plane radiation pattern of the dual-band coplanar antenna at 2.19 GHz

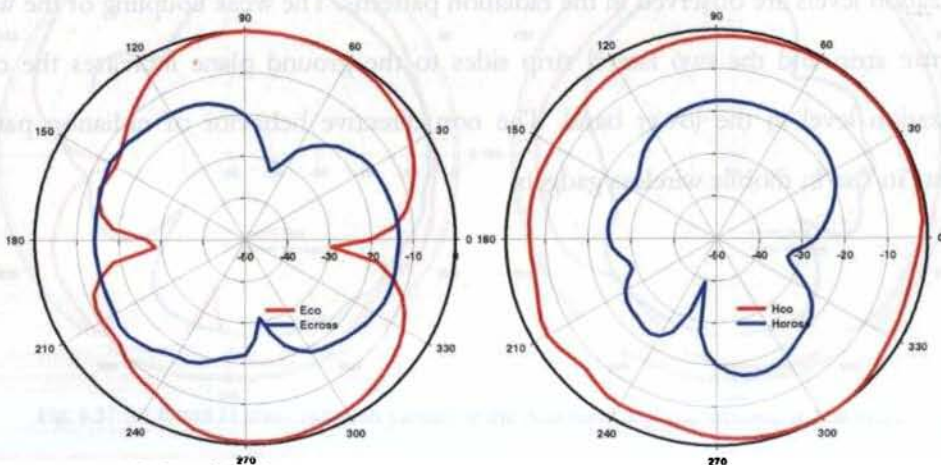


Fig. 6.36 (b) E and H plane radiation pattern of the dual-band coplanar antenna at 2.34 GHz

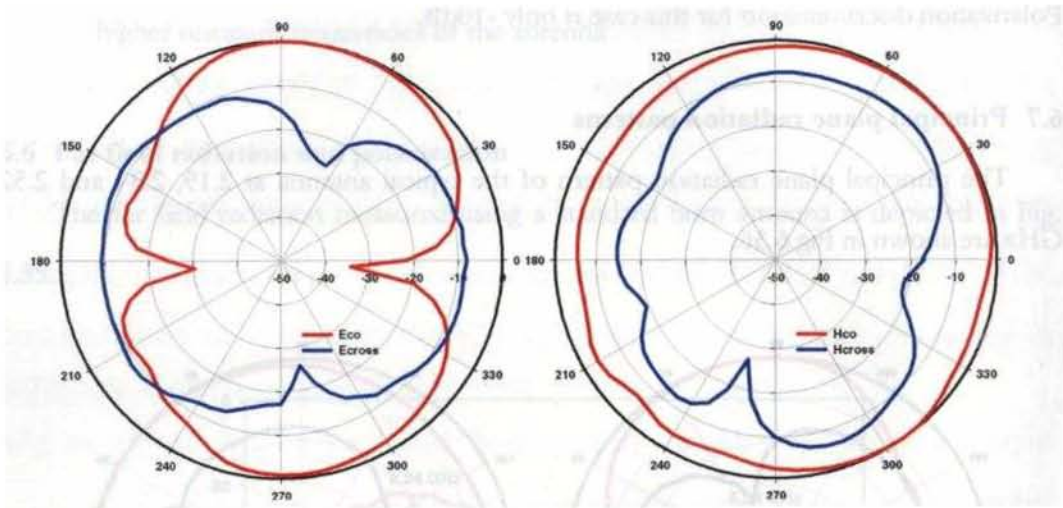


Fig. 6.36 (c) E and H plane radiation pattern of the dual-band coplanar antenna at 2.52 GHz

As expected the radiation pattern in the E plane has figure of eight shape, whereas the H plane radiation patterns are nearly non directive. The antenna has almost identical radiation pattern through out the 2:1 VSWR band width in the first band. Large cross polarization levels are observed in the radiation patterns. The weak coupling of the width of centre strip and the two lateral strip sides to the ground plane increases the cross polarization level in the lower band. The non directive behavior of radiation pattern suggests its use in mobile wireless gadgets.

Fig. 6.37 (a), (b) and (c) shows the E and H plane radiation patterns of the antenna at 4.84, 5.26 and 6.07 GHz respectively.

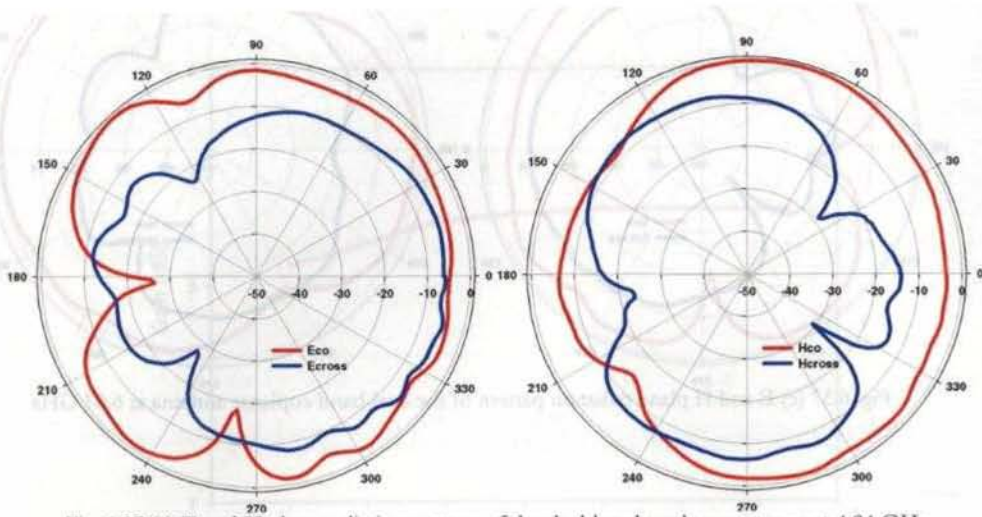


Fig. 6.37 (a) E and H plane radiation pattern of the dual-band coplanar antenna at 4.84 GHz

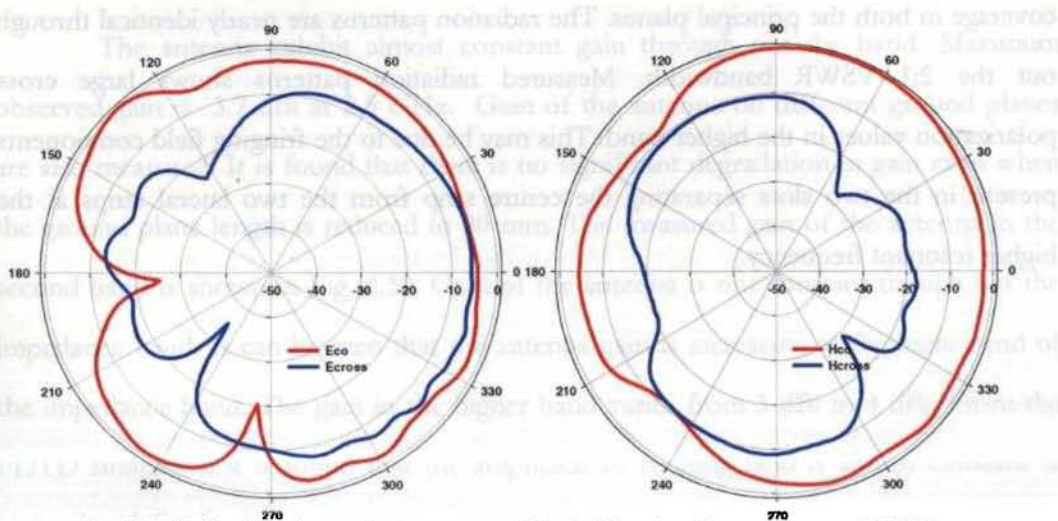


Fig. 6.37 (b) E and H plane radiation pattern of the dual-band coplanar antenna at 5.26 GHz

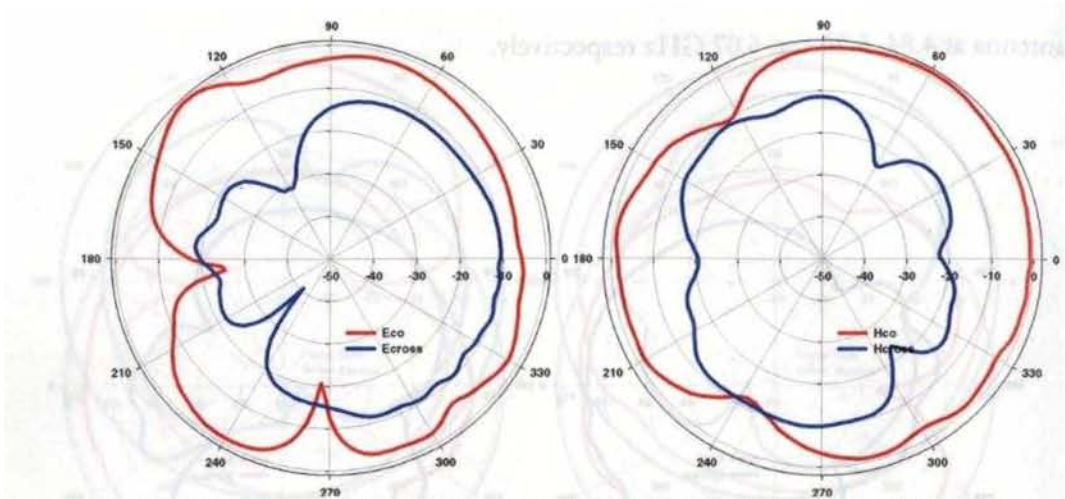


Fig. 6.37 (c) E and H plane radiation pattern of the dual-band coplanar antenna at 6.07 GHz

The radiation patterns in the higher band are found to have good radiation coverage in both the principal planes. The radiation patterns are nearly identical throughout the 2:1 VSWR bandwidth. Measured radiation patterns show large cross-polarization values in the higher band. This may be due to the fringing field components present in the two slots separating the centre strip from the two lateral strips at the higher resonant frequency.

6.8 Gain and radiation efficiency in the two bands

Gain of the coplanar antenna in the lower resonant band is shown in Fig. 6.38.

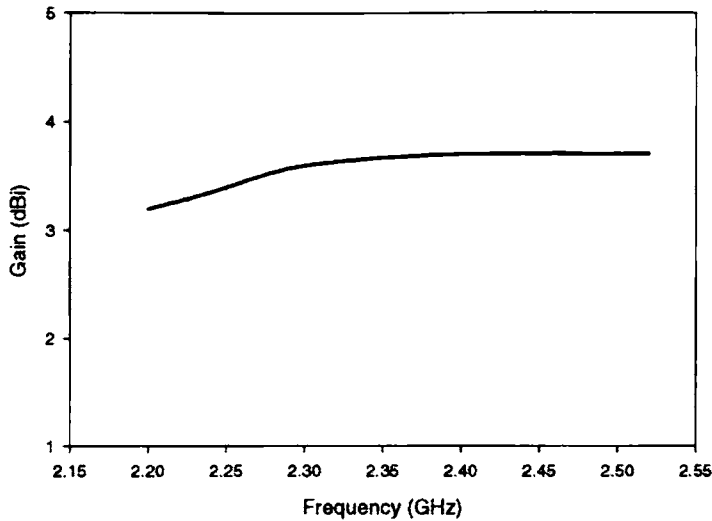


Fig. 6.38 Measured gain of the coplanar antenna in the lower band

The antenna exhibit almost constant gain through out the band. Maximum observed gain is 3.7 dBi at 2.5 GHz. Gain of the antenna on different ground planes are also measured. It is found that there is no significant degradation in gain even when the ground plane length is reduced to 20 mm. The measured gain of the antenna in the second band is shown in Fig. 6.39. Gain of the antenna is not constant though out the impedance band. It can be seen that the antenna gain is increasing at the higher end of the impedance band. The gain in the higher band varies from 3 dBi to 4 dBi. From the FDTD simulation it is found that the amplitude of fringing field is almost constant at higher band. So the gain increases with frequency.

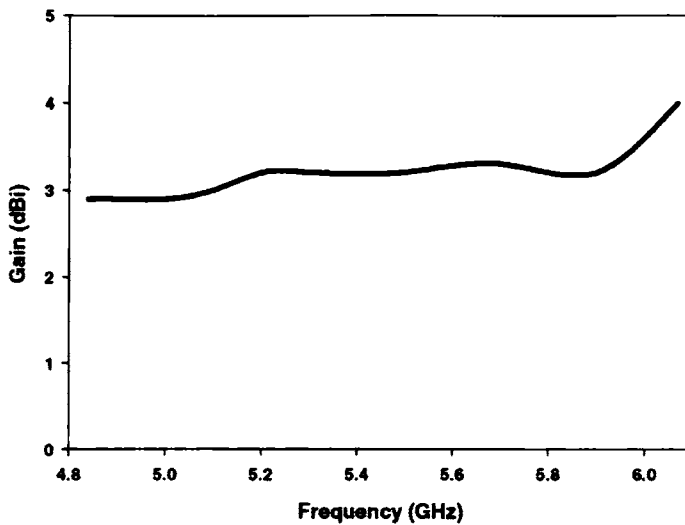


Fig. 6.39 Measured gain of the coplanar antenna in the second band

The estimated radiation efficiencies using IE3D simulation package is 85% in the lower band and 73% in the higher band when the antenna is fabricated on FR4 substrate. Note that the loss tangent of the FR4 substrate is 0.02, which reduces the radiation efficiency. The estimated efficiency is found to be increasing when the antenna is designed on RT duroid substrate. In this case the efficiency is 89% and 79 % respectively in the lower and higher bands of the antenna.

6.9 Design procedure

The experimental as well as theoretical investigations gave insight to radiation mechanism and effect of various antenna parameters on the radiation characteristics. Inferences of these investigations leads to the formation of design equations for the

microstrip fed dual-band coplanar antenna. The following equations can be used to design the antenna with good radiation characteristics.

1. Select any substrate with relative dielectric constant ϵ_r and thickness h , and calculate the width (w_1) of the microstrip transmission line for 50Ω characteristic impedance.
2. Calculate width of the centre strip (w) using the following equation.

$$w = \frac{c}{2f_2\sqrt{\epsilon_{re}}} \tag{1}$$

where c is the velocity of light and f_2 is the second resonant frequency.

Since the field components are not confined to the substrate alone the effective dielectric constant (ϵ_{re}) has to be used in calculations instead of relative permittivity of the substrate.

$$\epsilon_{re} = \frac{\epsilon_r + 1}{2} \tag{2}$$

3. The length l of the three rectangular strips is then calculated as

$$l = \frac{0.15c}{f_1\sqrt{\epsilon_{re}}} \tag{3}$$

Where f_1 is the first resonant frequency

4. Width of the lateral conductors (C) is calculated using the equation given below.

$$C = \frac{c}{2f_1\sqrt{\epsilon_{re}}} - \left(\frac{4l + 2h + w}{2} \right) \quad (4)$$

Where h is the thickness of the dielectric substrate.

5. Gap separating centre strip from the lateral strips is then calculated

$$g = \frac{0.014c}{f_1\sqrt{\epsilon_{re}}} \quad (5)$$

Where c is the velocity of electromagnetic signal in free space

The constants 0.15 and 0.014 in equations (3) and (5) respectively are obtained after exhaustive experimental and simulation studies.

6. Ground plane dimensions are calculated using the following equations.

$$L = \frac{0.12c}{f_1\sqrt{\epsilon_{re}}} \quad (6)$$

$$W = \frac{0.98c}{f_1\sqrt{\epsilon_{re}}} \quad (7)$$

The constants 0.12 and 0.98 are derived empirically after studying the effect of ground plane on the two resonant frequencies.

7. The two extreme corners of the lateral conductors are connected to ground plane of the microstrip line using vias or conducting pins.

In order to confirm the validity of above equations various antennas were designed using the above equations. The return loss characteristics of an antenna designed on RT duroid ($\epsilon_r=2.2$ and $h=1.5$ mm) substrate for 2.4/5GHz WLAN operation using the above equations are shown in Fig. 6.40. A photograph of the fabricated antenna is shown in Fig. 6.41. The antenna is resonating at 2.54 GHz and 5.59 GHz with 13% and 19% return loss bandwidth in lower and higher bands respectively.

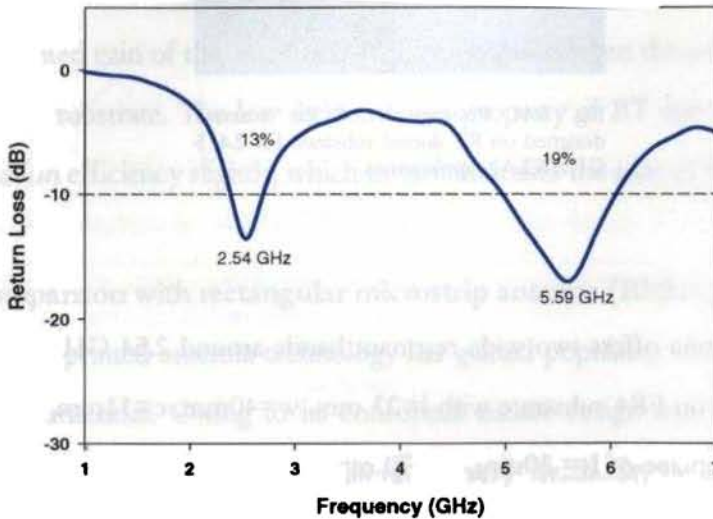


Fig. 6.40 Return loss characteristics of the antenna printed on RT duroid substrate for 2.4/5GHz WLAN applications

TABLE 6.1
CHARACTERISTICS OF ANTENNAS DESIGNED ON DIFFERENT SUBSTRATES

Sl.No.	Antenna Dimensions (mm)	FDTD		Experiment		Radiation Efficiency (IE3D) (%)		Average Gain (dB)	
		Band1	Band2	Band1	Band2	Band1	Band2	Band1	Band2
1	l=12 mm, w=17mm, c=6mm, g=1.5 mm w1=3.5 mm on a ground plane of L=40mm, W=50 mm RT Duroid substrate	2.49 GHz BW=14%	5.44 GHz BW=17%	2.54 GHz BW=13%	5.59 GHz BW=19%	89	79	3.6	4.1
2	l=23 mm, w=40mm, c=11mm, g=1 mm w1=3 mm on a ground plane of L=30mm, W=70 mm FR4 substrate	0.86 GHz BW=11%	1.86 GHz BW=12%	0.89 GHz BW=10%	1.91 GHz BW=14%	81	74	3.1	3.5

The measured gain of the antenna is slightly increased when the antenna is fabricated on RT Duroid substrate. The low dielectric loss property of RT duroid substrate increases the radiation efficiency slightly, which in turn increases the gain of the antenna.

6.10 Comparison with rectangular microstrip antenna (RMSA)

The printed antenna technology has gained popularity after the introduction of microstrip antennas. Owing to its conformal nature design and analysis of microstrip antennas have been addressed in literature very much. In this section the coplanar antenna is compared with a rectangular microstrip antenna in order to highlight its feasibility as efficient microwave antenna.

STANDARD RECTANTULAR MICROSTRIP ANTENNA (RMSA)	Coplanar Antenna
Half wave length resonant structures. Large size, nearly $\lambda d/2$ size long and width larger than $\lambda d/2$ to obtain maximum efficiency	Extremely compact. Nearly $\lambda/5 \times \lambda/14$ size.
Simple and low fabrication cost	Easy to fabricate and low fabrication cost
Easy integration with microwave circuits	Coplanar antennas can be easily integrated with microwave circuits.
Narrow bandwidth	Broadband
7.2 dBi gain	~3.7 dBi gain
Substrate losses are high	Substrate losses are minimum due to the weak interaction of field components with substrate material
Uni-polar radiation pattern	Bi-polar radiation pattern
Vias are essential for active antenna applications	The DC ground potential is available on the top layer on the lateral ground strips, avoids the need of vias in many active antenna applications

6.11 Conclusions

A novel planar antenna is designed using the concept of resonance and radiation in offset fed coplanar waveguides. The FDTD analysis has made an insight into the radiation phenomena of the coplanar antenna. Coplanar antenna element exhibit similar properties observed in the case of coplanar waveguides with offset feed discussed in Chapter 5. The radiating system is extremely compact. The radiation mechanism and resonance of the coplanar waveguide is exhaustively explained in the thesis using the FDTD and experimental observations. Parametric analysis is also done to optimize the antenna. Measured radiation patterns of the antenna are broad and demand its application in compact wireless modules. Ground plane dimensions of the antenna are not significantly affecting the resonant frequency in the two bands. But bandwidth in the two bands is strongly affected by the ground plane dimensions. Measured peak gain of the coplanar antenna is ~ 4 dBi in the two bands. The design relations are also developed to synthesize the coplanar antenna dimensions for any two bands.

Conclusion

This chapter explains the conclusions brought out from the numerical and experimental investigations explained in the previous two chapters. A novel planar, compact, efficient antenna with good radiation characteristics is thus derived out of a coplanar transmission line structure by properly exciting it using an asymmetrical feed system.

7.1 Thesis Highlights

This chapter brings the thesis to a close by summarizing the results obtained out of the numerical as well as experimental investigations conducted on the resonance and radiation characteristics of coplanar waveguide with conventional feed and offset feed and the coplanar antenna. Aim of this work was to develop a compact dual-band antenna suitable for compact wireless connectivity terminals such as mobile phones, wireless LAN etc.

An introduction to the overview of antenna research, state of the art antenna technologies, introduction of coplanar waveguides have been discussed in chapter 1. The literature review presented in chapter 2 clearly convinces the importance of the work in this direction and the novelty of work presented. It could be seen from the literature review that resonance phenomena on coplanar waveguides with offset feed scheme is not yet addressed anywhere. The literature review clearly indicate that the radiating mode excited with corner feed system is a novel concept for antenna applications.

The materials and methodology employed for experimental investigations have been explained in chapter 3. In chapter 4 the PML based FDTD technique has been discussed. Importance of PML based FDTD computation in the present work and the source model for fast FDTD convergence was also presented.

Investigations on resonant characteristics of conventional coplanar waveguides, offset fed coplanar waveguides were presented in chapter 5 with FDTD as well as experimental results. Chapter 6 is devoted for the novel coplanar antenna developed

based on the conclusions of chapter 5. The FDTD and experimental results were also presented. A design procedure is also presented after the rigorous parametric analysis to design the antenna for any two bands.

7.2 Inferences from investigations on Coplanar Waveguides

A conventional open circuit coplanar waveguide is exhibiting resonance phenomena at higher microwave bands. Fig. 5.2 in chapter 5 indicates the measured as well as computed return loss characteristics with poor return loss at 6.5 GHz. The conclusions arrived based on the experimental as well computed results are as follows.

- When the frequency of operation is sufficiently high, open circuited CPWs excites a resonant mode.
- The resonant frequency is more influenced by the structural parameters such as l , w , c , and the dielectric constant of substrate.
- Return loss characteristics of the system is observed to be very poor through out the parametric analysis
- The efficiency of the system is very low (nearly 20%)
- Maximum gain is -2.1 dBi when the centre strip width is wide.
- Radiation pattern is highly distorted

The far field radiation presented in Fig. 5.3 in chapter 5 indicates that the radiation intensity is very poor. The parametric analysis clearly gives an insight into the influence of structural parameters on resonance. The antenna offers, extremely low gain and distorted radiation pattern along with large size.

The key idea behind the ‘coplanar antenna’ presented in the thesis is the excitation of a resonance in conventional coplanar waveguide with offset feed scheme. The offset feed mechanism have resulted a resonance on conventional coplanar waveguides with excellent radiation characteristics. FDTD analysis, experimental results, parametric analysis and simulation have resulted many important points, which will be very useful for both antenna and electromagnetic compatibility (EMC) researchers.

When a conventional open circuit coplanar waveguide is excited with an offset feed, a new resonance is found on the structure at lower microwave bands. This is a very interesting phenomenon for antenna researchers, because the dimension of the new resonant system has a very small size ($\lambda/5 \times \lambda/14$, where λ is the free space wavelength of the fundamental resonance). The conclusions of the chapter are summarized below.

- An open circuit CPW with conventional feeding excite spurious resonance at higher microwave bands.
- The mode thus excited at higher bands are not radiating EM energy efficiently. The radiation pattern, gain and efficiency are not enough to consider it as efficient compact radiator.
- A coplanar waveguide structure is able to excite a resonant mode at a lower frequency band when the feed point is away from the center of the signal strip, along the width (usually at the corner).

- The new resonance is influenced mainly by the length l , signal strip width ' w ', and substrate parameters.
- The resonance is due to the 'U' shaped resonant path excited on the centre strip and the coupling between centre strip and the two lateral strips.
- FDTD analysis shows that the corner feeding excites in phase field distribution.
- FDTD analysis and measured far field radiation shows that the tangential component of the fringing fields radiates and produce a horizontally polarized EM radiation.
- The width ' w ' should be slightly wide to obtain broad side radiation.
- The measured gain of the device is -1.8 dBi
- Length ' l ' of the waveguide should be less than $\lambda_d/4$, to obtain a distortion less radiation pattern, where λ_d is the wave length in the dielectric corresponding to the desired resonance. This reduces the phase variation of the electric fields in the slots.

7.3 Inferences from investigations on 'Coplanar antenna'

The conclusions presented in the above section was used to implement the 'coplanar antenna' configuration. A microstrip line was employed to excite the system. The conclusions of FDTD analysis, simulation results, measured characteristics of the antenna and the parametric analysis are summarized below.

- The optimum ratio between width of the lateral strip to the signal strip of coplanar geometry is 1:2.5 for obtaining good 2:1 VSWR band width and nearly omnidirectional coverage.
- The antenna is operating in the dual mode.
- The lower resonant frequency of the antenna is due to the 'U' shaped resonant path on the centre strip and 'L' and reflected 'L' shaped resonant paths on right and left lateral strips respectively.
- The 'U' shaped current path on the center strip is half wave length in dielectric.
- 'L' and reflected 'L' current paths are quarter wavelength in the dielectric.
- Gap 'g' should be small compared to the wavelength corresponding to the lower resonance to obtain good electromagnetic coupling between the center strip and lateral strips.
- The upper resonant frequency is obtained due to the width of the centre strip, corresponding to a half wave length variation in substrate.
- Radiation of the antenna in the lower resonant band is due to the fields along the length at the two gaps separating center strips from the two lateral strips.

- The antenna at the lower resonant frequencies can be described as an array of two identical in phase sources separated by a distance.
- In order to maintain a nearly constant phase of the electric field at the two gaps, the dimension should be less than quarter wave length.
- The wide radiation coverage observed from the radiation pattern at the two resonant bands suggests its use in mobile gadget applications.
- The antenna fabricated on RT duroid substrate exhibits 89% efficiency.
- The equations presented in the thesis can be used to design the 'coplanar antenna' with $\sim 2\%$ accuracy.

7.4 Demerits of the present design

An important demerit that has been encountered is the requirement of a ground plane on the bottom layer of the substrate to excite the two possible modes on the structure. That is a completely uni-planar integration is not possible. All the merits furnished in the previous sections are being over ruled by this disadvantage. Moreover, gap 'g' in the design is very small compared to the operating wavelength. A small conducting dust on the gaps can perturb the fundamental mode of the antenna very much. A short in the gap will not support these resonant modes. An insulator material coating is highly required to protect it from any accidental shorting problems at the slots.

7.5 Suggestions for future work

The radiation phenomena of offset fed coplanar waveguide has resulted a new radiating geometry for compact antenna applications. But from the microwave circuit point of view this resonance/radiation will be a problem for circuit designers. For example, a coplanar waveguide based open circuited stub at the out put impedance matching circuit of a microwave amplifier may excite spurious resonance/radiation if the connection to the input of the coplanar waveguide stub has got an offset on the centre strip due to fabrication errors. This may produce unwanted radiation problems at the resonant frequency of the open circuited stub. This will also arise feed back problems, resonance in the system package etc. This aspect of the offset feed on coplanar waveguides is not yet been addressed. A case study and analysis of its consequences by a complete circuit modeling with offset fed coplanar waveguide stubs will be a good research topic.

A complete uni-planar coplanar antenna using coplanar waveguide feed may be explored to overcome the major demerit of the present design. Reconfigurable antennas are the other area where 'coplanar antenna' is found to be a good candidate. The varactor diodes integrated on the resonant path of the antenna element can tune its resonant frequency electronically. These reconfigurable design concept will be useful in realizing ultra compact reactively steered antennas using parasitic array concepts for automotive applications. Active antenna concept can be implemented in 'coplanar antennas'. Transistors, diodes, MOSFETs etc. can be integrated on the antenna element

for amplification, self oscillating systems etc. It is worth noting that the ground potential is available at the top layer of the antenna at the two lateral ground strips, avoids the use of vias for active device integration.

APPENDIX A

Compact planar Multi-band Antenna for GPS, DCS, 2.4/5.8 GHz WLAN applications

A compact single feed multi-band planar antenna configuration suitable for GPS, DCS, 2.4/5.8GHz WLAN applications is developed. The antenna of dimensions 38mm x 3mm x 1.6mm offers good radiation and reflection characteristics in the above frequency bands. The antenna has a simple geometry and can be easily fed using a 50 Ω coaxial probe. The wide 2:1 VSWR bandwidths at the three resonant bands along with moderate gain and radiation characteristics make the proposed antenna an ideal choice for multi-band wireless communication gadgets.

A.1 Introduction

The rapid progress in personal and computer communication technologies demand integration of more than one communication systems into a single compact module. To comply with the above requirement compact high performance multi-band planar antennas with good radiation characteristics are needed. A planar single feed dual L antenna of dimensions 30.5mm x 21.5mm x 13mm operating in GPS and PCS bands is proposed in [1]. The dual band antenna for the ISM band (2.4/5.8GHz) using a backed microstrip line proposed in [2] has an overall dimension of 30 x 20 mm² on FR4 substrate and offers a maximum gain of 4dBi. Dual frequency antenna configuration proposed in [3] uses triple stacked microstrip patch antennas with a slot in the middle patch, to achieve triple band operation.

This work presents a compact single feed planar antenna with three wide 2:1 VSWR operating bands around 1.8GHz, 2.4GHz and 5.8GHz respectively, covering four useful frequency bands namely GPS (1575.4MHz), DCS (1800MHz), 2.4GHz (2400-2485MHz) and 5.8GHz (5725-5825MHz) WLAN.

A.2 Antenna design

Geometry of the proposed antenna is shown in Fig. A.1. It is etched on FR4 substrate of relative permittivity, $\epsilon_r = 4.7$ and thickness $h = 1.6$ mm. The antenna has two arms of lengths $l_1 = 38$ mm, $l_2 = 33$ mm and widths $w_1 = w_2 = 1$ mm placed symmetrically on either side of a middle element of length $l_3 = 17$ mm and width $w_3 = 1$ mm. The feed point of the antenna is optimized to be at the middle of edge AB.

Good impedance matching is achieved by embedding a reflector of dimensions $L = 40\text{mm}$ and $W = 25\text{mm}$ on the bottom side of the substrate at an offset $d = 0.5\text{mm}$ from the edge AB as shown in the figure.

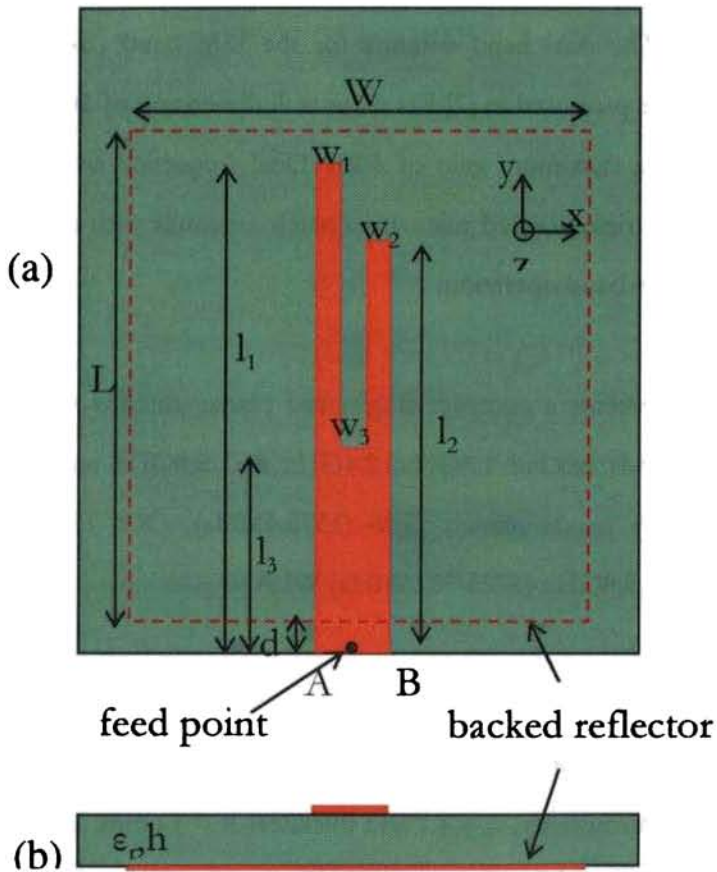


Fig. A.1 Geometry of the proposed antenna (a) Top view (b) Side view
 $L=40\text{ mm}$, $l_1=38\text{mm}$, $l_2=33\text{mm}$, $l_3=17\text{mm}$, $W=25\text{ mm}$, $w_1= w_2=w_3=1\text{mm}$, $h=1.6$
 mm , $d=0.5\text{mm}$

From the experimental and simulation results, it is understood that the lower resonance can be tuned by varying the length l_1 of arm 1. Resonance in the 2.4GHz band is influenced by the length $l_1 + l_2 - 2 l_3$. When length l_3 of the middle element is increased, the second resonance shifts upwards whereas, it gets lowered when the length l_2 is increased. Dimensions of the reflector affect both the resonance frequency and impedance matching in the 5.8GHz band. Another antenna with $l_1=79.4\text{mm}$, $l_2=77.48\text{mm}$ and $l_3=60.54\text{mm}$, exhibits resonance at 940MHz, 1.85GHz and 5.2GHz respectively suitable for GSM/DCS/5.2GHz WLAN applications.

A.3 Results and Discussion

The measured return loss characteristic of the proposed antenna is shown in Fig. A.2.

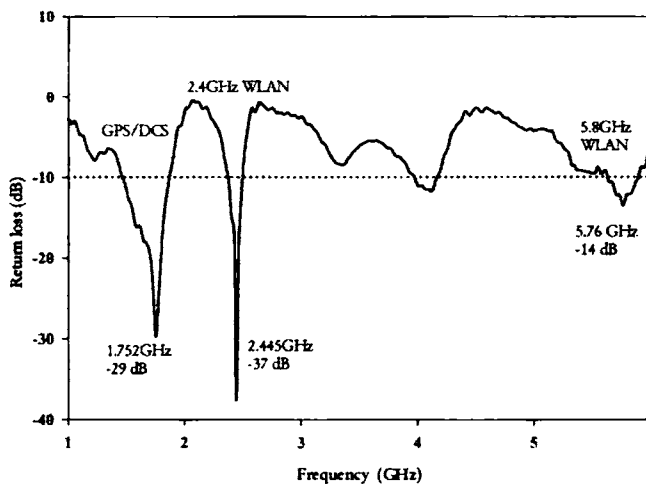


Fig. A.2. Return loss characteristics of the antenna

Three resonant bands are observed at frequencies 1.75 GHz, 2.45GHz and 5.76GHz with 2:1 VSWR bandwidths of 23%, 5% and 4.5% respectively. The lower

resonant band with 406MHz (1466-1872) bandwidth is wide enough to cover the GPS/DCS bands. The higher resonant bands with 124MHz (2372-2496) and 260MHz (5630-5890) bandwidths cover the 2.4GHz and 5.8GHz WLAN bands respectively.

The normalized E-plane and H-plane radiation patterns measured at the centre frequencies of the respective bands are shown in Fig. A.3. The patterns are observed to be nearly omni directional in the H-plane, with a cross polar level better than -15dB in the bore-sight direction. The antenna exhibits similar radiation characteristics in all the desired bands.

The measured antenna gain against frequency is presented in Fig. A.4. The antenna offers a peak gain of 7.38dBi in the GPS band. The maximum gain observed in the DCS, 2.4GHz WLAN, 5.8GHz WLAN bands are 3.73dBi, 4.22dBi and 4.65dBi respectively.

The radiation performance of the antenna in all the above bands is summarized in Table. It is observed that all bands except the 5.8GHz band are linearly polarized along Y direction. The 5.8GHz band is orthogonal to the other bands.

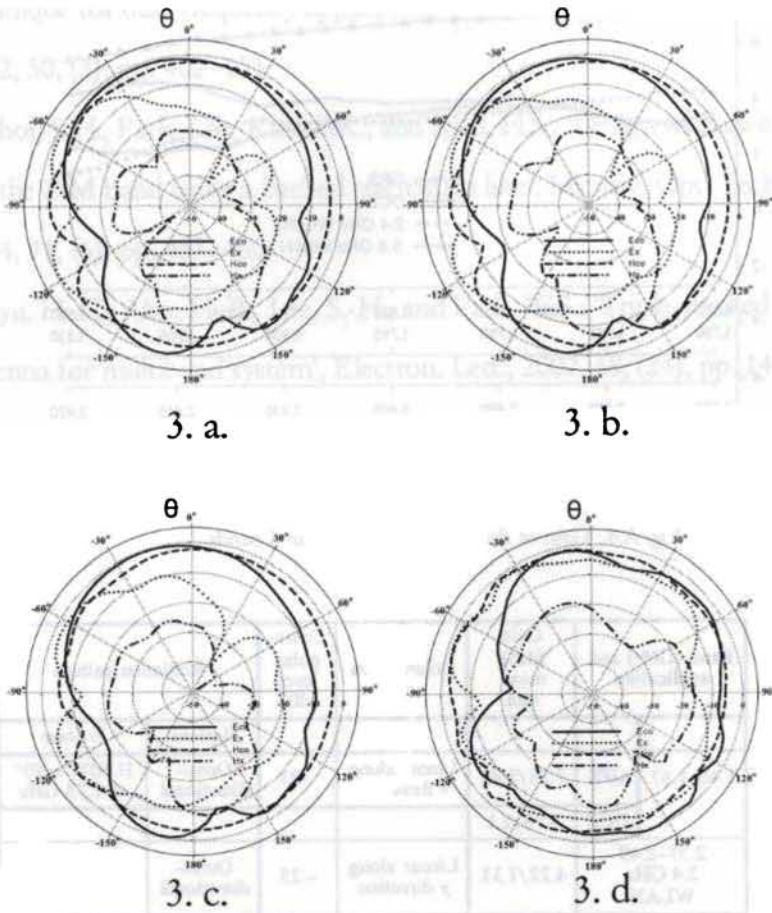


Fig. A.3: Radiation Patterns at the centre frequency of the desired bands
3.a GPS band 3.b. DCS band 3.c. 2.4GHz WLAN band 3.d. 5.8GHz WLAN
band

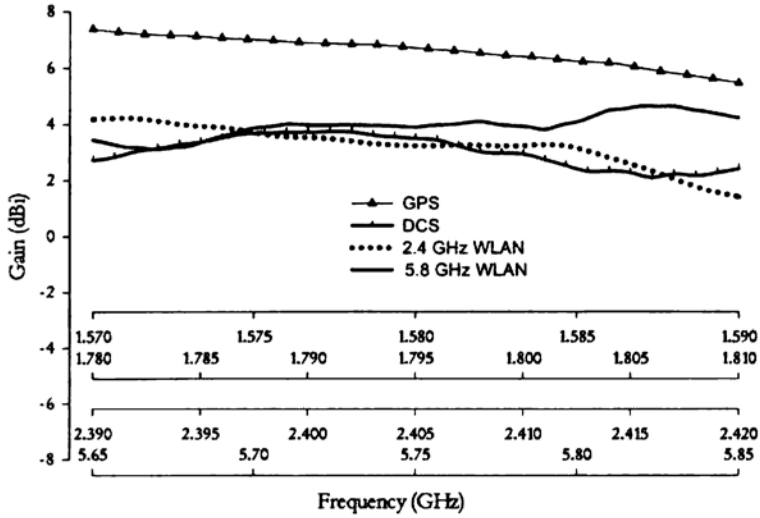


Fig. A.4. Gain of the antenna in the desired bands

Band (GHz) and application	Gain (dBi) max/min	Polarisation	Cross-polar level (dB)	Radiation pattern		
				H-plane	E-plane	
1.46–1.87	GPS	7.38/5.45	Linear along y direction	-23	Omni-directional	HPBW = 90° at 1.75 GHz
	DCS	3.73/2.1				
2.37–2.49 2.4 GHz WLAN	4.22/1.31	Linear along y direction	-25	Omni-directional	HPBW = 80° at 2.45 GHz	
5.63–5.89 5.8 GHz WLAN	4.65/3.12	Linear along x direction	-19	Omni-directional	HPBW = 126° at 5.76 GHz	

A.4 References

1. Chen, Z., Ganjara, A.D., and Chen, X.: 'A dual-L antenna with a novel tuning technique for dual frequency applications', *IEEE Trans. Antennas. Propag.*, 2002, 50, (3), pp. 402–403
2. Choi, S.H., Park, J.K., Kim, S.K., and Kim, H.S.: 'Design of dual-band antenna for the ISM band using a backed microstrip line', *Microw. Opt. Technol. Lett.*, 2004, 41, (6), pp. 457–460
3. Ryu, H.-C., Ahn, H.-R., Lee, S.-H., and Park, W.S.: 'Triple-stacked microstrip antenna for multiband system', *Electron. Lett.*, 2002, 38, (24), pp. 1496–1497

APPENDIX B

Compact Amplifier Integrated Microstrip Antenna

A compact microstrip antenna integrated with an amplifier having an area reduction of 70%, compared to the standard circular microstrip patch antenna, is presented in this section. The antenna also provides an enhanced gain of 10 dB more than its passive counter part. The measured 2:1 VSWR band width is 4% at 790 MHz, which is 2.5 times larger than that of the passive microstrip antenna.

B.1 Introduction

There is a growing tendency for portable equipment to be made smaller and smaller as the demand for personal communication rapidly increases, and the development of very compact handheld units has become urgent. Various compact microstrip antenna designs have been reported in the literature to overcome the size problem of the conventional microstrip patch antenna, such as embedding slots in microstrip patch and shorting pins placed between radiating element and the ground plane [1, 2].

For most compact antennas, the gain and radiation efficiency is much lower than the conventional microstrip antenna. In this work, area reduction is achieved by the patch geometry [3], which is obtained by modifying standard rectangular and circular microstrip patches, and gain is enhanced by integrating an amplifier to it.

The active integrated antenna has become a growing area of research in recent years, as microwave-integrated circuits and monolithic microwave-integrated circuit (MMIC) technology have become more mature, thus allowing for high-level integration. Active integrated antennas also have strong potential for commercial applications in wireless communications and radar. An amplifier-type active integrated antenna integrates a two-port active device to a passive antenna element at its input or output port.

The implementation of an amplifier in a passive antenna structure increases the antenna gain and bandwidth, and improves the noise performance. Such an active slotted equilateral-triangular microstrip antenna with an amplifier circuit has already been illustrated in [4]. In this work, a compact microstrip receiving antenna with enhanced gain and wide-impedance bandwidth is presented.

B.2 Active Antenna Design

Fig. B.1 shows the top view of the proposed amplifier-integrated microstrip antenna.

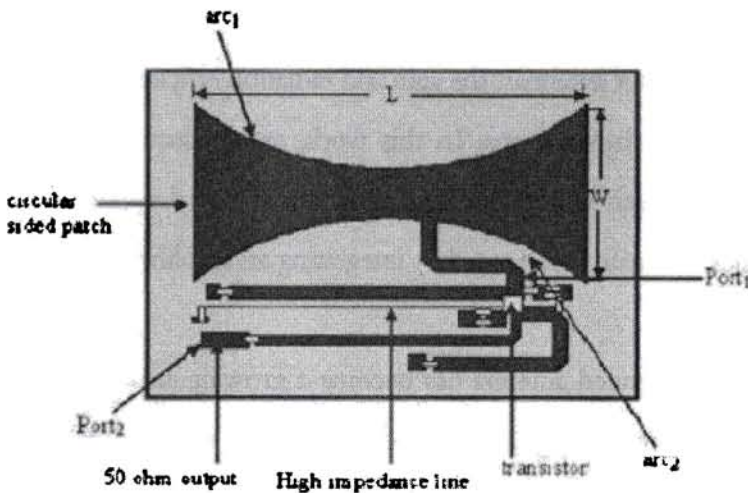


Fig. B.1. Active antenna configuration

The antenna geometry is based on a rectangular geometry with its resonating edges replaced by two circular arcs of radii $r_1 = r_2 = 6$ cm on two sides. The antenna and the amplifier circuit are etched on a substrate of thickness $h = 0.148$ cm and relative permittivity 3.95, as shown in figure.

The antenna output is coupled to the input port of the amplifier using 50 ohm microstrip feed line. Signal transmission can also be carried out using the same circuit by connecting the amplifier output to antenna input. The schematic diagram of the amplifier circuit is shown in Figure B.2. The transistor used is an NEC 2SC3357, with input impedance of $51 + j0.3084$ ohm and output impedance of $91.67 + j43.56$ ohm at 800 MHz. The amplifier is biased for class A operation. The input and output of the transistor are conjugate matched to the source and load impedance, respectively, using microstrip short-circuited stubs and impedance transformers [5].

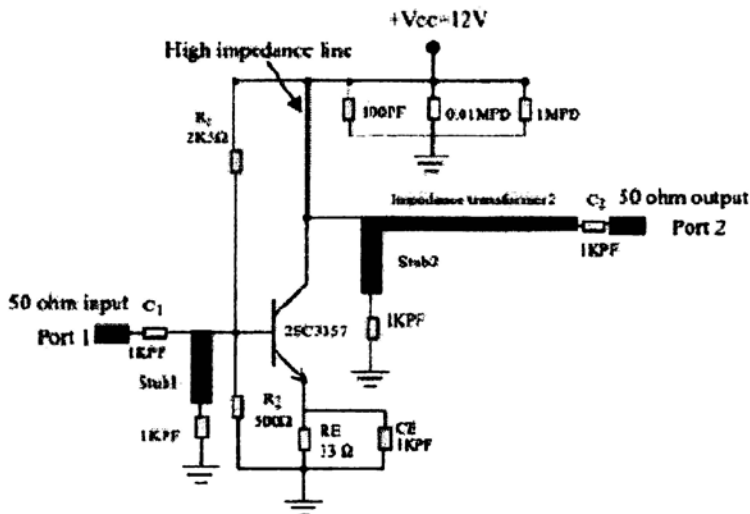


Fig. B.2. Schematic diagram of the BJT amplifier.

A high impedance microstrip line is used as load impedance at the collector of the transistor. $R1$ and $R2$ are potential divider bias resistors and RE is the emitter resistor. $C1$ and $C2$ are input and output coupling capacitors and CE provides emitter bypass capacitance.

B.3 Results and discussion

The active receiving microstrip antenna is fabricated and the impedance bandwidth, relative gain, and radiation patterns are measured using an HP 8510C vector network analyzer. Fig. B.3 shows the return-loss curve of the active receiving antenna. Relative gain of the active antenna compared to the passive element is also plotted in the figure. It is observed that the proposed antenna has an impedance bandwidth of 4% and a gain enhancement of 10 dB, compared to that of the passive counter part. E and H plane radiation patterns of the antenna at 790 MHz are shown in Fig. B.4. The patterns are broad as in the case of standard rectangular microstrip patch and cross-polarization levels are better than 20 dB.

The overall size of the antenna including the amplifier circuit is 36 cm², whereas the size of a circular microstrip antenna operating at this frequency is 121 cm². Thus, the size of the new antenna is only 30% of the circular microstrip antenna.

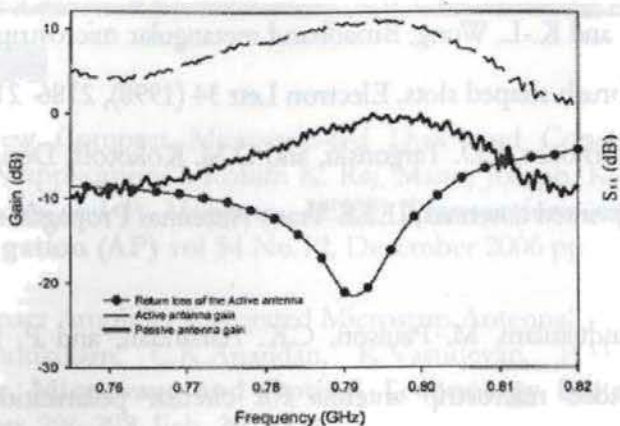


Fig. B.3. Return loss and gain curves of the passive and active antenna

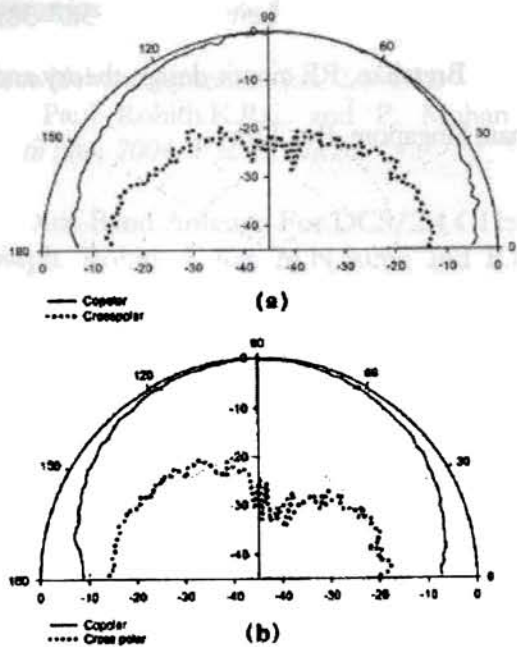


Fig. B.4. Radiation patterns of the active antenna at 790 MHz
(a) E plane; (b) H plane

B.4 References

1. J.-Y. Sze and K.-L. Wong, Broadband rectangular microstrip antenna with a pair of toothbrush-shaped slots, *Electron Lett* 34 (1998), 2186–2187.
2. R.B. Waterhouse, S.D. Targonski, and D.M. Kokotoff, Design and performance of small printed antennas, *IEEE Trans Antennas Propagat.* AP-46 (1998), 1629–1633.
3. S.O. Kundukulam, M. Paulson, C.K. Aanandan, and P. Mohanan, Compact circular-sided microstrip antenna for circular polarization, *Microwave Opt Technol Lett* 34 (2002), 176–177.
4. M.-C. Pan and K.-L. Wong, A broadband active equilateral-triangular microstrip antenna, *Microwave Opt Technol Lett* 22 (1999), 387–389.
5. R. Ludwig and P. Bretchko, *RF circuit design theory and applications*, Addison Wesley Longman, Singapore, Pvt. Ltd.

List of Publications of the author

International Journals

1. "A New Compact Microstrip-fed Dual-band Coplanar Antenna for WLAN applications", Rohith K. Raj, Manoj Joseph, K.Vasudevan, C. K. Aanandan and P. Mohanan, **IEEE Transactions on Antennas and Propagation (AP)** vol 54 No.12, December 2006 pp 3755-3762.
2. "Compact Amplifier Integrated Microstrip Antenna", Rohith.K.Raj, Sona O.Kundukulam, C.K.Aanandan, K.Vasudevan, P.Mohanan, Praveen Kumar, **Microwave and Optical Technology Letters**, USA, vol.40, no.4, pp. 296-298, Feb. 20, 2004.
3. "Compact planar multiband antenna for GPS, DCS, 2.4/5.8 GHz WLAN applications" Rohith.K.Raj, M. Joseph, B. Paul and P. Mohanan, **IEE Electronics Letters**, vol.41, no.6, pp. 290-291, 17th March 2005.
4. "Compact wideband antenna for 2.4 GHz WLAN applications", M. Joseph, B. Paul Rohith.K.Raj, and P. Mohanan, **IEE Electronics Letters**, 11th Nov. 2004, Vol.40, No.20.
5. "Compact Dual-Band Antenna For DCS/2.4 GHz WLAN Applications" Manoj Joseph, Rohith K.Raj, M.N.Suma and P.Mohanan, **Microwave and Optical Technology Letters**, Vol.48, No.5, May 2006, pp-856-859
6. "Microstrip-fed Dual band Folded Dipole Antenna for DCS/PCS/2.4GHz WLAN Applications" Manoj Joseph, Rohith K. Raj, Suma M. N, C. K. Aanandan, K. Vasudevan and P. Mohanan., **International Journal for Wireless and Optical communications (IJWOC)** December 2006
7. "A Compact Dual Band Planar Branched Monopole Antenna for DCS/2.4GHz WLAN Applications" Suma M.N, Rohith K Raj, Manoj Joseph, Bybi P.C and P. Mohanan **IEEE Microwave and Wireless Components Letters**, vol. 16, no.5, May 2006, pp 275-277

8. "Planar Branched Monopole Antenna for UWB Applications", K. Francis Jacob, Suma M.N, Rohith K. Raj, Manoj Joseph and P. Mohanan, **Microwave and Optical Technology Letters**, USA vol 49 , No.1 January 2007,pp 45-47
9. "Compact Ultra wide Band Planar Serrated Antenna with Notch band ON/OFF Control" Shameena V.A, Suma M. N, Rohith K. Raj, Bybi P.C, and P. Mohanan, **IEE Electronics Letters**.
10. "Dual band uniplanar antenna for WLAN applications" , Deepu V, Rohith.K.Raj, Manoj Joseph, Suma M.N ,C.K.Anandan,K. Vasudevan and P.Mohanan " **IEE Electronics Letters** ,Vol 43,no.2 January 2007,pp 70-72.
11. "Compact asymmetric coplanar strip fed monopole antenna for multiband applications" Deepu V, Rohith.K.Raj, Manoj Joseph, Suma M.N , and P.Mohanan **IEEE Transactions on Antennas and Propagation (AP)**

International and National Conferences

12. "Compact Active microstrip antenna", Rohith.K.Raj, Sona O.Kundukulam, C.K.Anandan, K.vasudevan, P.Mohanan and Praveen Kumar, ICMARS 2003, 15th -19th Dec. 2003, jodhpur.
[paper presented]
13. "Compact Slotted active microstrip antenna", Rohith.K.Raj, Sona O.Kundukulam, Shynu S.V, C.K.Anandan, K.vasudevan, P.Mohanan and Praveen Kumar, International Conference on Computer and Devices for Communication (CODIC-04), Jan. 1-3, 2004, Institute of Radio Physics and Electronics, Calcutta.
14. "Single-Fed Dual-Frequency Dual polarized microstrip antenna with Hexagonal slot" Shynu S.V, Rohith.K.Raj, Anupam R.Chandran, C.K.Anandan, P.Mohanan and K.Vasudevan, IEEE APS 2004.

15. "A New Compact Coplanar Antenna", Rohith K. Raj, Manoj Joseph, C. K. Aanandan, K. Vasudevan and P. Mohanan URSIGA2005, Communicated.
[paper presented]
16. "A New compact printed antenna with coplanar configuration", Rohith K. Raj, Manoj Joseph, C. K. Aanandan, K. Vasudevan and P. Mohanan, IEEE APS 2005.
17. "Planar multiband antenna", Manoj Joseph, Rohith K. Raj, Binu Paul, P. Mohanan, IEEE APS 2005.
18. "A Novel Compact wideband antenna", Manoj Joseph, Rohith K. Raj, Binu Paul, C. K. Aanandan, K. Vasudevan and P. Mohanan, URSIGA2005.
19. "Fractal PBG microstrip antenna", Rohith.K.Raj, Jayaram.P, Sreedevi K.Menon, K.Vasudevan, C.K.Aanandan, P.Mohanan, National Symposium on Antennas and Propagation (APSYM-2002), 9-11 Dec. 2002, Dept. of Electronics, Cochin University of Science and Technology, Cochin.
[paper presented]
20. "Compact Coplanar antenna for Active Antenna Applications", Rohith.K.Raj, Manoj Joseph, C.K.Anandan, K.vasudevan, P.Mohanan, National Symposium on Antennas and Propagation (APSYM-2004).
[paper presented]
21. "Compact wideband antenna for Bluetooth applications", Manoj Joseph, Rohith K. Raj, Binu Paul, K. Vasudevan, C. K. Aanandan and P. Mohanan, National Symposium on Antennas and Propagation (APSYM-2004).
22. " Compact asymmetric coplanar strip fed multiband antenna for wireless applications", Deepu V, Rohith K.Raj,Manoj Joseph, Suma M.N ,C.K.Aanandan,K. Vasudevan and P.Mohanan (APSYM-2006).

23. "Compact Dual band antenna for WLAN applications" Deepu V, Rohith K.Raj,Manoj Joseph, Suma M.N , and P.Mohanan (IEEE APS-2007,Honolulu,Hawaii,USA)



◆ Reference to the Paper

1. "Compact planar multiband antenna for GPS, DCS, 2.4/5.8 GHz WLAN applications" R.K Raj, M. Joseph, B. Paul and P. Mohanan, IEEE Electronics Letters, vol.41, no.6, 17th March 2005.
2. "Planar Branched Monopole Antenna for UWB Applications", K. Francis Jacob, Suma M.N, Rohith K. Raj, Manoj Joseph and P. Mohanan, Microwave and Optical Technology Letters, USA vol 49 , No.1 January 2007,pp 45-47
3. "A Compact Dual Band Planar Branched Monopole Antenna for DCS/2.4GHz WLAN Applications" Suma M.N, Rohith K Raj, Manoj Joseph, Bybi P.C and P. Mohanan IEEE Microwave and Wireless Components Letters, vol. 16, no.5, May 2006, pp 275-277.
4. "Compact wideband antenna for 2.4 GHz WLAN applications", M. Joseph, B. Paul R.K. Raj, and P. Mohanan, IEEE Electronics Letters, 11th Nov. 2004, Vol.40, No.20.

Resume of the Author

Rohith K. Raj

Senior Research Fellow

Centre for Research in Electromagnetics and Antennas

Department of Electronics

Cochin University of Science and Technology

Cochin-22, Kerala, India

Email: rohith_research@yahoo.com

OBJECTIVE

A motivated scholar having keen interest in Microwave electronics with specialization in Printed antenna technology, seeking a position in R&D level.

RESEARCH ACHIEVEMENTS

1. **Young Scientist Award of International Union of Radio Science (URSI)**, and had an official meeting with the **President of India**
2. **International Patent** is under process for the design of an Ultra Compact Coplanar Printed Antenna useful for **RFID, WLAN** cards, Chip antennas etc.
3. Published papers in International Journals such as **IEEE, IEE**, etc., National and International Symposia

EDUCATION

M.Sc Applied Electronics

P.S.G College, Coimbaore, Tamil Nadu, India.

Score: First class with Distinction

MEMBERSHIPS IN PROFESSIONAL BODIES

- **Radio Scientist** Membership of International Union of Radio Science (URSI)
- Possess Grade I Amateur Radio License for experimenting, operating and maintaining an Amateur Wireless Station in India, issued by Ministry of Communications, Government of India (Call sign VU2FMR).

TRAINING

1. Attended Agilent's training on ADS at Bangalore, India
2. Completed 6 months training in Rubber Research Institute of India (RRII) during Masters Thesis, and developed an updated version of ageing chamber to determine the Plasticity Retention Index (PRI) of natural rubber
3. Successfully completed a training from Kerala Electronics Ltd. (KELTRON), Govt. of Kerala, India.

TECHNICAL PAPERS PRESENTED

1. Presented the paper "Fractal PBG microstrip antenna" in National Symposium on Antennas and Propagation (APSYM-2002), 9-11 Dec. 2002, Dept. of Electronics, Cochin University of Science and Technology, Cochin
2. Presented the paper "Compact Slotted active microstrip antenna" in International Conference on Computer and Devices for Communication (CODEC-04), Jan. 1-3, 2004, Institute of Radio Physics and Electronics, Calcutta
3. Presented the paper "Compact Coplanar antenna for Active Antenna Applications" in National Symposium on Antennas and Propagation (APSYM-2004), 21-23 Dec. 2004, Dept. of Electronics, Cochin University of Science and Technology, Cochin
4. Poster presentation of the paper entitled "A New Compact Coplanar Antenna" during URSI GA 2005, New Delhi.

PUBLICATIONS

International Journal	: 11
National & International conference	: 12

RESEARCH EXPERIENCE

1. Completed the project entitled 'Pseudorandom Polarization Hopping communication system (PPH)' for Polarzone Technologies, Malaysia
2. Worked in the project 'Design development and analysis of a compact printed antenna for 2.4 GHz sensor network applications' for Wireless People, Malaysia
3. Worked as a Project Fellow in the Research Project entitled 'Development of Compact Antenna with reduced radiation hazards suitable for use in Mobile Communication handsets, funded by University Grants Commissions (UGC), Govt. of India.

3

3D radiation pattern · 140, 175, 192, 197

A

Aanandan · 47, 69, 72, 73, 74, 75, 289, 290, 291, 292, 293
Active antenna · 269
AMC · 13
Amplifier · 29, 30, 31, 282, 290
Anechoic Chamber · 91, 93, 100
Antenna design · 273
Antenna miniaturization · 78

B

Bandwidth · 30, 95
Bose · 3

C

Compact · 28, 34, 38, 52, 66, 69, 70, 72, 74, 75, 79, 185, 271, 282, 289, 290, 291, 292, 293, 294, 295, 296, 297
Compactness · 35
Conducting pin · 203, 239
Coplanar antenna · 34, 258, 259, 267, 293, 296
CPW · 15, 16, 17, 18, 19, 22, 24, 26, 31, 44, 49, 54, 56, 57, 59, 60, 63, 71, 75, 78, 79, 82, 85, 139, 135, 136, 137, 140, 142, 143, 144, 145, 147, 148, 150, 151, 155, 156, 159, 161, 162, 164, 166, 168, 170, 171, 173, 174, 177, 179, 182, 209, 265
Current distribution · 173

D

Dominant mode · 31
Dual band · 290, 291, 293

E

E plane · 248
EBG · 13
Efficiency · 141
Electric field · 81, 179
Electromagnetic radiation · 20
Even mode · 26
experimental · 25, 34, 41, 45, 48, 58, 86, 94, 96, 166, 171, 238, 252, 254, 259, 261, 263, 264, 265, 275

F

FDTD · 60, 86, 105, 106, 107, 110, 112, 113, 114, 115, 116, 121, 122, 126, 127, 128, 129, 130, 131, 132, 134, 135, 136, 137, 135, 137, 143, 144, 145, 146, 147, 149, 150, 151, 155, 156, 157, 158, 161, 164, 167, 168, 170, 172, 176, 180, 182, 206, 207, 208, 209, 210, 213, 215, 216, 221, 222, 223, 230, 231, 251, 257, 259, 263, 265, 266, 267
FFT · 148, 214
Field distribution · 17
Finite Difference Time Domain · 35, 85, 102, 115
Flow chart · 147
Fractal antenna · 77

G

GPS · 26, 38, 43, 70, 271, 273, 276, 277, 290, 293

H

Handset · 36, 65, 67
 Hertz · 3
 HfSS · 25, 86, 98, 99, 100, 214, 215, 239
 HP 8510C · 91, 155, 287

I

IE3D · 25, 86, 97, 100, 140, 173, 175, 189, 191, 194, 252
 Impedance matching · 142
 Inferences · 252, 264, 267
 Internal antenna · 70

K

Kraus · 27, 100

L

Low profile · 77

M

Magnetic field · 151
 Marconi · 3, 27
 Maxwell · 3, 61, 82, 105, 106, 107, 110, 115, 116, 136
 MEMS · 19
 Metamaterial · 13, 15, 27
 Microwave substrates · 89
 Millimeter wave · 27
 Mobile communications · 7
 Mohanan · 68, 69, 70, 72, 73, 74, 75, 76, 100, 289, 290, 291, 292, 293, 294
 Monolithic · 31
 Monopole antenna · 8
 Multi-band · 34, 41, 271
 Mur · 113, 115, 136

N

Numerical dispersion · 111

O

Odd mode · 17, 26, 143

P

Parametric analysis · 26, 135, 166, 200, 259
 Pattern reconfigurable · 63, 85
 PCS · 26, 35, 38, 39, 55, 56, 77, 79, 273, 290
 Photolithography · 88
 PMI · 25, 60, 61, 99, 102, 114, 115, 116, 118, 120, 121, 123, 124, 125, 126, 148, 151, 208, 209, 231, 263
 Polarization · 171, 247, 297
 Polarization discrimination · 247
 Principal plane · 247
 Propagation · 27, 28, 65, 66, 67, 68, 69, 70, 71, 72, 73, 74, 75, 76, 77, 78, 79, 80, 81, 82, 83, 84, 85, 136, 290, 291, 292, 293, 296
 PTFE · 10

R

Radiation · 67, 82, 98, 143, 144, 169, 175, 222, 264, 268
 Radiation boundary · 98
 Radiation pattern · 143, 175, 264
 References · 27, 65, 100, 136, 280, 289
 Resistive source model · 128
 Resonance · 59, 136, 137, 143, 275
 Return loss · 95, 135, 137, 156, 190, 206, 208, 213, 215, 233, 264
 RI² potential · 178
 Rumsey · 27

S

Sarabandi · 54, 77, 78
 Sheen · 61, 82
 Sine function · 133

Staircase transition · 130
Switches · 19

T

TEM · 16, 198
Theoretical analysis · 86
THRU calibration · 96, 97
Time domain · 105, 136
Transistors · 269

V

Vasudevan · 68, 74, 75, 100, 290, 291, 292, 293
Vector Network Analyzer · 91
VNA · 91, 95
VSWR · 34, 48, 51, 55, 57, 95, 248, 250, 267,
271, 273, 276, 282

W

Waveguide · 19, 28, 29, 30, 135
Wen · 15, 28, 35, 38, 40, 46, 49, 56, 59, 65, 66,
67, 68, 72, 75, 79, 81
WLAN · 26, 35, 38, 39, 43, 45, 46, 50, 56, 63, 70,
72, 75, 76, 85, 255, 271, 273, 275, 276, 277,
290, 291, 293, 294, 295
Wong · 35, 37, 38, 40, 48, 65, 66, 67, 68, 74, 289

Y

Yagi-Uda · 4
Yee · 61, 82, 105, 108, 114, 115, 129, 131, 136,
208, 209
YIG · 92